

SILESIA UNIVERSITY OF TECHNOLOGY  
FACULTY OF MECHANICAL ENGINEERING  
DEPARTMENT OF FUNDAMENTALS OF MACHINERY DESIGN



**Doctoral dissertation**

M. Sc. Eng. Szymon Żymełka

DEVELOPMENT OF SEMI-ACTIVE SHOCK ABSORBER DYNAMIC  
MODEL AND PARAMETERS IDENTIFICATION METHODOLOGY

Supervisor:

Marek Fidali, BEng, PhD, DSc

Gliwice, 2023

# Contents

<b>1</b>	<b>Introduction</b>	<b>7</b>
1.1	Problem statement . . . . .	7
1.2	Objectives . . . . .	8
1.3	Scope of the research . . . . .	9
1.4	Plan of industrial implementation . . . . .	10
1.5	Hypothesis . . . . .	11
<b>2</b>	<b>Automotive suspension and shock absorbers - theoretical background</b>	<b>12</b>
2.1	Historical perspective . . . . .	12
2.2	Current state of the semi-active suspension systems development . . . . .	13
2.3	The function of the shock absorber in the automotive suspension . . . . .	16
2.4	Shock absorber design and operation principles . . . . .	18
2.4.1	Mono-tube design . . . . .	18
2.4.2	Double-tube design . . . . .	20
2.4.3	Semi-active damper . . . . .	21
2.5	Valving design . . . . .	23
2.5.1	Passive valves . . . . .	23
2.5.2	Active valve . . . . .	25
2.6	Noise related problems background . . . . .	25
2.7	Standard shock absorbers measurements methods . . . . .	30
2.7.1	Shock absorber performance . . . . .	30
2.7.2	Valve level measurement . . . . .	31
2.7.3	High frequency response . . . . .	32
<b>3</b>	<b>Literature survey of modeling techniques</b>	<b>35</b>
3.1	Empirical models . . . . .	35
3.2	Physical models . . . . .	36
3.3	Conclusions . . . . .	40
<b>4</b>	<b>Proposed model description</b>	<b>42</b>
4.1	Rod forces . . . . .	42
4.2	Hydraulic system . . . . .	43

4.3	Chamber compliance . . . . .	44
4.4	Valves submodel . . . . .	46
4.5	Top mount . . . . .	52
4.6	Rod friction . . . . .	54
4.7	Study of alternative valve modeling techniques . . . . .	56
4.7.1	Impact of the valve stiction forces . . . . .	57
4.7.2	Impact of the valve level friction . . . . .	57
4.8	Conclusion . . . . .	58
<b>5</b>	<b>Parameters estimation methodology</b>	<b>61</b>
5.1	Theoretical introduction . . . . .	62
5.1.1	Parameter estimation . . . . .	62
5.1.2	Optimization . . . . .	63
5.2	Parameter estimation methods used in this dissertation . . . . .	63
<b>6</b>	<b>Parameters calibration study – approach 1</b>	<b>68</b>
6.1	Description of the design used for the calibration exercise . . . . .	68
6.2	Calibration of valves related parameters . . . . .	69
6.2.1	Experimental set-up and results . . . . .	70
6.2.2	Estimation of the parameters of the valve model . . . . .	72
6.2.3	Results of the calibration process . . . . .	75
6.3	Calibration of compliance related parameters . . . . .	75
6.3.1	Description of the compliance estimation procedure . . . . .	76
6.3.2	Results of the compliance estimation . . . . .	77
6.4	Calibration of top mount related parameters . . . . .	77
6.4.1	Description of the methodology . . . . .	77
6.4.2	Results of the calibration process . . . . .	80
6.5	Assesment of the model quality based on experimental measurements . . . . .	84
6.5.1	Results of the comparison . . . . .	85
6.6	Conclusions . . . . .	89
<b>7</b>	<b>Parameters calibration study – approach 2</b>	<b>101</b>
7.1	Sensitivity-based parameters estimation procedure . . . . .	103
7.2	Description of the parameter estimation procedure . . . . .	104
7.3	Results of the calibration process . . . . .	107
7.4	Conclusions . . . . .	113
<b>8</b>	<b>Summary and discussion</b>	<b>119</b>
8.1	Industrial implementation . . . . .	122

## Abstract

The shock absorber is one of the most important parts of the automotive suspension which is primarily influencing the ride and handling properties of the vehicle. Apart from this traditional low-frequency range of operation, automotive dampers can be a source of undesired high-frequency content that might lead to a range of expensive and difficult-to-solve problems, particularly when detected at the late stage of the design development project. With the growing popularity of advanced shock absorber designs, there is a demand for the ability to predict the dynamic behavior of the damper by means of computer modeling. Due to the multi-physical complexity of the shock absorber and the large number of physical characteristics involved, this task poses a significant challenge for the design teams, despite the rich scientific material and literature in that field. In order to address the aforementioned needs, the presented dissertation includes a review of the current state of the art in the field of automotive shock absorbers and methods of computer modeling of their behavior. Based on this knowledge and needs formulated during cooperation with the industrial partner engineering community, a model of the semi-active shock absorber has been proposed which is capable of reliably reproducing axial dynamics of the shock absorber up to 500 Hz by capturing various physical aspects of the valve operation and compliance of the damper as well as vibroisolators. In order to facilitate the practical application of the proposed model, a calibration procedure was necessary to estimate the values of the parameters that could not be directly obtained from the technical documentation. The first approach included parameter estimation performed at isolated test setups which required multiple experimental measurements. Despite the good quality of the model calibration, due to complex testing procedures, this approach was deemed difficult for industrial implementation. For that reason, a second approach was proposed. It relied on a much simpler experimental procedure thanks to the advanced sensitivity-based parameter estimation method. Throughout the project, the quality of the model and reliability of parameter calibration has been proven using multiple measurements performed at various assembly level.

## Streszczenie

Amortyzator to jedna z najistotniejszych części zawieszenia samochodowego, która w dużej mierze wpływa na właściwości jezdne pojazdu związane z przyczepnością i komfortem. Oprócz podstawowego (niskoczęstotliwościowego  $< 30$  Hz) zakresu pracy zawieszenia dla jakiego amortyzatory samochodowe są projektowane i kalibrowane, konstrukcje te, mogą być również źródłem niepożądanych drgań wysokoczęstotliwościowych, których rozwiązanie nierzadko jest trudne i kosztowne, zwłaszcza jeśli problemy te zostają wykryte na późnym etapie rozwoju konstrukcji. Wraz z postępującym rozpowszechnieniem zaawansowanych konstrukcji amortyzatorów trudności w ocenie ryzyka wystąpienia niepożądanych charakterystyk dynamicznych rośnie. Stwarza to potrzebę rozwoju komputerowych narzędzi pozwalających na ocenę dynamicznego zachowania amortyzatorów nawet na wczesnym etapie projektowania. Pomimo bogatego zasobu literatury naukowej w zakresie modelowania komputerowego tego typu konstrukcji, ze względu na wysoką złożoność amortyzatora i dużą liczbę cech fizycznych z nim związanych, zadanie to stanowi istotne wyzwanie dla środowiska przemysłowego. Wychodząc naprzeciw powyższym potrzebom, w prezentowanej rozprawie dokonano przeglądu aktualnego stanu wiedzy w zakresie amortyzatorów samochodowych oraz metod komputerowego modelowania ich zachowania. W oparciu o tę wiedzę i potrzeby określone we współpracy ze środowiskiem inżynierskim partnerów przemysłowych zaproponowano model amortyzatora półaktywnego, który jest w stanie wiarygodnie odtworzyć dynamikę osiową w zakresie do 500 Hz poprzez dokładne oddanie aspektów fizycznych wpływających na działanie systemu amortyzatora. Ze względu na złożoność zaproponowanego modelu, istotnym utrudnieniem uniemożliwiającym jego praktyczne wykorzystanie jest konieczność rzetelnego określenia wartości parametrów wejściowych. Z tego powodu, kolejnym etapem pracy było przygotowanie procedury kalibracji parametrów modelu, których nie można uzyskać bezpośrednio na podstawie dokumentacji technicznej. W celu jak najlepszego dostosowania rozwijanych metod do potrzeb środowiska przemysłowego, w toku doktoratu zaproponowano dwa odrębne od siebie podejścia które pozwalają na kalibrację modelu. Pierwsze podejście polegało na szacowaniu wartości parametrów w oparciu o pomiary przeprowadzane na wyizolowanych podukładach amortyzatora. Podejście takie ułatwiało proces kalibracji gdyż, możliwe było odseparowanie od siebie grup parametrów które podlegały kalibracji. Niestety podejście to wymagało przeprowadzenia kilku niezależnych od siebie badań eksperymentalnych co z organizacyjnego punktu widzenia może stanowić wyzwanie w środowisku przemysłowym. Druga zaproponowana metoda kalibracji miała na celu zniwelowanie tego problemu. Opierała się ona na znacznie prostszej procedurze eksperymentalnej (przeprowadzanej na pełnym złożeniu amortyzatora) która, dzięki zaawansowanej metodzie estymacji parametrów opartej o czułości pozwalała na kalibrację wielu parametrów modelu w ramach jednej pętli optymalizacyjnej. W trakcie projektu jakość modelu jak i niezawodność kalibracji parametrów sprawdzono poprzez wielokrotne pomiary przeprowadzane na różnych poziomach złożenia amortyzatora. Zaproponowany model jak i opracowane metody jego kalibracji posłużyły do stworzenia narzędzia obliczeniowego gotowego do wykorzystania w warunkach przemysłowych.

*Pragnę wyrazić wdzięczność wszystkim tym, którzy pomogli mi przygotować poniższą pracę. Przede wszystkim, podkreślić chciałem pomoc mojego promotora dr hab. inż. Prof. PŚ Marka Fidali oraz opiekuna przemysłowego dr inż. Damiana Sławika, bez których realizacja doktoratu nie byłaby możliwa. Jako, że doktorat realizowany był w trybie projektu wdrożeniowego chciałbym podziękować partnerowi przemysłowemu, firmie Tenneco Automotive Eastern Europe Sp. z o.o. w tym, w szczególności mojemu przełożonemu dr inż. Tomaszowi Łukasikowi oraz śp. Piotrowi Grzance, a także wszystkim pozostałym pracownikom którzy okazali mi wsparcie przy realizacji tej pracy. Dziękuję również mojej żonie za pomoc oraz wyrozumiałość w trakcie realizacji tego doktoratu.*

# Chapter 1

## Introduction

With over 80 years of service history, telescopic, hydraulic, shock absorbers are hardly a new invention. However, despite the time laps, they remain an important part of modern automotive suspension. One of the reasons for their popularity is that this design facilitates relatively easy changes of the damping characteristics making a shock absorber a primary component that is used to fine-tune the behavior of the suspension of the car according to the subjective requirements of the car manufacturers.

### 1.1 Problem statement

The natural frequency range of the operation for which the automotive shock absorbers are designed to operate and control the suspension is usually approximately 0-30 Hz (low-frequency range). Frequency content above that range is traditionally considered a domain of the elastomeric vibro-isolators which are meant to stop higher-frequency content from transferring to the rest of the car. An important part of that high-frequency content is not only vibrations that come from the road disturbances and wheel but also those that due to high nonlinearities related to valves opening and closing, originate directly at the shock absorber's chambers (self-induced shock absorber vibrations). As the damper designs are progressing, and getting more complex (often by means of electronic control) to meet the demand for better ride and handling properties of the car, performance within their natural domain is indeed improving but as a side effect, often, such designs are prone to more pronounced unwanted high-frequency dynamic phenomena that might arise at the damper even under just a low-frequency excitation. If it fails to be isolated by the top mount, such high-frequency vibrations might lead to noise-related problems as well as disruptions to the control algorithms. These problems are further exacerbated by the rapid proliferation of electric cars, which (due to lack of engine noise) are much quieter and high-frequency vibrations are more easily distinguishable and picked up by the driver. It is also important to emphasize that most of the dynamic, high-frequency

problems are difficult and expensive to solve when detected at the late stages of the development project (when the field test and full vehicle ride works are performed) owing to the fact that, this type of problems are inherently related to the complete system and altering its characteristics often requires changes to the key design parameters. All the above reasons, create a situation in which the ability to numerically simulate and predict the dynamic characteristics of the newly designed shock absorbers is very valuable.

Fortunately, as shown in the survey (see chapter 3) there is a wide range of documented modeling techniques specifically developed for the hydraulic automotive suspension and damping systems that allow for performance and characteristics estimation across a wide range of frequencies. However, they are difficult to be practically employed as part of standard industrial procedures due to the following challenges:

- difficulty related to establishing suitable modeling techniques to address the problems of high-frequency vibrations at the semi-active dampers
- lack of established parameter estimation procedures
- difficulty handling a large number of parameters, parameters conditioning methods as well as results and reporting

## 1.2 Objectives

As a result of the described needs of the industry, the goals of the project were formulated. The most important goal is to enable the practical utilization of the advanced modeling techniques of the semi-active automotive shock absorbers in the industrial environment. To achieve that it is required to perform research on the existing knowledge related to the automotive shock absorber, their role in the suspension and most importantly modelling techniques allowing to reproduce their behaviour. Based on this review as well as based on the available techniques present in the automotive industry, a computer model is to be proposed. In order to fully utilize the formulated simulation techniques, a parameter estimation procedure has to be developed and the quality of the result should be estimated. The described goals of the project have been summarized in the form of the following list:

- Review of the existing knowledge regarding hydraulic, telescopic shock absorbers as well as techniques of reproducing their high-frequency ( $<500\text{Hz}$ ) dynamic behavior with computer modeling methods.
- Proposal of the numerical model of the semi-active shock absorber that can be used for the following purposes:
  - Analysis of the damper performance at low-frequency behavior with accurate hysteresis representation which can be adopted for vehicle ride and handling performance studies

- Optimization of the control algorithms
- Risk prediction of the structure-borne noise due to the high-frequency dynamic behavior of the shock absorber
- Reduction of the damper performance-related experimental testing
- Proposal of the complete parameters estimation procedure
- Verification of the model accuracy in relation to the experimental measurement of the high-frequency behavior of the shock absorber
- Implementation of the developed methods into the engineering procedures of the industrial partner company

### 1.3 Scope of the research

In order to address the goals that were formulated for the project the first step was to perform a study of the existing knowledge in the domain of automotive suspension systems as well as in the field of computer modeling of shock absorbers (these parts can be found in chapters 2 and 3). After establishing the main guidelines and assumptions for the simulation techniques, a numerical model is proposed in chapter 4. Due to the wide range of physical phenomena that influence the dynamic behavior of the semi-active shock absorbers, a multi-domain, lumped parameters model was employed. Due to the high level of complexity of the model, parameter estimation become a particularly important task. Given the large amount of documented work devoted to the modeling of the shock absorbers, techniques related to parameterization (model calibration) are much more sparse, making parametrization an important limiting factor that is preventing the wider adoption of the numerical models. The problem of model calibration was addressed with two approaches:

- classic parameters characterization procedure that is done on isolated subsystems
- sensitivity-based parameter estimation procedure utilizing a series of concurrent genetic algorithms for optimization purpose

The first method (described in chapter 6) allows to establish values of the input parameters that are difficult to obtain from the technical documentation of the designs. Three main subsystems are considered separately: valves (valve stiffness being the main estimated parameter), oil compliance (amount of undissolved gas being the main estimated parameter) as well as top mount dynamic's model parameters. The advantage of that method of estimating the parameters is the high flexibility of the application since it allows for verifying the designs that were not yet prototyped. On the downside, it requires a relatively complex calibration procedure in terms of the experimental testing part and the quality of the model prediction depends on the accuracy of the measurement, these shortcomings are mitigated with the second parameter estimation approach.

The second method of parameter estimation requires performing calibration testing at the complete shock absorber assembly as the only experimental measurement used for the parameter estimation. This greatly simplifies the experimental part of the process (because there is only one, relatively simple test) but the large amount of parameters calibrated at the same time poses a challenge. To mitigate this difficulty a sensitivity-based parameter estimation procedure is applied. It allows to use of only one test result as a source of multiple objective functions, each oriented at the specific subsystem for which the parameters will be estimated. Such a proposed method simplifies the experimental part of the calibration procedure and results in higher fidelity of the model results. After such calibration, a model effectively becomes a digital twin of the calibrated sample.

Each of the calibration methods was discussed in detail and the results of each procedure were evaluated. This together with the parameter sensitivity study provides the confirmation that the model is able to correctly reproduce the dynamic behavior of the shock absorber. However, the last remaining obstacle preventing the application of the developed methods within standard design procedures was the complexity of the input and output data processing. In order to manage this, over the course of the project, a simulation environment has been prepared using Python scripting language that couples the calibration methods, data and simulation engine (Simcetner Amesim) allowing for easy manipulation of input parameters and simulation results without a deep understanding of the constituent parts of this system.

## 1.4 Plan of industrial implementation

Presented Ph.D. dissertation is prepared as part of the Industrial Implementation Program (conducted in cooperation with industrial partner: Tenneco Automotive Eastern Europe Sp. z o.o.) which exerts strong emphasis on the practical application of the knowledge and methods obtained over the course of the project. For that reason, apart from the already formulated goals, conducted scientific research should result in tools, methods and processes that are practically applied in the industrial environment. Since the subject of the project is the development of the computer model which might involve advanced and complex procedures, it is planned that for future usage, an easy-to-use interface will be prepared. The main goal of this interface is to enable engineers to access the developed functionality without a deep understanding of the theory behind it and without a need for the installation of specialized software. A prepared interface together with the developed methods should help solve already existing engineering problems in a tangible manner. In the case of the dynamic behavior of the shock absorber, this means improving the design using knowledge obtained from the calibrated, dynamic model of the semi-active shock absorber.

## **1.5 Hypothesis**

With the computer model which is proposed based on the literature study, through the use of a series of experimental tests at the level of individual components and/or the entire assembly, it is possible to identify the parameters that are necessary to simulate the dynamic operation of an automotive, semi-active shock absorber with the accuracy that allows making practical conclusions regarding high-frequency (above secondary ride mode range) behavior of the shock absorber. Furthermore, this process can be practically implemented into standard industrial procedures.

# Chapter 2

## Automotive suspension and shock absorbers - theoretical background

This chapter provides an overview of the subjects related to automotive suspension and shock absorbers so that the reader can easily understand the circumstances and needs for the numerical model and identification techniques developed in later parts of this dissertation.

### 2.1 Historical perspective

Well-designed and appropriately tuned damper should not draw the attention of the passengers of the car. Therefore, it is easy to underestimate the role of the shock absorber. At the beginning of the XX century, when motored vehicles were slowly gaining traction, shock absorbers were still a relatively rare occurrence. Earlier, due to the low speeds attained by horse-drawn carriages, shock absorbers were not particularly useful and definitely too complicated for manufacturers in that era. Additionally, the function of the shock absorbers was somehow reproduced by the frictional forces that arise at the surfaces of the leaf springs which were commonly used at the time. As a result, the first mass-produced cars did not feature any kind of automotive damper design along with the leaf or coil springs. This included a famous Ford Model T for which the manufacturer not only didn't include a shock absorber but in its 1915 owner's manual, discouraged the use of them on the grounds of the safety [78, 28]. This provided early adopters of the motored vehicles with an unpleasant opportunity to experience the consequences of a lack of the proper damping device. The inconvenience produced by the usage of such automotive suspension was sufficient for car owners to find a solution on their own. As a result, it has become relatively common to retrofit early cars with after-market shock absorbers. The demand for this kind of solution was high enough to make their manufacturers commercially successful [40]. Some of the most popular brands of shock absorbers

at that time included:

- Truffault-Hartford Shock Absorber (scissor-action dry friction damper)
- Andre-Hartford (scissor-action dry friction damper)
- Hassler Shock Absorber (conical spring for Ford Model T)
- Lovejoy (lever-arm hydraulic damper)
- Gabriel (belt snubbers)

From a technical perspective, early shock absorbers relied mainly on the dry friction forces produced by preloaded discs or block and belt snubbers which are most commonly operated via a scissor or lever mechanism. Some of the designs included a link for the driver to adjust damper force which functioned as a break for the body motion. Although hydraulic and telescopic designs of shock absorbers were known much earlier they've become popular in the second half of the twenties by replacing friction-based lever and scissor-based designs. The next notable advancement in the history of the shock absorber came with the introduction of the MacPherson strut which dominated the market of the front suspension since the late 1940s. The main reason for the popularity of this type of suspension was cost, simplicity and compact size [79]. Further progress in the technology of automotive suspensions was oriented toward the improvements of electronic control of shock absorber systems. Although passive shock absorbers and struts still comprise a bulk of the automotive suspension systems sold across the world, however, some semiactive systems reached large-scale production numbers and their volumes are already counted in millions of units sold. Apart from semi-active dampers progress in the development and modeling of stroke and frequency-dependent dampers should also be recognized since due to relatively low price and noticeable improvement in ride comfort this class of designs is also gaining a notable portion of the market [58, 54, 55].

## 2.2 Current state of the semi-active suspension systems development

Most commonly, electronically controlled suspension systems are divided into two types: active and semi-active systems. Active systems are defined as those for which the external energy is supplied so that the force exerted by the damper can be independent of the damper's travel or velocity. On the other hand, semi-active suspension systems only adjust the parameters of the damper to the current conditions on the road and they don't use external energy for the damping force creation [105]. Semi-active systems are usually divided into two groups:

- adaptive shock absorbers – those systems allow to adjust the parameters of the damper but the feedback loop is not closed at the time of damper operation,

- semi-active dampers – those systems utilize the feedback loop to continuously adjust the damping characteristics.

Both semi-active and active systems might operate in variously limited vibration bandwidths. Depending on the design, the characteristics of the damper might be adjusted at different rates and the adaptivity of the characteristics might be performed independently for each stroking direction or both together. Although there is a large amount of different technical solutions available for engineers to apply, only a few were used in the automotive industry on a large scale. The section below provides an overview of the technical solutions for electronic control of damping from the perspective of their popularity in the automotive industry. The simplest and cheapest type of semi-active suspension system is the introduction of the electronically controlled bypass valve that can be remotely closed or opened. This provides an opportunity to choose either a ‘soft’ or ‘sport’ suspension setting. All major shock absorber suppliers included in their portfolio some variation of this type of damper system. Notable examples of such products are Tenneco’s DualMode [92] and Bilstein’s DampTronic-Select [114]. Although relatively cheap, this type of adjusting the damper systems is slowly being replaced by designs that allow for continuous adjustment of the characteristics. In terms of technical methods of achieving such continuous control, there are only two families of designs that are currently relevant in the industry: MR/ER dampers and Electronically controlled valve systems [114].

**MR/ER dampers** - operate by employing magnetorheological or electrorheological fluid as a hydraulic medium and electromagnetic coil which produces a magnetic field to control the flow resistance through a valve. This method of continuous control of the damper characteristics doesn’t require a complex mechanical valve, making it relatively simple and cheap in design. Lack of moving parts and mechanical simplicity also means that this type of damping force control is very quick in terms of response time and has a high dynamic range (turn-up ratio) [64]. Other advantages include the quiet operation of the valve and low power consumption when compared with other semi-active systems. Development of the MR dampers technology started in 1990 at the Lord Corporation and resulted in Motion Master Ride Management System which found its first application in Class 8 trucks in 1997. The first broad-based automotive application came with the introduction of the MagneRide systems from Delphi Automotive Systems which was first used in the 2002 Cadillac Seville STS and Chevrolet Corvette. Since then MagneRide system has undergone its 4th revision and was used in at least 1 million vehicles [112, 30, 5]. So far MagneRide remains the only large-scale, commercially successful system utilizing MR dampers. Some disadvantages that stifle the growth of the MR/ER dampers originate from the fact that magnetorheological fluids comprise in large part of iron particles which cause the hydraulic medium to be more abrasive, heavier and susceptible to oxidation and particle settling (when not used for longer periods of time). Although

manufacturers mitigate a lot of those problems in different ways, high-damping force nonlinearities still pose challenges.

**Electronically controlled valve** (ECV) – this type of continuous adjustment of the damping force utilizes a valve that in most cases is controlled by the solenoid actuator (a regular servo-valve would be too complex and expensive for such application). Since the solenoid is capable of exerting only relatively low forces, ECVs usually employ a hydraulic leverage mechanism to control high pressures in the damper. Due to the packaging challenges and production costs, such an electronically controlled valve is usually attached to the side of the damper and operates alongside regular passive valves. Oil flow is directed to the ECV via an additional chamber created by adding a third tube. Such design facilitates the damping force's continuous control in both stroking directions but not independently. A strong advantage of this solution is the similarity of the design to a classical passive damper which makes it easier for adoption by the existing production facility. Triple tube design with one, unidirectional ECV is currently by far the most common and commercially successful application of semi-active shock absorbers thanks to the following product lines in the portfolio of the suspension systems suppliers [114]:

- Monroe's CVSAe featuring Ohlins's CES valve – produced by Tenneco with approximately 20 million units sold and applied for 75 different passenger vehicles [8, 38]
- Sachs CDC – produced by ZF Friedrichshafen with approximately 34 million units sold so far [6]
- Bilstein DampTronic B6

Due to the popularity of the aforementioned design, this particular semi-active shock absorber layout has been selected as an object of the numerical model described in this dissertation. Detailed layout and operating principle have been described in detail in paragraph 2.4.

A natural, further development of this design is an application of two electronically controlled valves which allow for independent tunability of damping force in compression and rebound stroke. Due to increased cost, this solution is less popular than one valve design but it is also gaining popularity in the form of the following products:

- Monroe's CVSA2
- Sachs CDC [7]
- Bilstein DampTronic Sky

The most advanced automatic suspension development is a fully active system however the price of the system itself as well as the power consumption during operation so far prevents commercial application of this type of system.

## 2.3 The function of the shock absorber in the automotive suspension

Dynamic characteristics of the automotive dampers cannot be fully discussed outside of the broader context of vehicle dynamics, therefore, this paragraph aims at providing a practical description of the role that shock absorber plays in the operation of the automotive suspension. In the scientific literature, multiple approaches to describing and explaining the function of automotive suspension can be found. At the most general level, the vehicle dynamics approach usually indicates two primary roles of the suspension: isolation and control. Isolation is concerned with separating passengers from the disturbances caused by road defects as well as vehicle maneuvers. On the other hand, control is defined as an ability to safely enforce steering commands provided by the driver [22]. Most often, those functions are discussed in terms of ride comfort (isolation but mainly related to straight-line driving) and road holding and handling (control, particularly during maneuvers), which traditionally constitute conflicting objectives for which the compromise has to be found. Since both aforementioned aspects of the vehicle dynamics are influenced by various characteristics of the vehicle, not only originating at the suspension (e.g. engine, wind, seating etc.) and due to the fact that both are relatively subjective, finding a good compromise is not a trivial task. Multiple attempts were made in the past to find an objective measure of how well both functions of the suspension are accomplished for given settings but so far such objective measures only serve as an aid to the ride engineers and the end decision regarding the suspension tuning is primarily subjective [126]. Particularly, ride comfort is notoriously difficult for finding reliable objective measures. Ride comfort is often considered in terms of two frequency ranges called: primary and secondary ride modes. Primary ride mode is usually considered as rigid body motions of the vehicle body which is taking place at a frequency range of 0-3Hz. On the other hand, the secondary ride mode is used to describe the dynamic motion of the unsprung mass in relation to the road and vehicle body which takes place at approximately 3-30 Hz [13]. If the wheel suspension is analyzed using a simple quarter car model, its secondary ride mode is dominated by the natural frequency of the wheel (wheel hop frequency) which is usually in the range of 10-20Hz for passenger cars. The human body is considered to be most sensitive to vibration in a range of 0.5-0.75 Hz due to motion sickness [69], 3 and 11 Hz are important for the torso [1] while head and neck are most susceptible in range of 18-20Hz [13]. Therefore objective measures of ride comfort usually focus on vertical, secondary ride mode. Lateral accelerations at lower frequencies are also relevant but they are used to a lesser degree since the primary ride modes can easily be confused with the handling aspects [13]. In terms of the road holding and handling the objective quantity is mainly related to the dynamic loads transferred

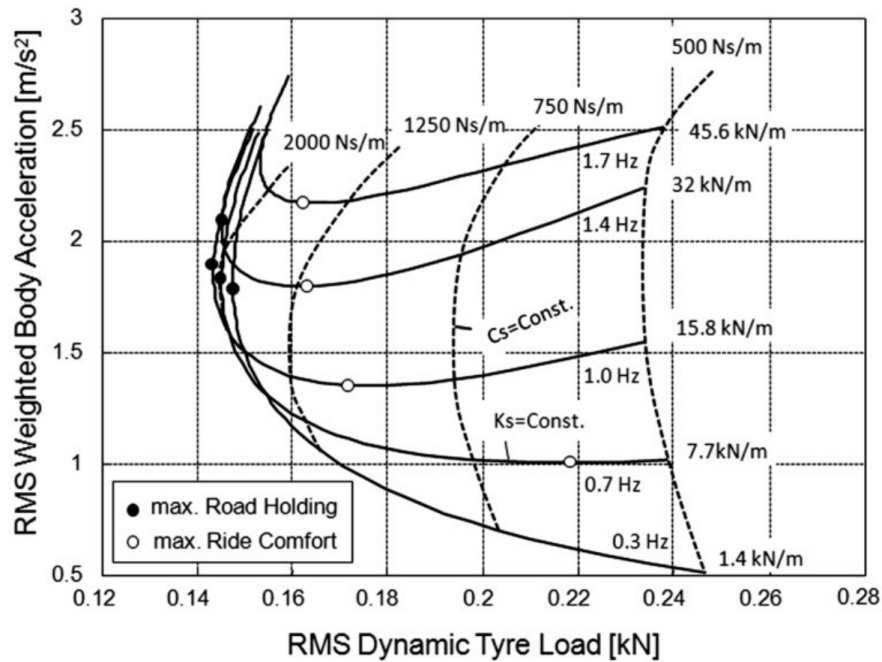


Figure 2.1: Relationship between ride and handling objective measures for various suspension damping and stiffness settings [114, 82]

by the tire which should be uniform across the wheels and as low as possible. However, in practice lateral body accelerations and side slip angles are used as well [126].

With the help of the simple quarter car model, it is possible to analyze the influence of the two most important parameters of suspension damping and stiffness over the indicators of ride comfort and road holding. The result of such a study performed in [82] is shown in fig. 2.1 where dotted lines show constant damping whereas solid lines indicate the constant stiffness. Inspection of this graph reveals the Pareto front which illustrates the famous problem of compromise between ride and handling. Each new car or suspension system before it is rolled out to the broad market has to go through the process of suspension tuning which aims at finding the best compromise/settings of the suspension. Much like the musical instrument tuning process, such a process involves a combination of formalized subjective and aforementioned objective measures in order to find the best possible combination of ride and handling. In practice, for modern passenger cars, this balance is usually achieved by the use of a relatively low-stiffness suspension spring element which is controlled by relatively high damping forces [59]. Such an approach is a result of the relationship shown in Fig. 2.1 but also of the fact that the damper's key characteristics such as force vs velocity and force vs displacement can be strongly non-linear and easily adjusted. For that reason, the shock absorber is the most important component from the perspective of controlling the behavior of the automotive suspension. In general, with the higher forces generated by the damper for a given velocity (steeper force-velocity characteristic) vehicle handling is improved at

the cost of degraded ride comfort and vice-versa. However proper suspension tuning involves many more aspects of the damper behavior (described in detail in [87, 14]) such as damper's force-velocity relationship progressiveness, low-speed characteristics as well as blow-off level and shape. Important to the perceived comfort might also be hysteresis in the force-velocity characteristic. Despite relatively high flexibility in adjusting the damper parameters, passive shock absorbers always have to find a compromise for a conflicting objective of ride comfort and handling. Perfect damper setting (lack of need for compromise) for a given road condition can only be achieved by the application of a fully active system. However, passive systems, even those with low adaptability rates, thanks to a wide range of potential damping characteristics can provide significant improvement to all aspects of the vehicle dynamics.

## 2.4 Shock absorber design and operation principles

On the most basic level, all the telescopic, hydraulic shock absorbers generate the resistive damping force either by inducing pressure differential over the piston or by an increase in overall internal pressure which acts on the cross-section of the piston rod (see eq. 4.1). Both pressure differential and overall pressure increase are a result of the restriction to the flow from one chamber of the damper to another. For such a mechanism of damping force generation to work properly it is required for the hydraulic medium to be relatively incompressible, otherwise, the damper would operate more like a capacitive element. However, during the actuation of any telescopic damper, the volume of a piston rod is either pushed into or pulled out of a constrained volume of a shock absorber tube. Since valves have to operate within the incompressible fluid, part of the damper has to be devoted to a compressible chamber that facilitates this alternating volume. The way in which this problem is solved is the main differentiator of the two most common types of hydraulic shock absorbers: mono-tube and double-tube designs (see figures 2.2b and 2.2a). Although this dissertation focuses on the semi-active damper design, understanding the operating principles of the passive designs is very helpful to later analyze and model the dynamic behavior of the more complex systems.

### 2.4.1 Mono-tube design

In a mono-tube design (fig. 2.2a), the volume of the piston rod can freely enter and exit the damper thanks to the gas chamber that is separated from the compression (oil) chamber by a floating piston. Since gases are highly compressible, with the correct sizing of the chambers, the volume of the rod during compression stroke causes only a small increase in internal damper pressure (and vice versa for the tension stroke). Since the floating piston, by design, can slide within the tube of the damper without restriction,

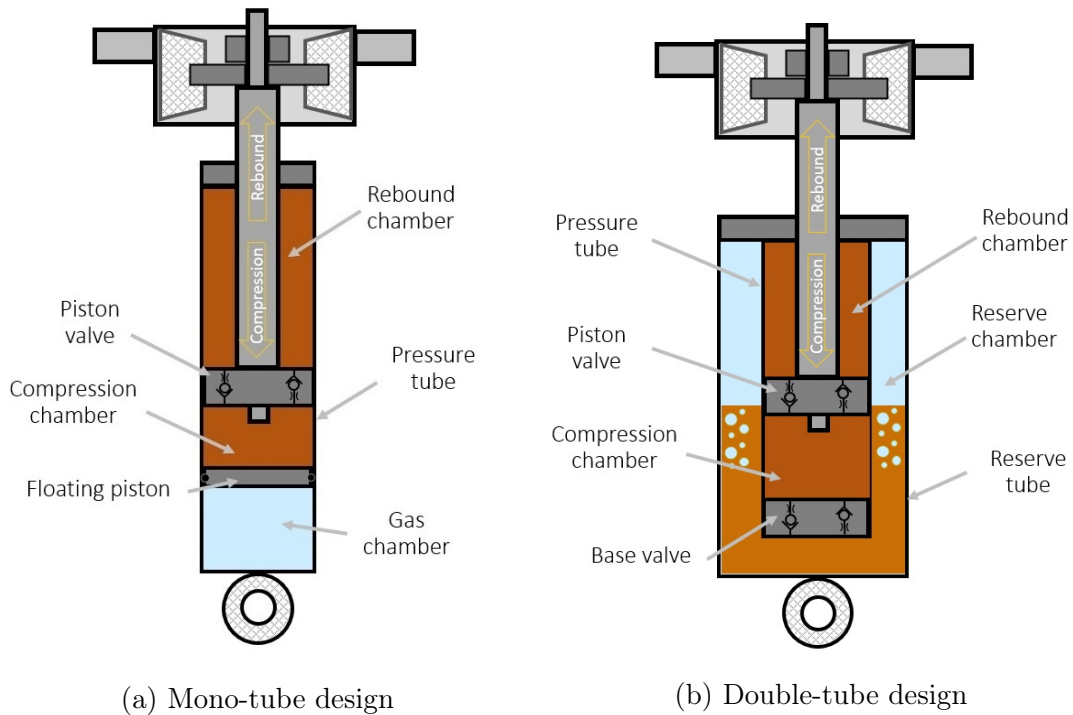


Figure 2.2: Layout of the two most common passive damper designs

the pressure in a gas chamber and compression chamber remains virtually constant. This means that pressure in the compression chamber cannot rise at all in relation to the damper velocity. During the rebound stroke, this is not an issue since the pressure in the rebound chamber can easily rise and create the required pressure differential. However, in the compression stroke, the pressure differential has to be obtained not by an increase in the compression chamber pressure but, by the drop of the pressure in the rebound chamber. It is important to point out that the pressure in any oil chamber cannot fall below a certain value (which is usually close to zero bar in relation to atmospheric pressure) since then according to Henry's law, oil would lose its hydraulic properties. The solution for mono-tube dampers is simply to increase initial pressure. Therefore the maximum compressive force of the mono-tube damper is limited (for the given dimensions of the damper) by the value of precharge pressure. For a typical mono-tube damper, a pre-charge pressure ranges between 20 - 40 bar and during the rebound stroke it can rise significantly. Given the fact that loss of precharge pressure constitutes immediate degradation of the damping performance, this type of hydraulic damper requires very advanced and therefore expensive rod guide sealing. However, thanks to the floating piston design, monotube shock absorbers are characterized by relative mechanical simplicity. By having only one valve, the damping forces can usually be more precisely controlled (compared to other designs of shock absorbers), there is less disturbance related to the opening and closing of the valves and as a result the vehicle dynamics aspects particu-

larly those related to the handling are improved (wheel control is more consistent and predictable). Despite the advantages of the mono-tube design, the necessity of maintaining high internal pressure in the damper is a significant drawback of this type of shock absorber design which is mitigated in the case of the double-tube design. It is worth emphasizing that the damping forces in the mono-tube damper are primarily built by the pressure differential whereas the overall increase of the pressure is not significant (this is a fundamental difference when compared with double tube design).

## 2.4.2 Double-tube design

In the case of a double-tube damper design, piston rod volume displaces the oil into the reserve chamber which is partially filled with gas. The reserve chamber is separated from the rest of the damper not by the floating piston like in the mono-tube design but by the base valve (see section 2.2b). During rebound stroke, damping force is built in a similar way as in mono-tube design - by an increase of the pressure in the rebound chamber which creates a pressure differential over the piston. It is important though that in the case of double tube design, the restriction at the base valve in the rebound direction (base valve intake) has to be low enough not to lead to aeration in the compression chamber during rebound stroke. However, in the case of the compression stroke direction, a completely different mechanism of force build-up is used. In the compression stroke, oil displaced by the rod volume entering the damper has to pass through the base valve. Any restriction to the flow through the base valve will cause an increase in both, compression and rebound chambers. Since the compression surface of the piston is larger than the rebound surface (by the value of the piston rod cross-section), the uniform rise of pressure in both chambers will result in force generated at the piston rod. Due to increased pressure in the rebound chamber (caused by the restriction at the base valve), it is possible to also involve the restriction at the piston, since the pressure in the rebound chamber can fall without risk of going under precharge pressure value. In such a case, force at the piston rod is also developed by the pressure difference at the piston. Double tube valving configuration which generates the force by both valves is referred to as "full displacement" whereas the configuration that only utilizes base valve restriction is called "rod displacement" (comparison of the pressure characteristics for both configurations can be found in figure 2.3). During compression stroke in rod displacement damper, pressure in rebound and compression chamber remains similar due to low restriction of the piston compression valve (piston intake). On the other hand, when the full displacement damper configuration is used, restriction at the piston compression valve has to be always (at each flow rate value) lower than the restriction of the base compression valve, otherwise, pressure in the rebound chamber would immediately drop below precharge values, causing so-called "valve imbalance" which is characterized by large free stroke in next rebound

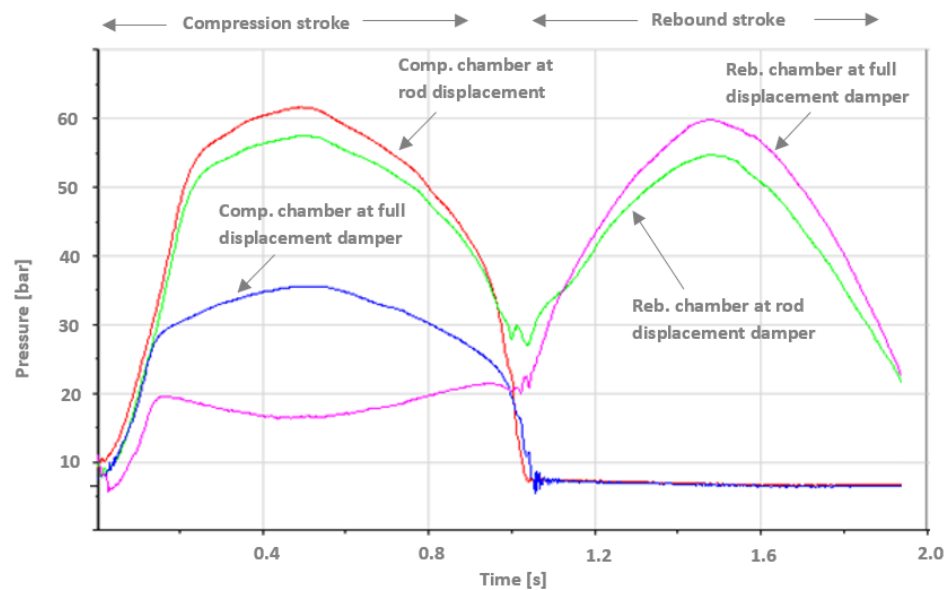


Figure 2.3: Example of the pressure changes in the compression and rebound chambers in dampers with rod and full displacement configuration during sinusoidal excitation

cycle.

A strong advantage of the double-tube damper design over the mono-tube design is much lower precharge pressure (usually at around 2-5 bar) which decreases the production cost. Also, in the event of partial loss of internal pressure, a double-tube damper will in most cases continue to operate normally (albeit with degradation of the damping performance) whereas the internal pressure loss in a monotube damper would cause significant free strokes in the compression direction. The disadvantage of the double tube is the necessity of having two separate passive valves and an additional tube. Double tube dampers usually are limited to operation in a vertical position although designs with floating pistons or buffer springs also exist. On the other hand, monotube dampers have to be much longer compared to double-tube designs. From the perspective of performance, small rod diameter monotube dampers provide much higher responsiveness due to low compliance and therefore hysteresis in force-velocity characteristic.

### 2.4.3 Semi-active damper

The semi-active shock absorber for which the model is studied generates the velocity-dependent forces largely on the principles of the double tube damper configured to operate in rod volume displacement regime for which adjustable bypass flow is introduced (see figure 2.4). This flow is channeled via the annular cavity created by the third tube (third tube chamber) to the active valve. Rod volume displaced regime is required due to the fact that an active valve can only be used with flows going in one direction and in the considered design there is only one active valve. Similar to the double tube design,

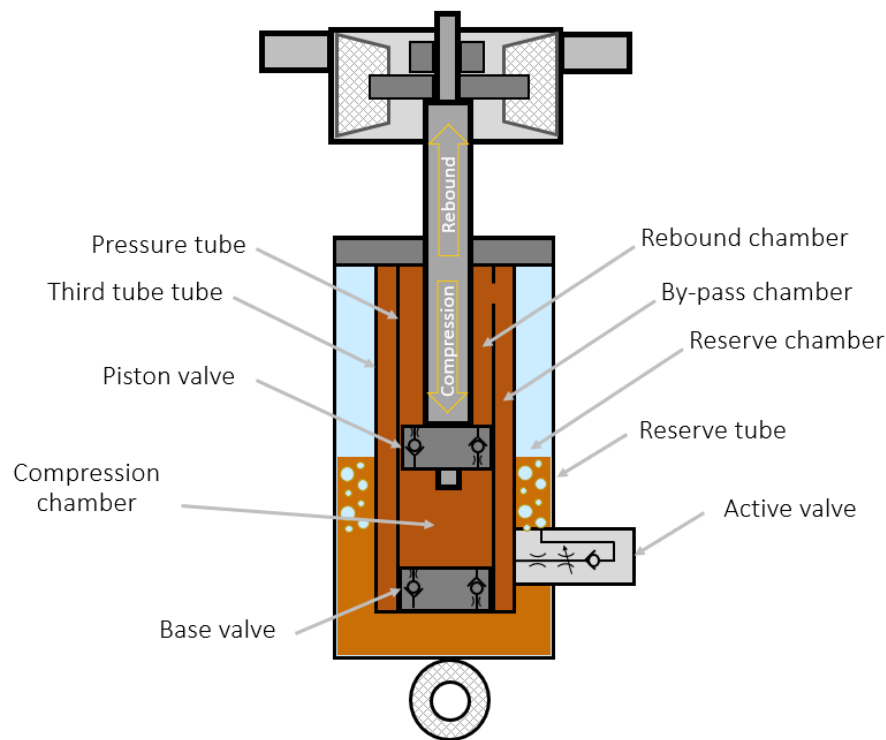


Figure 2.4: Schematic view of the triple tube semi-active shock absorber with one unidirectional active valve

within such a regime, the majority of the damping force during the compression stroke is built by the base compression valve (pressure rises in all chambers) while the piston compression valve acts only as a check valve. Conversely, in the rebound direction, the majority of the force is built on the piston rebound valve, since any significant pressure drop caused by the base rebound valve restriction would lead to the pressure in the compression chamber falling below the pressure in the reserve chamber and in turn to the aeration problems. As a result of the rod displacement valve configuration of the semi-active damper, both rebound and compression strokes create higher pressure in the rebound chamber than in the third chamber. This pressure drop can be influenced by the active valve which controls the flow from the third tube chamber to the reserve chamber. Application of the full displacement valve configuration would result in the loss of damping force adjustability during the compression stroke. The ability to control both directions with only one active valve is the main advantage of the considered design of the semi-active damper since the electronically controlled valve is the most expensive part of the damper. Unfortunately, as explained earlier such an approach necessitates the usage of a rod displacement configuration which as demonstrated in the following sections might be challenging from the perspective of the high rod acceleration problems particularly when a relatively small rod diameter is used.

## 2.5 Valving design

### 2.5.1 Passive valves

The role of the valves in the hydraulic dampers is to introduce the desired restriction to flow between different chambers which in turn, induces pressure differential and finally a force at the piston rod. Hydraulic properties of this restriction are usually characterized by the pressure vs flow rate relationship (abbreviated as P/Q curve, see figure 2.5). In order to supply appropriate damping force at different dynamic motions of the car and undamped mass (as discussed in section 2.3), P/Q characteristic is usually desired to be strongly non-linear. As explained in sections 2.3, some of the valves, act as check valves only (intake valves), therefore their restriction should be as small as possible, however, the opening and closing of those valves should not induce excessive vibrations in the hydraulic system.

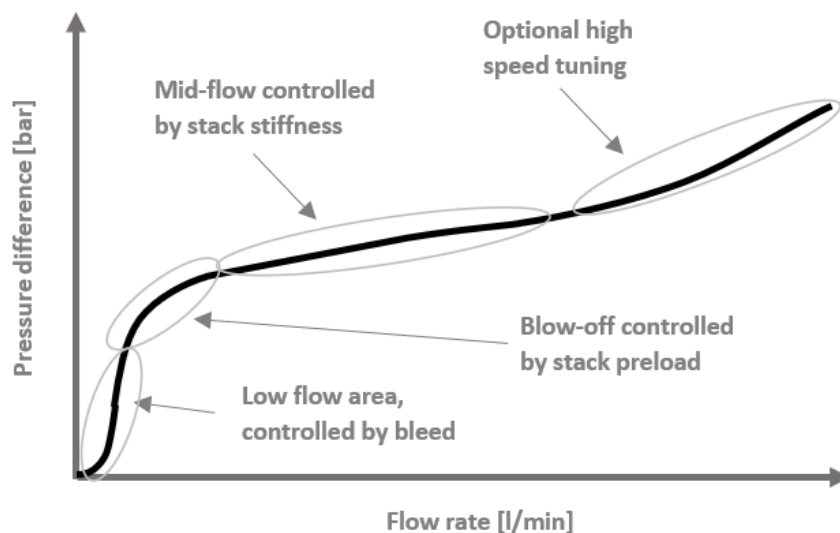


Figure 2.5: Exemplary PQ curve with the description of its distinct ranges

**Shim stack valves** Shim stack valves are by far the most common type of valves used in hydraulic dampers to control their characteristics. The primary reason for their popularity is the ease of setting even complex, non-linear P/Q curves by changing the stiffness and/or preload of the shim stack. The stiffness of the shim stack is changed, simply by adding shim disks or using thicker ones, whereas the preload is changed by adding or removing preload discs at the base of the stack. Shim stack preload mainly influences the pressure difference at which the opening (also referred to as blow-off) of the valve takes place whereas the slope and shape of the P/Q curve after blow-off is more

impacted by the stiffness. At pressure differences lower than those causing valve opening (at low flow rates),  $P/Q$  characteristic is dominated by a purposefully created slot in the first shim disc which is called a bleed area. Conversely, at higher pressures and flow rates, the  $P/Q$  curve can be increased by physically constraining the valve opening (the outer diameter of the disk is supported) creating so-called high-speed tuning. The impact of the design features of the shim stack valve mentioned above has been illustrated in figure 2.5. Since the valving system is a key element determining the behavior of the suspension in a car, apart from the main design features of the valve described in this section, each shock absorber manufacturer has a range of small design details that help to improve the subjective reception of the damper. Moreover, as a result of continuous improvement of this part of the shock absorber, there is a large number of shim stack design variations in use which include conical springs acting on the shim valve, clover-shaped valve lands, etc.

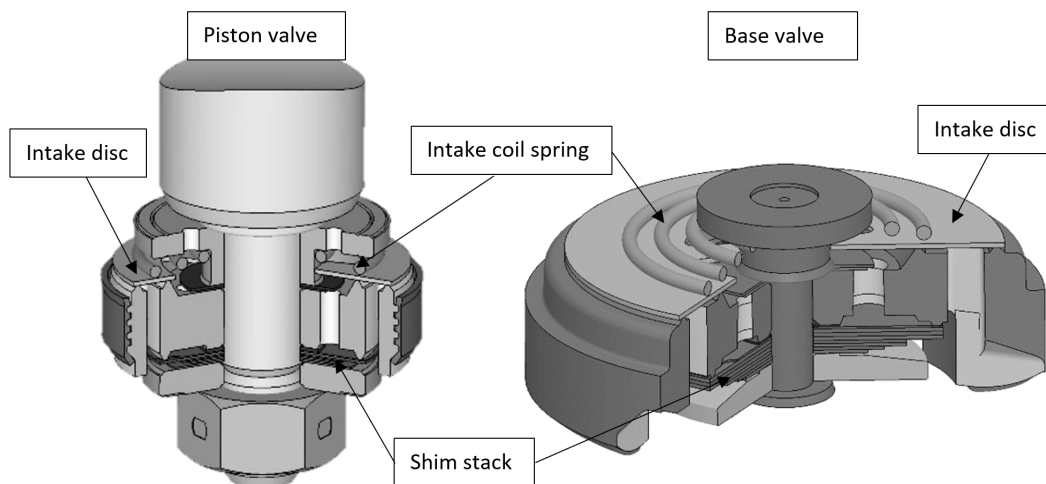


Figure 2.6: Overview of the valve design

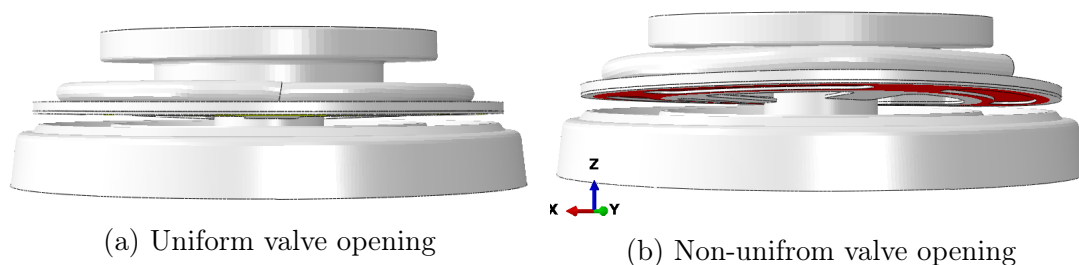


Figure 2.7: Simulated intake valve opening shapes

**Intake valves** Since intake valves (piston compression side and base valve rebound side) act as check valves, in contrast to the shim stack valves, they usually have a much simpler  $P/Q$  relationship. It is usually desired for the intake valve to induce a relatively

low-pressure drop for a given flow rate without excessive vibration of the flow and valve mechanical structure. In most cases, such an objective can be achieved by the application of a single check disk and conical spring (see fig. 2.6 b). Depending on the parameters such as the height of the preloaded intake spring, outer diameters and stiffness of the spring, the force exerted by the spring might be more or less uniform around the circumference of the intake disk. Non-uniform opening of the intake valve (see fig. 2.7b) creates smoother P/Q characteristics.

### 2.5.2 Active valve

The role of the active valve is to facilitate electronic control over the restriction to the flow between the third tube chamber and the reserve chamber. This is achieved by the application of the two-stage proportional control valve which is actuated by the electromagnetic solenoid (see fig. 2.8), manufactured by Swedish company "Ohlins" under the commercial name of CES (Continuously Controlled Electronic Suspension) valve [94, 12]. In principle, the valve consists of two poppets (see fig. 2.9). The first poppet functions as a simple proportional valve which is responsible for exerting restriction to the main path of the flow (counter proportional to the pressure difference). The second poppet (called pilot poppet) also acts as a proportional valve but is additionally (apart from the spring) actuated by the solenoid force. Opening of the second stage poppet creates a pressure drop under the main poppet which induces a proportionally larger opening to the main flow path. In other words, the second stage acts as a hydraulic leverage that operates the main poppet. In this way, even low force input coming from the solenoid is able to efficiently influence large pressures and flow rates going through the valve. By setting the correct spring stiffness, diameters of the poppets as well as slots diameters it is possible to obtain desired relationship between the current applied at the solenoid coil and pressure drop vs flow rate through the valve. The exemplary range of P/Q characteristic adjustability has been shown in figure 6.2.

## 2.6 Noise related problems background

In normal driving circumstances, automotive shock absorbers should not be the source of the distinguishable noises, however, in some cases, due to wrong damper designs or the unfortunate combination of the dynamic properties of the damper and the car, this requirement is not satisfied.

Noise-related problems can be divided into air-borne and structure-borne. In the case of automotive suspension, airborne vibrations are considered as those that originate at a certain part of the suspension and then are transferred directly to the passengers via the acoustic medium. A structure-borne noise is defined as the vibrations that originate

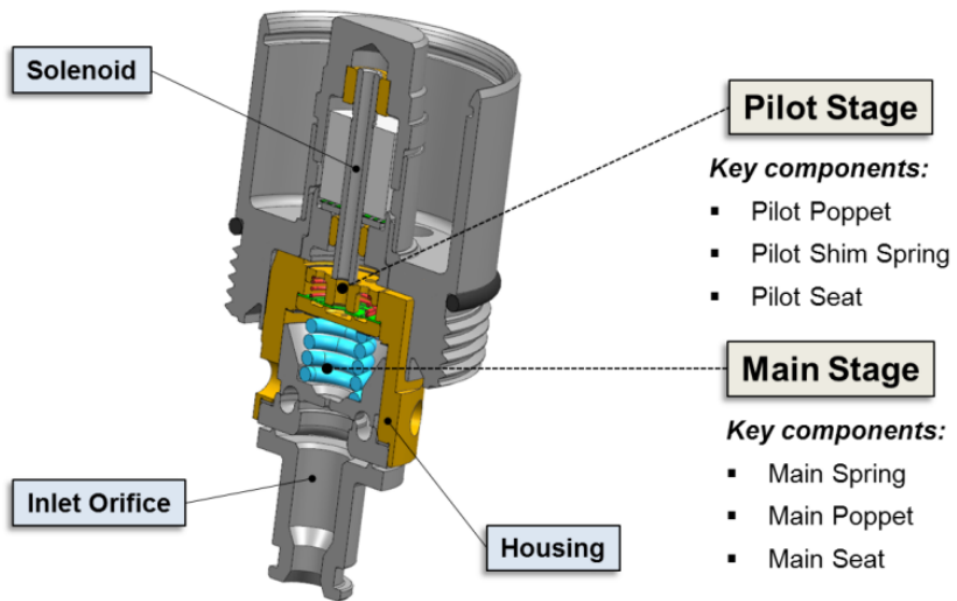


Figure 2.8: Cross section of CES8700 valve [94]

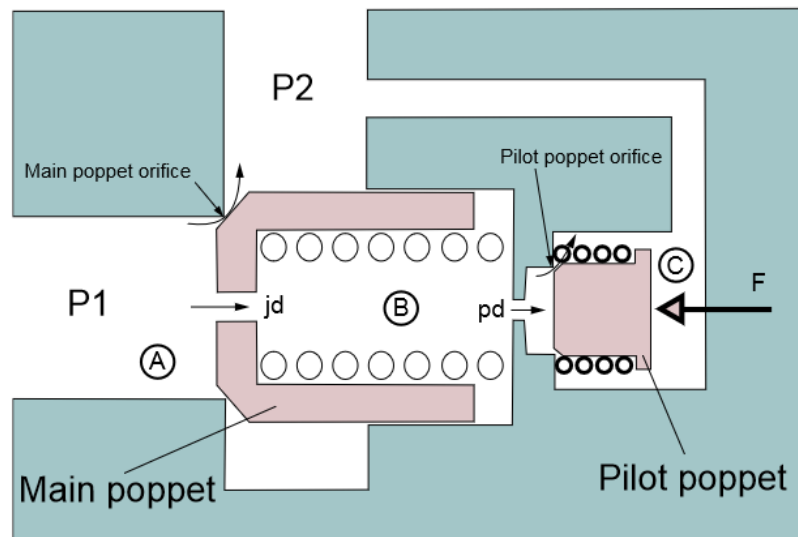


Figure 2.9: Schematic layout of the CES valve [12]

at one part of the suspension but are then transferred via mechanical and structural connection of the chassis to the elements of the car interior where they induce secondary vibration and audible noise. The system-level modeling approach studied in this dissertation is primarily suitable for the analysis of the structure-borne noise, therefore methods and tools developed in this work are only applicable to structure-borne related problems. The main challenge in dealing with the structure-borne noise coming from the automotive suspension is the fact that the vibrations themselves are only half of the problem. The second part is the question of whether the vibrations, do induce undesired acoustic effects. In other words, suspension vibrations are the inputs to the structure and how the structure reacts determines whether vibrations constitute a problem or not. Unfortunately, to answer this question the entirety of the vehicle structure would have to be considered. Given the current state of the computational and experimental testing capabilities, it is not practical to do so. Instead, good practice rules and general guidelines are being used to determine the risk of noise occurring in the car for each of the noise mechanisms. The difficulty with the structure-borne vibrations is further exacerbated by the fact that (as it can be concluded based on the section 2.3) historically, a primary, vehicle dynamics-oriented domain of operation for the automotive damper in terms of frequency is approximately within the range of 0-30Hz. It is usually considered that the problem of higher frequency content should be simply isolated by the application of proper elastomeric bushings. Particularly important is in this case the shock absorber top mount since the damper is often the main source of unwanted structure-borne vibrations. Yet another challenge in dealing with structure-borne noise is related to the fact that there are at least three different mechanisms that can induce excessive vibrations in the suspensions:

- Axial vibrations of the piston rod
- Lateral vibrations of the shock absorber structure
- Friction induces vibrations

**Axial vibrations of the piston rod** A common misconception regarding structure-borne noise is that the vibrations that cause the problem originate from the road irregularities and later are failed, to be properly isolated by the suspension. In reality, high-frequency (100-500 Hz) vibrations described in this paragraph are often a result of only low-frequency actuation (0-30 Hz) of the shock absorber itself. The true origin of this type of noise mechanism is due to forces created by abrupt pressure changes in the damper chambers which are caused by the nonlinearities in the P/Q characteristics of the valves [123, 102, 68]. These forces induce high acceleration excitation which (with the unfortunate combination of the parameters impacting modal parameters) can initiate the rod vibration. The main mode of this vibration is related to the inertia of the rod mass whereas the stiffness is provided at the top mount bushing and damper compliance

[23, 117]. As a result of such shape of the main vibration mode, the relationship between damper characteristics and top mount stiffness is particularly important [48, 115].

The vibrations of the rod caused by the aforementioned mechanism can be transferred to the chassis of the car and from there, it can propagate to the cabin and its occupants in the form of audible noise. Figure 2.10 shows the comparison of the vibration levels at various parts of the suspension in the function of the frequency. In that figure, primary and secondary ride modes are easily distinguishable below 20Hz, but it can also be clearly observed that the overall vibration level at higher frequencies is elevated at the rod when compared with the damper's knuckle. This indicates that much of the vibration measured at the rod is self-induced at the damper level.

The risk of such noise mechanism occurring in the car is usually detected at the modular damper assembly level with the use of the clatter noise test set-up described in paragraph 2.7 where rod accelerations are analyzed in time domain using periodic excitation signal as well as in the frequency domain when typical unsprung mass noise is used as a drive signal. The relationship between rod acceleration characteristics and risk of noise due to the fact that the complete structure of the car is involved constitutes a complex subject. However, over the past decades, shock absorber suppliers developed an experience-based set of KPIs (Key Performance Indicators) that are focused on quantifying the undesired characteristics of the rod acceleration signal which might contribute to the undesired noise. Although the ability to estimate the risk of structure-borne noise based on the rod acceleration signal is important know-how of the damper suppliers some methods are openly published [16, 47, 81].

**Lateral vibrations of the shock absorber structure** The second type of noise mechanism originates from the dynamic properties of the shock absorber structure. In particular, the bending modes of the damper can be excited by the operation of the suspension and cause undesired resonance which is transferred to the cabin [81]. Risk of the noise problems related to this type of damper vibrations is usually diagnosed by performing a modal analysis of the structure of the damper with a focus on the lateral directions. Both, car manufacturers as well as shock absorber suppliers have good-practice requirements that are based on the natural bending frequencies of the damper that help to avoid this type of problem. For example, bending modes at around 200Hz are often considered risky. Rao et al. in [100] observed that lateral bending modes of the damper may have an even higher contribution to the noise problems than the axial direction at higher frequencies (in that case, 145-155 Hz). Finite element simulations provide a reliable and cost-effective method of determining the bending mode particularly given the fact that the assessment should be performed at the early stages of the project since solutions of this type of noise mechanism often require significant changes in the design [132]. Modal parameters can only be altered by the changes to the mass or stiffness

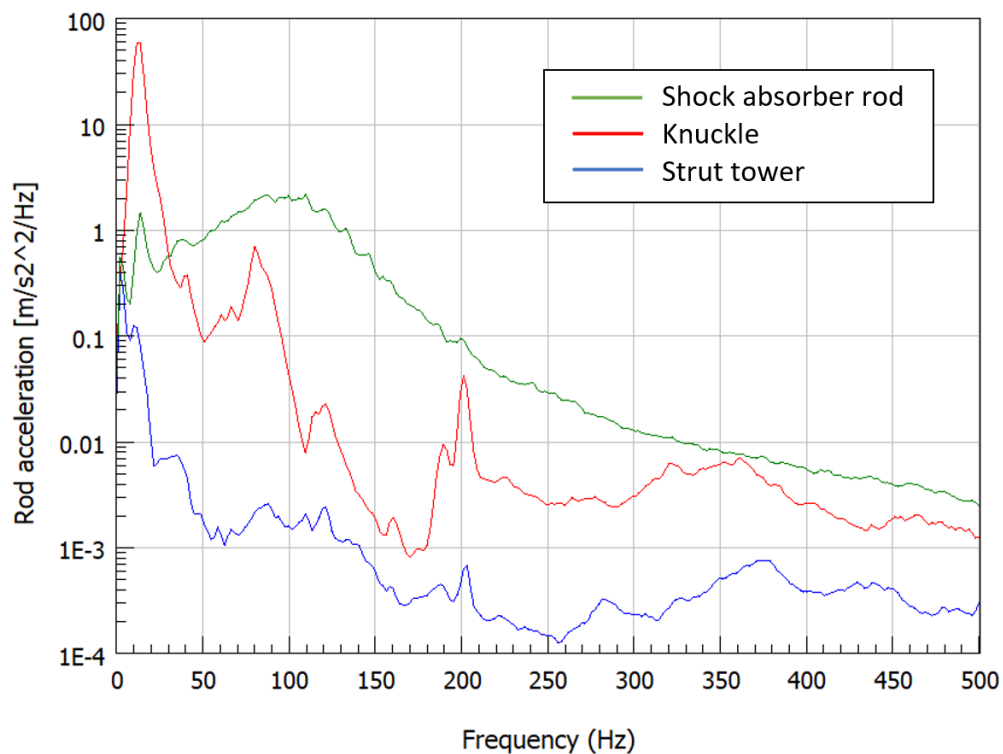


Figure 2.10: Comparison of the PSD profile of the acceleration signals measured at various parts of the automotive suspension

of the structure. One of the potential solutions for such cases is the addition of the mass damper to the damper design, an example of such a part is shown in Fig. 2.11.

**Friction induces vibrations** The last discussed physical phenomenon that can contribute to the NVH (Noise Vibration and Harshness) related problems are frictional forces that emerge at the sliding bearings (rod guide and piston bearing) and sealing of the damper. Damper friction can contribute to the increased vibration level at the chassis of the car in two distinct ways. The first mechanism is related to static friction, since axial forces prior to the damper movement (contact surfaces slippage) will be carried directly to the top mount and further to the car chassis. This increased transmissibility at the low amplitude forces of the suspension vibration by itself can cause undesired sensations to the passengers [72]. The second type of friction-related problem is caused by the so-called stick-slip phenomenon. This type of rod vibration (which is discussed in detail in [62]) occurs when due to road excitation damper experiences a high-frequency transitioning between the sticking and slipping phases of friction. Based on the work of Yamauchi et al. in [128] it can be concluded that apart from the aforementioned friction-related NVH problems, frictional forces serve as an important link in the overall dynamic behavior of the telescopic dampers that are allowing to influence each other, the axial and lateral rod



Figure 2.11: Exemplary design of mass absorber used to alter dynamic properties of the shock absorber structure (source: Courtesy of Tenneco Automotive Eastern Europe Sp. z o.o.)

vibration mechanisms that have been described earlier. However, the role and impact of the frictional forces on lateral vibrations of the damper remain a difficult subject for reproduction using modeling and simulation tools.

## 2.7 Standard shock absorbers measurements methods

Due to the widespread application of automotive shock absorbers, there are numerous standard methods of measuring various characteristics of the damper. Each method is designed to quantify specific characteristics of the shock absorber. In order to facilitate an easy introduction of the new numerical tools into the existing industrial development processes, standard methods are intended to be used as much as possible. This section aims at introducing the reader to those standard methods while custom methods devised for parameter estimation of the specific subsystems are discussed in their corresponding sections.

### 2.7.1 Shock absorber performance

In terms of assessing the performance-related characteristics of the shock absorber, the most commonly used type of experimental characterization method is force-displacement as well as force-velocity graphs (abbreviated as FSV graphs, an example can be seen in figure 2.12). As described by Duym et al. in [44], shock absorber force plotted in the function of the velocity is also referred to as characteristic diagram whereas force in the

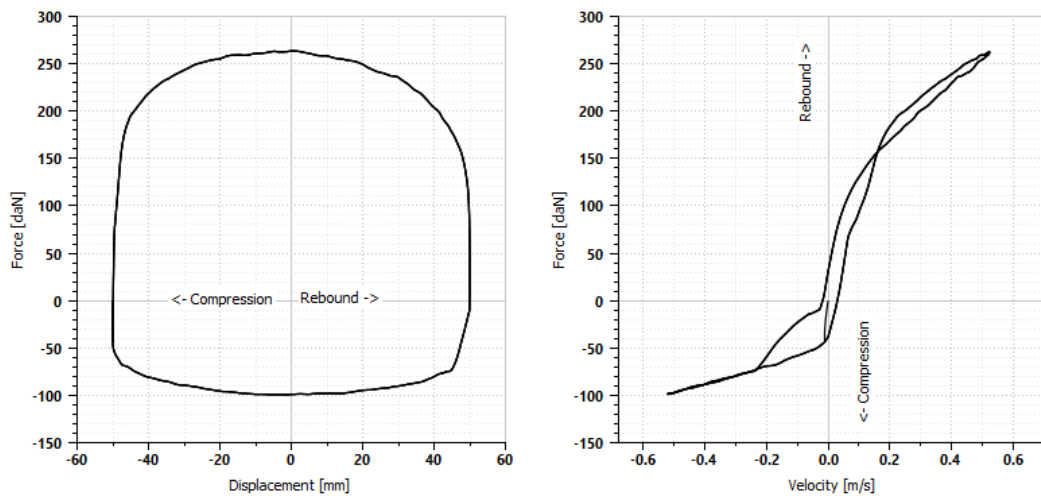


Figure 2.12: Exemplary force-displacement and force-velocity characteristics

function of damper displacement is known as work diagram. Both graphs are produced on the same test bench which in most cases involves a servohydraulic actuator that is used to induce triangular or sinusoidal displacement signals (at relatively large strokes  $>5\text{cm}$ ) at different velocities, to the shock absorber while reaction force is measured via strain-gauge based force transducer. Examples of the commonly used test benches used for low-frequency measurements can be found in figures 6.6, 6.15a and 7.3a. The damper is usually not featured with any compliant mounts as it would significantly conceal the force that is attributed to the hydraulic system of the damper. The main advantage of this measurement is the ability to capture strong non-linearities of the shock absorber related to the operation of the valves (FV graph) as well as force characteristics produced by the end-stop systems (compression and rebound stop systems). This makes both characteristics a primary method of controlling the influence of the damper on the behavior of the car in a wide range of road events. However, since these diagrams are created based on the measurements performed only at certain conditions and do not cover the higher frequency or lower strokes domain they are not able to reflect the influence of the damper on the car ride and handling completely. Two different dampers that share very similar FSV characteristics can produce noticeably different vehicle dynamics behavior.

## 2.7.2 Valve level measurement

During the designing process of a new shock absorber or new valve system, it is advantageous for the engineers to be able to measure the characteristics of the valve without the influence of other subsystems of the shock absorber. This is facilitated by the application of the valve-level test machine (commonly referred to as flow-bench, shown in fig. 2.13) which allows for establishing a relation between flow rate and pressure drop

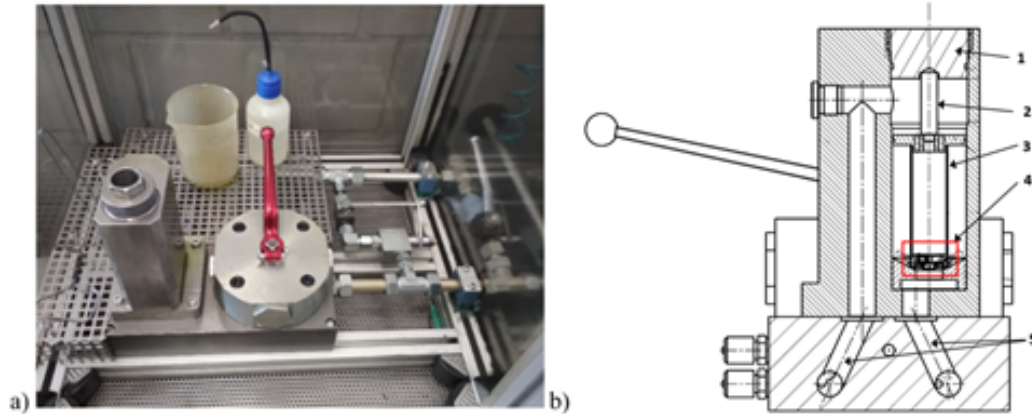


Figure 2.13: a) flow test bench, b) cross-section of the metal column: 1 – sealed nut, 2 – pin, 3 – inner tube, 4 – valve location, 5 – inflow/outflow channel [25]

for the individual valve (abbreviated as P-Q characteristic). The test is performed by inducing a controlled flow through the valve while pressure sensors are placed at different positions of the flow path to register the pressure differential produced by the valve restriction. Flow with the desired rate and acceleration is obtained by two servo pumps each optimized for different flow conditions. The ability to isolate a singular valve is a strong advantage of this test setup. Another advantage is easy access to the measured sample which makes it possible to test multiple valves in a short period of time. On the other side, a significant limitation of the currently existing measurement machines of this type is low flow rate acceleration which makes it impossible to study a dynamic effect of the flow at the valve level.

### 2.7.3 High frequency response

At the previously discussed test setups which aimed at measuring shock absorber force characteristics quasi-statically, compliant mounts were not been preset during the test and as a consequence, the piston rod was held fixed. Since the vibration of the rod depends strongly on the stiffness and damping of those compliant elements of the structure, in order to correctly capture the dynamic properties of the system, the test set-up has to include those parts as well. As demonstrated in [39, 48], the top mount is the most important vibro isolator that influences the high-frequency content of the damper vibrations whereas due to the relatively high stiffness of the lower bushing (and partially high inertia of the lower assembly), it is influencing rod accelerations in much lesser extend. Due to the above reasons, tests that are designed to reveal the high-frequency behavior of the damper in most cases are performed at the modular level (while the modular assembly is defined as the assembly of the shock absorber and parts that are mounted to the suspension together with it). Since it is convenient to analyze the vibrations produced by

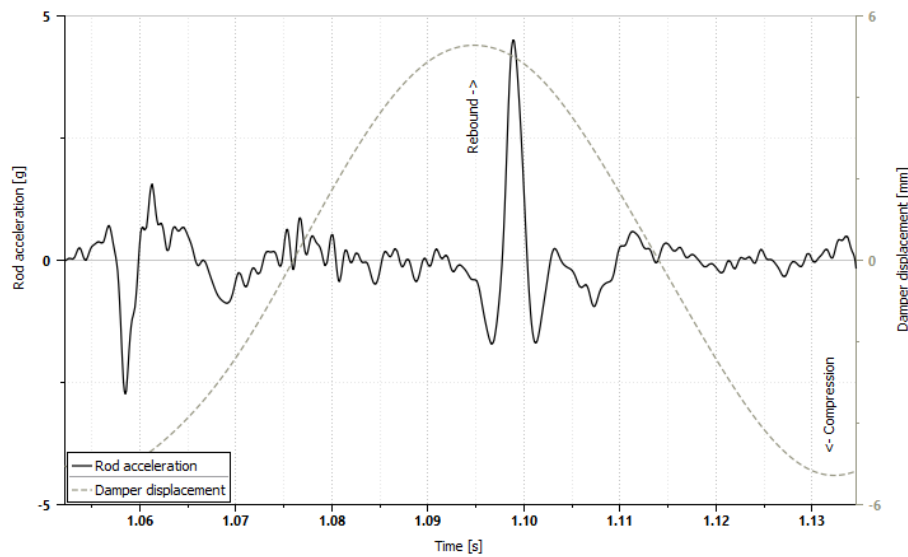


Figure 2.14: Exemplary sinusoidal excitation test results for the high-frequency rod acceleration analysis

the damper both in the time and frequency domain, high-frequency tests are performed in two variants (as proposed in [123]). In both cases, the sample is actuated using a servo-hydraulic or electromagnetic actuator while rod accelerations are registered via a piezoelectric accelerometer. Typical test set-up used for this type of test can be found in figures 6.15b and 7.3b.

For the time domain analysis, the damper is usually excited with a range of sine signals. Although worst-case excitation frequency is usually not known (from the perspective of the rod acceleration magnitude and noise risk), the typical excitation frequency used for this type of test is at the level of secondary ride mode ( $\sim 10\text{-}15\text{Hz}$ ). For this level of excitation frequency, stroke is usually well below 5cm, which is much lower than for the FSV characteristic measurements. During the test, as an output, rod accelerations are captured by the data-acquisition system. Exemplary sine test results for the time domain analysis of the rod acceleration are presented in Figure 2.14. This type of graph allows for observing rod acceleration during various stages of the damper operation, e.g. opening and closing of the valves, compression and rebound accelerations and peaks. In certain cases, this type of analysis allows, to identify parts of the damper that are related to elevated values of the rod acceleration and therefore indicate the most likely source of the noise.

In the case of the frequency domain, the shock absorber is excited with various noise signals that aim to reproduce the vibration profile of the unsprung mass or excite uniformly certain parts of the frequency spectrum (quasi-pink noise excitation). The results of such a test can be used to judge the risk of inducing structure-borne noise by the in-

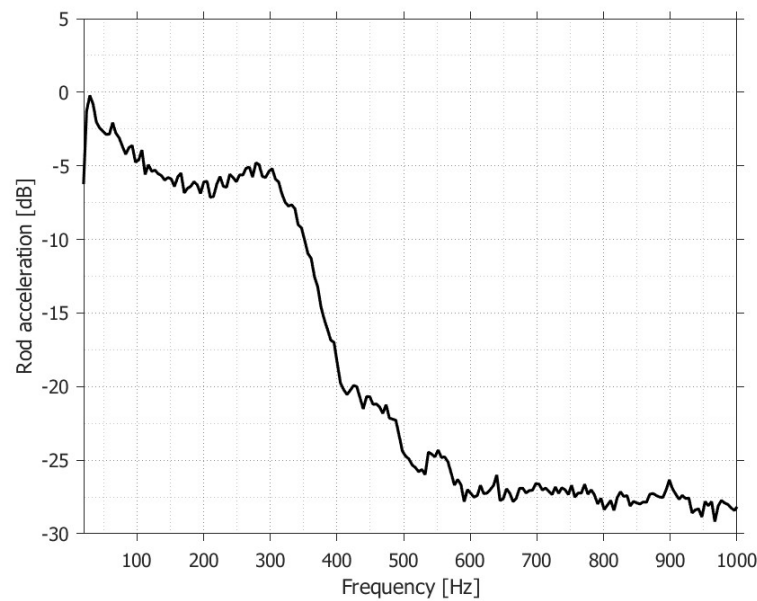


Figure 2.15: Exemplary spectrum of rod acceleration resulting from noise excitation test

investigated shock absorber. Since the structure-borne noise problems not only depend on the source of the vibration (in this case damper) but also on other parts of the structure, such risk evaluation is not trivial and as a result, is often performed using a comparative approach where validated designs are used as a benchmark. Examples of both sinusoidal, time domain, as well as noise, and frequency domain test results, have been shown in figures 2.14 and 2.15.

Another approach for studying the high-frequency behavior of the shock absorber is to perform the sine sweep or noise excitation test on the test set-up without the top mount and analyze only force frequency content in the range of  $\sim 50$ -500 Hz. This approach (used for instance in [18]) is less useful for investigating the noise problems but thanks to the simplification resulting from the lack of top mount, allows for easy comparison with the numerical results. Additionally challenge with this type of set-up is that the popular strain-gauge-based force transducers have limited capability to register high-frequency content, while piezoelectric sensors (as accelerometers used for standardized tests) are much more robust in this domain. As a consequence instrumentation used for this type of study has to be carefully evaluated.

# Chapter 3

## Literature survey of modeling techniques

The main objective of this paragraph is to describe the process of establishing the guidelines and assumptions for the modeling techniques of the automotive shock absorbers that will be used for further consideration in this dissertation. This is achieved by reviewing and organizing the knowledge and observations available among the scientific and engineering community. Given the fact that computer modeling of hydraulic shock absorbers is already a well-established part of automotive engineering with a long history of peer-reviewed publications, there is a rich collection of already developed and described models that are capable of reproducing various dynamic behaviors of the shock absorber. Depending on the purpose, the complexity of these models varies significantly. On the highest level, the models can be classified into empirical (data-based, black-box) models and physical (first-principle, mechanistic, white-box) models.

### 3.1 Empirical models

Since the empirical models are more computationally efficient and don't require a deep understanding of the underlying physical phenomena they are well suited for the purposes of representing the behavior of the damper in the larger assemblies e.g. car models or multibody simulations [11, 35, 15, 99]. Nevertheless there are many examples of such models that are used for the purpose of the analyzing and studying damper force characteristics, hysteresis and performance. The following list summarizes the most common modeling techniques that utilize in various degrees the empirical modeling principles:

- equivalent linearization approach [124, 66]
- restoring force method (force state map method) [44, 119]
- rheological modelling [131]
- non-parametric modelling [125]

- artificial neural networks [53]

Unfortunately in most cases, empirical data-based models are very limited in their ability to extrapolate the results outside of the scope of data that they were trained on. The nature of those models makes them not practical for the purpose of learning and understanding low-level physical phenomena governing operations of the shock absorber and therefore don't allow for exploration of new improvements and methods related to the design and physical parameterization. For those reasons, the majority of the models that are intended for the damper designing process are largely based on the physical modeling principle. These models usually involve a larger number of parameters and are more computationally expensive but allow for the prediction of the damper characteristics in a wide range of conditions. Therefore, they can be used for the estimation of damper performance, and risk of noise issues as well as for the purposes of the design and calibration process of the damper itself as well as the control system (in the case of semi-active suspension). It is important to emphasize that the majority of physical models incorporate also elements of the data-based approach to a certain degree (e.g. grey box modeling).

## 3.2 Physical models

Over the course of the last 50 years, a large number of physical-based models of automotive shock absorbers were proposed and documented. These models vary significantly in terms of complexity and the amount of physical phenomena that they cover. The majority of the models choose to follow the lumped parameters modeling approach to manage the complexity by spatially separating the considered systems into relatively independent subcomponents. Due to the large number of publications related to the physical modeling of shock absorbers, the tabular overview was prepared in the table 3.1 by expanding the survey performed in [11]. This summary provides a clear, chronological overview of the most important publications in the field of physical modeling of the shock absorber with an outline of physical phenomena that are captured by each model.

**Early physical models** From the historical perspective one of the earliest first-principle models of the shock absorber was proposed by Lang in [83, 108]. Although this modeling approach emerged relatively early it involved a complex representation of the valves and oil. With 83 parameters, solved on an analog computer, this model was able to take into account the effects of compressibility and inertia of the fluid. Extensive work was performed to characterize the discharge coefficient used in describing the pressure-flow relation at the orifice of the valve in turbulent flow conditions. Experimental tests confirmed the validity of the assumptions made by Lang for the frequency range up to 20

Literature source			Physical phenomena included in the model											
Autor	Year	Ref	Type of damper*	Friction	Oil compliance	Chamber compliance	Cavitation	Gas solubility	Laminar flow	Turbulent flow	Valve dynamics	Shim stack stiffness	Stiction force	Thermal effects
Lang	1977	[83]	D	✓	✓		✓		✓	✓	✓			
Hall and Gill	1986	[67]	D	✓	✓		✓			✓				
Surace et al.	1991	[119]	M	✓	✓		✓			✓				
Reybrouck	1994	[101]	M	✓	✓					✓	✓			✓
Lee	1997	[85]	M	✓	✓					✓				✓
Duym et al.	1997	[44]	D		✓		✓			✓	✓			
Duym et al.	1998	[43]	D	✓	✓					✓	✓			✓
Duym	2000	[42]	D,M	✓	✓					✓	✓			
Purdy	2000	[97]	D	✓	✓		✓		✓					
Czop	2001	[33]	T		✓									
Young et al.	2002	[130]	M	✓	✓					✓	✓			
Talbott	2002	[121]	M		✓				✓	✓	✓	✓		
Park	2005	[91]	T		✓	✓				✓	✓			
Benaziz	2015	[20]	D	✓	✓				✓	✓	✓	✓	✓	
Sikora	2021	[111]	D	✓	✓			✓	✓	✓	✓		✓	

Table 3.1: Summary of the physical phenomena related to the automotive shock absorbers reproduced by models across publications

\* abbreviation of damper types: M - monotube, D - double tube, T - semiactive triple tube with one unidirectional active valve

Hz. A similar model but for the monotube damper was documented by Lee in [85]. In contrast to early detailed models presented by Lang, Segel and Lee, there were also multiple approaches to deriving much simpler models as in [101]. In those types of models, valve restrictions are often parameterized with non-physical coefficients [97]. An overview of such simplified modeling techniques that were based on the simple mathematical relations combined with data-based models was provided in [44]. Together with [42] it discussed also aspects of parameters identification for this class of models.

**Improvements in modeling hysteresis** In parallel to the physical modeling capabilities advancements, attempts were taken to better represent the hysteresis by improving the reproduction of the oil compliance [118, 41]. Duym proposes a method that takes into consideration the effect of the non-dissolved gas on the bulk modulus of the oil in [43]. Effects of the chamber compliance over the hysteresis of the double tube shock absorber

have been studied in detail in [84] and proposed a chamber mathematical model that was based on the thick-walled cylinder equations.

**Improvements in modeling the valves** One of the earliest attempts to include the shock absorber valves as a separate mechanical system was published in [67] by Hall and Gill. In this work, a full-body diagram was considered for the valve but the valve stiffness was included in the form of a linear spring. Later publications by Talbott et al. [121] and Eyres et al. in [50] involved first attempts at incorporating stiffness of the valves and shim stacks in form analytical formulas. Similarly, Farjoud et al. in [52] studied the model of shock absorber with the shim opening governed by the tick plate theory. Works of Czop, in [31, 34, 32] focused on modeling of isolated shim valves using analytical and numerical methods such as finite element method, computational fluid dynamics as well as fluid-structure interaction. Similarly, Bell and Beale in [17] used FE and CFD methods for the shim stack simulations within the monotube damper. The hybrid modeling approach of the shim stack stiffness using the beam deflection method was proposed by Xu in [127]. With this approach, thanks to efficiency, shim stack stiffness can be relatively easily included in the system-level models. Later models proposed by Benaziz in [20, 18] also included valve stiffness estimated using finite element methods. A very detailed study using fluid-structure interaction modeling technique was delivered by Nillson and Pelosi in [88].

**High frequency models** In terms of capturing higher frequencies produced by the damper, one of the first publications was delivered in [130] and [129] but the mathematical models are not described in detail and are based heavily on the empirical approach. Czop et al. in [33] demonstrated an advanced physical model that was capable of reproducing the high-frequency response of the shock absorber together with the servohydraulic actuator. Significant simplification assumed in this work was that valves have been represented in the form of the empirical look-up table approach. A much more detailed approach to modeling valves has been demonstrated in [19, 20] where each valve constituted a separate mechanical system. An important advancement in modeling the valves has been made by including the stiction force that is acting on the flat surfaces of the intake valves. This allowed a better representation of the high-frequency vibration caused by the intake valve opening. A similar model of a double tube shock absorber has been studied by Sikora in [110, 111]. This model has been specifically oriented on the problem of structure-borne noise caused by the operation of the shock absorber. In terms of ER/MR damper, high frequency model of has been studied by Goldasz in [63].

**Semi active dampers** With the adoption of semi-active suspension systems by the mass market, the demand for the capabilities of simulating and the performance of such

technologies significantly increased. One of the first publications on modeling semi-active dampers was prepared by Park in [91]. It dealt with the same semi-active damper type (namely triple tube design with one unidirectional active valve) but the description of the damper model (which was prepared in a Matlab Simulink environment) is very limited. A more detailed study was performed by Pellegrini in [93] but the semi-active layout differed significantly from the one that is considered in this dissertation. Over the course of the last decade, a series of master theses was prepared by the scientific community in cooperation with Ohlin's engineering center. These studies were primarily oriented on the active valve and its dynamic response, examples: [61, 12, 94].

**Vibro-isolators** As discussed in 2.6 rod accelerations produced by the operation of the shock absorber strongly depend not only on the dynamics of the shock absorber but also on the behavior of the elastomeric vibroisolators. The impact of the top mount on the noise and harshness aspects of driving comfort has been studied in detail by Eickhoff et al. and Sonnenburg et al. in [48, 115]. As a result, in order to virtually predict dynamic aspects of the shock absorber, a detailed model of the top mount has to be included. This is not a trivial task since due to their inherent viscoelasticity and viscoplasticity, for most of the vibroisolators designs, their dynamic behavior depends on multiple external variables such as amplitude, frequency and preload of the excitation as well as on environmental conditions such as temperature and humidity. Fortunately, since elastomeric vibroisolators are widely used across many transportation industries, over the last century, there have been many attempts at representing their behavior with various numerical and rheological models. Historically the simplest one was Kelvin-Voigt cell which consists of spring and dashpot elements connected in parallel. Usually, the steady state and dynamic response of the bushings, for a given preload and amplitude are described in the frequency domain using dynamic stiffness and loss angle [80, 96].

As it can be observed in figure 3.1 this model is capable of capturing the stiffness (for selected amplitude, see eq.) but fails at reproducing loss angle dependency on frequency. Despite its deficiencies, this model has been used in multiple models that aimed at studying damper dynamics [20, 110].

As an attempt to improve the fidelity of the bushing models, multiple models have been proposed by combining the following elementary cells: Kelvin-Voigt, Maxwell and Zener. The performance and characteristics of these models have been compared by Polach in [96]. Particularly popular has been a parallel rheological framework which uses multiple Maxwell cells connected in parallel with other elementary cells [37, 74, 122]. As an attempt to make the application of various rheological models more flexible, a modular approach has been proposed in [29] and [107]. Another popular family of models has originated from the attempt to capture various behaviors related to softening or hardening of the bushing by combining a regular rheological model with the Bouc-Wen differential

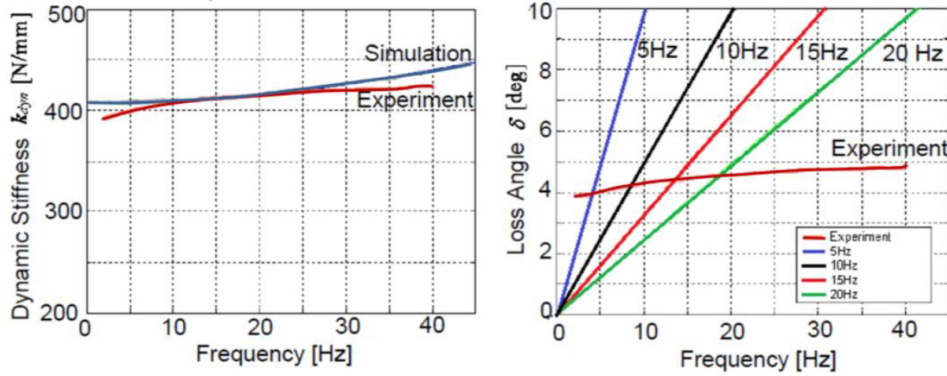


Figure 3.1: Representation of the dynamic stiffness and loss angle by the Kelvin-Voigt model [106]

model [24] that allows capturing time-history dependent hysteretic force [89]. Correct representation of the dynamic bushing behavior is particularly important in the domain of multi-body simulations. For that reason, virtually all MBS (Multi-Body simulation) software packages have developed their own versions of the mathematical models of the bushings and hydro-mounts dynamic behaviors (e.g. MSC Adams [10], Simpack [9], MotionView [2]). In most cases, models included within MBS packages involve a large number of parameters so that they are capable of covering a wide range of possible bushing designs and behaviors. This versatility comes at the cost of a more challenging process of parameter estimation.

### 3.3 Conclusions

Based on the performed survey and consultations with the engineering community, generic guidelines for the model architecture were established. As in most of the contemporary damper models, lumped parameters modeling approach will be used due to the flexibility in working with multiple subsystems. Also, due to the ease of introducing changes at the subsystem level and integration with other systems across the industry, Simcenter Amesim was selected as a modeling environment.

In terms of modeling the damper chambers and flows, the mass flow approach was selected similarly as in [33] and [20]. Shock absorber tube elasticity is represented using thick-wall cylinder theory as in [84] since it allows for a simple estimation of the compliance related to the deformations of the damper structure.

As emphasized already in previous sections, dynamic valve level behavior is essential to the performance of the shock absorber in the domain of vehicle dynamics, therefore shock absorber suppliers constantly look for ways to improve the design of the valves. This results in a large number of design modifications and design variants of the classical shim stack valve that appear on the market. As a result, a proposed model must be

characterized by a high level of adaptivity otherwise it might become quickly outdated. However, due to multiple physical phenomena that are involved in the operation of the passive valves of the shock absorbers, modeling the dynamic behavior of the passive valves is a complex subject that requires mathematical formulation that is very specific to the physics it attempts to capture. As a result, a compromise has to be found between model flexibility and how detailed is the physical representation of the valve behavior. Based on the study of the existing models it has been observed that the high diversity of the valve designs, mainly impacts the stiffness characteristics of the valve (due to the application of various shapes of the shim discs, coil-springs, preloads and support surfaces, etc.), whereas the physics related to other aspects of the damper valve operating (friction, stiction force, jet forces, restriction) remain relatively similar to the majority of the designs. As a result, it has been decided that each passive valve will be represented as a separate mechanical system but the stiffness of the valve should be represented using an empirical approach (in the form of valve level, load-deflection curve).

This decision is further justified by the fact that together with the advancements in the designs of the valves, simulation and experimental tools that are allowing for the prediction of the valve characteristics (in this case valve stiffness) are also progressing at a fast pace. Therefore it is more desirable to develop a model that can easily accept data from external, specialized tools and methods (in this case for representing the stiffness of the valve) than include this complexity in the system-level model of the shock absorber. This is particularly true in the case, of the active valve, since due to the complexity involved, entire engineering departments, are devoted exclusively to the problem of modeling its behavior. Based on the observations and conclusions in [33]) it has been decided that for the purpose of the semi-active damper model development at the system level, the active valve will be represented using the data-based approach in the form of 3D look-up tables.

As discussed in section 3.2, modeling of the vibroisolators is a well-established discipline that is widely used by various engineering teams of the shock suppliers. In order to capture complex dynamic characteristics (dependency on frequency and amplitude) but also to make the model compatible with existing procedures it has been decided to adopt a bushing model that is part of MBS package (Altair MotionView) that is already commonly used in the automotive industry.

In terms of the main considered applications of the developed model (noise and control-related aspects, discussed in section 2.6) the side loads acting on the damper are not considered. Therefore, the friction-induced between the rod and damper tube assembly is relatively low. However, due to the importance of the damper friction for the vehicle performance, as well as due to the recent advancements in modeling delivered in [72] a high-fidelity model of the friction should also be used.

# Chapter 4

## Proposed model description

This chapter describes the semi-active shock absorber model which was proposed based on the survey of already existing computer modeling techniques and guidelines formulated in chapter 3 as well as on the consultation with the engineering community of the industrial partner company. A model introduced in this chapter will be used for all further considerations in this dissertation.

Despite knowledge resulting from the performed survey and consultations, the process of establishing modeling techniques involved also a trial-and-error learning activity with various simulation tools. Due to practical reasons, intermediate models that were used during the process of experimentation and testing were not included in this paragraph however observations related to some relevant alternative modeling techniques were described in section 4.7. Together with the survey, these observations provide a rationale for selecting the specific modeling approach.

An important part of developing the model is also establishing the strategy for calibrating the parameters. The main goal of this chapter in regard to parameter calibration is to classify how the value of any given input parameter used in the proposed model will be obtained. In the case of parameters that require complex procedures to establish their value, a separate procedure should be proposed in subsequent chapters. However, in order to facilitate an easy application of the developed model, it is desired to either based on the experimental and virtual methods or based on the literature knowledge, fix the value of as many parameters as possible so that calibrating them does not consume engineering resources for future use of the model.

### 4.1 Rod forces

As the main role of the shock absorber is to generate the damping force during the actuation of the suspension, the first described part of the model is force equilibrium at the rod. At the most general level, the shock absorber model is used to estimate the force

it exerts on the piston rod when the external excitation is applied to its lower mount. The calculation of this external force starts with equation 4.1 where it is established from the internal pressures, their corresponding surface areas as well as frictional force. This equation is used when the shock absorber is rigidly fixed.

$$F_d = P_r(A_b - A_r) - P_c A_b + F_\mu \quad (4.1)$$

where:  $P_r$  and  $P_c$  correspond to rebound and compression pressure whereas  $A_r$  and  $A_b$  refer to the cross-sectional area of the rod and inner diameter of pressure tube (bore) according to the equations 4.2 and 4.3.

$$A_r = \pi(D_{PT}^2 - D_R^2)/4 \quad (4.2)$$

$$A_b = \pi D_{PT}^2/4 \quad (4.3)$$

In practice, however, the dynamic force which is transferred to the top mount dome and car frame is dependent also on the dynamic characteristics of the top mount elastic bushing. When the complete modular assembly is taken into account by the model, the equation 4.1 has to be expanded by the rod equation of motion, as in eq. 4.4

$$M_{rod}\ddot{x} + F_{tm} = P_r(A_b - A_r) - P_c A_b + F_\mu \quad (4.4)$$

where:  $M_{rod}$  correspond to mass of the piston rod assembly, and  $F_{tm}$  to the force coming from the top mount bushing. The friction force that appears between the rod guide and rod is obtained based on the equations 4.38 - 4.41 in section 4.6.

## 4.2 Hydraulic system

In order to model the behavior of the hydraulic system, the damper is divided into three control volumes: rebound, compression and by-pass chamber. Pressure changes in each of the volumes depend on the changes in volume (resulting from the motion of the damper), flows through the corresponding valves in and out of the chambers and on the overall compliance. Control volumes are related to the damper position by the following equations 4.5 - 4.7.

$$V_r = A_r \cdot (l_{r0} - x_{tube}) \quad (4.5)$$

$$V_c = A_c \cdot (l_{c0} + x_{tube}) \quad (4.6)$$

$$V_b = const \quad (4.7)$$

In order to make a link between pressure and volumetric change of the control volumes,

equation 4.8 for the mass flow is introduced based on the principle of conservation of mass.

$$\frac{dm}{dt} = \frac{d}{dt}(\rho V) = \rho \frac{\partial V}{\partial t} + V \frac{\partial \rho}{\partial t} \quad (4.8)$$

With the assumption of constant density over the control volume and by introducing bulk modulus  $K$ , equation 4.8 can be transformed into:

$$Q = \frac{\partial V}{\partial t} + \frac{V}{K} \frac{\partial p}{\partial t} \quad (4.9)$$

where  $Q$  is the net volumetric flow in and out of the control volume through the valves. The first term of the equation 4.9 relates to the changes in the volume caused by the movement of the shock absorber whereas the second term comes from the total compliance of the chamber that is represented by a control volume. Based on the above equation, the following relationships (equations 4.10 - 4.12) can be formulated for rebound, compression and by-pass control volumes respectively:

$$\frac{\partial P_r}{\partial t} = -\frac{K_r}{V_r} \left( \frac{\partial V_r}{\partial t} + Q_p + Q_{bp} \right) \quad (4.10)$$

$$\frac{\partial P_c}{\partial t} = -\frac{K_c}{V_c} \left( \frac{\partial V_c}{\partial t} - Q_p + Q_{bv} \right) \quad (4.11)$$

$$\frac{\partial P_b}{\partial t} = -\frac{K_b}{V_b} (Q_a - Q_{bp}) \quad (4.12)$$

The sign convention is established in such a way that the rebound direction produces a positive value of the tube displacement.

### 4.3 Chamber compliance

In the general case, the total bulk modulus of the chamber originates from the bulk modulus of the hydraulic medium as well as from wall compliance of the inner tubes of the damper that are subjected to the pressure differentials (according to equation 4.13).

$$\frac{1}{K_{total}} = \frac{1}{K_{eml}} + \frac{1}{K_{wall}} \quad (4.13)$$

For the purpose of parameter identification, both sources of compliance are estimated separately. Since parameters related to oil compliance are much more volatile (as explained below) wall compliance is calculated first based on Hooke's law while experimental identification of compliance only concerns a bulk modulus of the hydraulic medium.

**Compliance of the hydraulic medium** Oil is the primary hydraulic fluid used in the considered design of the shock absorbers, however, due to the fact that the reserve (rod volume compensation) chamber is filled with nitrogen, oil is subjected to mixing with the gas during the operation of the shock absorber. As a result of this mixing process, part of the gas is dissolved into the fluid and part is dispersed in form of an oil-gas emulsion. Since oil-gas solution and oil-gas emulsion differ significantly in terms of bulk modulus, in order to derive the bulk modulus of the fluid it is necessary to establish what fraction of the gas is undissolved for given conditions in the chamber at a given point in time. In the presented model, this is realized by introducing such parameters as saturation pressure and oil vapor pressure. Above saturation pressure, the entire gas is deemed to be dissolved and the bulk modulus of the hydraulic medium is virtually equal to the bulk modulus of pure oil. Below vapor pressure, the entire gas is considered to be freed and the vaporization process of oil is starting. The pressure range between oil vapor pressure and saturation pressure is governed by Henry's law in such a fashion that the volumetric fraction of undissolved gas ( $\theta$  in equation 4.14) depends linearly between saturation pressure and vapor pressure. The fact that the value of oil vapor pressure is the same as the value of pressure for the complete release of gas from the solution is a simplification but in normal working conditions, the shock absorber always operates above these values [40].

$$\theta(P) = 1 - \frac{P - P_{vap}}{P_{sat} - P_{vap}} \quad (4.14)$$

With the assumptions of the constant bulk modulus of oil and independence of oil's bulk modulus of temperature, the density of the emulsion can be estimated according to the equation 4.15 [4, 3].

$$\rho_{eml}(P, T) = \frac{(1 - \chi) \cdot \rho_{oil}(P_{ref}, T_0) + \chi \cdot \rho_{gas}(P_{ref}, T_0)}{(1 - \chi) \cdot \exp\left(-\frac{P - P_{ref}}{K_{oil}(P_{sat}, T)}\right) + \theta(P) \cdot \chi \cdot \frac{T}{T_{ref}} \cdot \left(\frac{P_{ref}}{P}\right)^{\frac{1}{\Gamma}}} \quad (4.15)$$

$$K_{eml} = \rho_{eml} \cdot \frac{\partial P}{\partial \rho_{eml}} \quad (4.16)$$

Where  $\Gamma$  is a polytropic index of the gas and  $\chi$  is the volumetric gas content of the emulsion. With such an approach, the only parameter that poses difficulty in characterization is gas content since this value is changing depending on the mixing and sloshing condition in the reserve chamber.

**Volumetric compliance of the structure** The model presented in this dissertation considers structural compliance originating only from volumetric flexing of the tubes while axial stiffness of the rod and tubes is neglected. Nevertheless, mentioned volumetric compliance takes into account longitudinal and hoop stresses resulting from the pressure

differential acting on a tube. Volumetric wall compliance of the chamber can be estimated using thick pressure vessel theory with the equation 4.17. This formula is only applied to the outer wall of the by-pass chamber and the outer wall of the compression chamber since the restriction between the rebound chamber and by-pass chamber is usually small resulting in a small pressure differential that allows for simplification of the model.

$$\psi = \frac{2}{E} \cdot \left( \frac{r_o^2 + r_i^2}{r_o^2 - r_i^2} + \nu \right) - \frac{2}{E} \cdot \nu \cdot \frac{r_i^2}{r_o^2 + r_i^2} \quad (4.17)$$

Based on equation 4.17 from which the bulk modulus of the chamber can be derived with equation 4.18.

$$K_{wall}(P) = \frac{1 + \psi \cdot P}{\psi} \quad (4.18)$$

## 4.4 Valves submodel

For a given excitation velocity, forces exerted by the shock absorber originate primarily from the pressure difference in the rebound and compression chamber. The role of the valves is to control the pressure differential for given flow conditions, therefore their mechanical and hydraulic properties are responsible for setting P/Q characteristics (delta pressure vs flow rate). The design of the valves facilitates easy adjustments of the shim stack stiffness which is used to control P/Q characteristics and therefore valves are the primary component through which the behavior of the shock absorber is influenced [40]. Additionally, as described in section 2.4, the behavior of the valving system must prevent pressure in various chambers from reaching undesirably low or high values. This creates a need for valves that are significantly different in terms of P/Q curves. Therefore, in the considered type of semi-active shock absorber, two types of valves can be found (see figure 2.6):

- shim-valves which are primarily responsible for setting up a pressure - flow rate characteristics of the damper
- intake-valves which for the most part, play a role of a check valve, which in the flow direction exerts as low restriction as possible.

Due to design limitation influence of the intake valves on the forces generated by the damper cannot be neglected. Due to significant differences in the design, different 1D mechanical models are prepared to correctly reproduce pressure difference for a given flow condition. The primary difference between the models can be found in flow paths but as demonstrated in subsequent sections, such characteristics as valve stiffness, friction and stiction forces are very different as well.

Apart from the passive valves that have been described above, part of the flow in the considered design of the semi-active damper is channeled through the by-pass chamber to the active valve. This valve is continuously electronically controlled in terms of flow restriction. The control is performed by the means of solenoid exerting force on the hydraulic leverage valve. As demonstrated in [33], for the study of the dynamic aspects, this valve can be reproduced with the data-based approach as a three-dimensional look-up table. Such an approach greatly simplifies what otherwise would be a complex sub-system.

**Valves mechanical model** Schematic layout of the mechanical hydraulic models for both types of the valves can be observed in figure 4.1. It consists of an elementary mechanical spring and dash-pot system with a mass element that is restricting the flow of the fluid. Spring element reproduces the non-linear stiffness of either shim stack or coil spring, depending on the design of the valve. The non-linear load-deflection characteristic of a stiffness element is approximated by a two-term exponential function as in equation 4.19. Although in most cases this approximation approach is sufficient, due to the highly non-linear shape of the valve stiffness characteristic of some of the valves that can be encountered in industrial applications, alternative stiffness approximation strategies were used as well. This included bi-linear approximation (or in some cases three-linear) for which the transition point has been smoothed using Bezier splines [49]. An additional benefit of such an approach is that the parameter values are much more intuitively interpreted which allows for defining more realistic boundaries for the optimization algorithm used for model calibration. On the other hand, using such an approximation formulation requires a more complex procedure for the stiffness characteristic evaluation.

$$F_k(x_v) = a \cdot \exp(b \cdot x_v) + c \cdot \exp(d \cdot x_v) - F_{preload} \quad (4.19)$$

Apart from the stiffness, the 1d valve model takes into consideration also following forces that are described in detail, in the subsequent paragraphs:

- $F_{\Delta p}$  - force due to pressure difference,
- $F_m$  - force due to change of flow momentum,
- $F_{st}$  - Stiction force,
- $F_\mu$  - Valve friction forces.

As a result, for each valve, it is possible to write the equation of motion in the form of eq. 4.20.

$$m_v(\ddot{x}_v) + c_v\dot{x}_v + F_k(x_v) = F_{st} + F_{\Delta p} + F_\mu + F_m \quad (4.20)$$

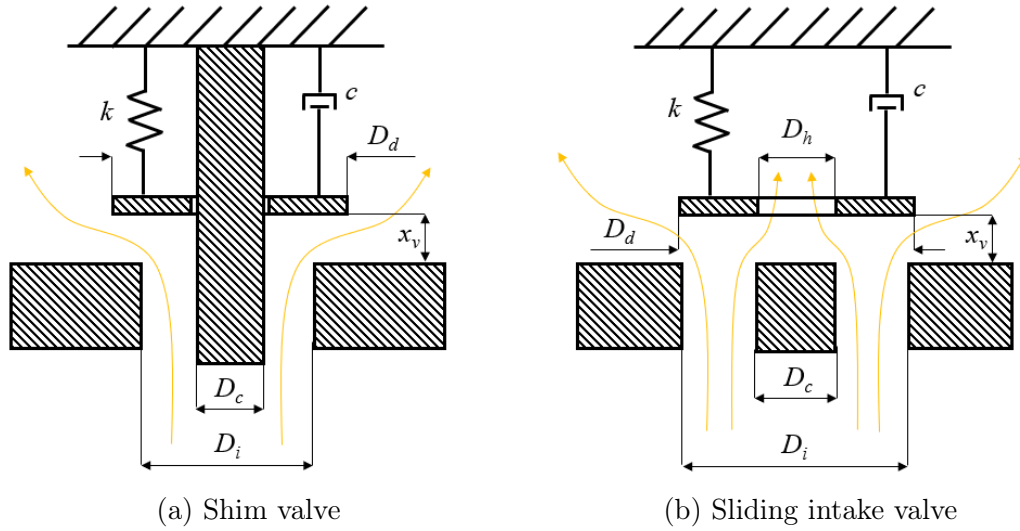


Figure 4.1: Schematic drawings of the valve model

**Force due to pressures difference** When the pressure differential is present between two chambers, force  $F_{\Delta p}$  is exerted on the valve mass element in the opening direction. Since the shim stack opens by tilting discs at an angle in relation to the support, for this type of valve, the non-constant pressure distribution is considered between  $D_d$  and  $D_i$  as in eq. 4.21, fig. 4.1a. On the other hand, for the intake valve, pressure is deemed to stay constant through the opening meaning that for this type of valve, force  $F_{\Delta p}$  is calculated according to eq. 4.22, fig 4.1b.

$$F_{\Delta P} = \frac{\pi}{12} \cdot (D_d - D_i) \cdot [D_d \cdot (2p_1 + p_2) + D_i \cdot (p_1 + 2p_2)] \quad (4.21)$$

$$F_{\Delta P} = \frac{\pi \cdot (p_1 - p_2)}{4} \cdot (D_d^2 - D_h^2) \quad (4.22)$$

**Force due to change of flow momentum** Apart from the force exerted by the difference in pressures, during the opening and closing of the valve, part of the stream of oil is inevitably deflected by the geometry of the valve. This creates a change in the momentum of the oil flow which generates the reaction to the jet force  $F_m$  that acts on the surface of the shim stack. In an idealized case, the jet force can be approximated by 4.23.

$$F_m = Q\rho V_f \sin \zeta = \rho A_f V_f^2 \sin \zeta \quad (4.23)$$

By incorporating the equation used for the volumetric flow rate (see eq. 4.29), the above equation can be converted into eq. 4.24.

$$F_m = 2C_q^2 \cdot A_f \cdot \Delta P \cdot \sin \zeta \quad (4.24)$$

Where  $\zeta$  is the angle of the deflected oil stream,  $A_f$  is a flow area that depends on the valve opening (calculated with eq. 4.27 and 4.28) and  $V_f$  is flow velocity. The main challenge with the proper incorporation of the influence of the jet force over the shim stack is to estimate the angle at which the flow is deflected. Since this quantity is difficult to measure, a rough estimation is done based on the study of the spool valves in [21] for which the angle is established at the value of  $70^\circ$ . Based on the study performed for the estimated values of the parameters, it has been established that jet force, exerts only a minor influence on the valve opening when compared with other forces acting on the passive valve.

**Valve stiction force** Apart from the forces described above, as observed in [20, 111], from the perspective of the dynamic behavior of the valve, stiction force is also relevant. It emerges when a thin oil film is trapped in between two flat surfaces that are being separated. In such a case, fluid has to flow into the slit and fill the volume that is being created by the separation of the adjacent surfaces. Flow restriction causes pressure drop on the surfaces being separated at a high rate. The process has been described mathematically for similar geometry in [77], from which the equation 4.25 is used for the estimation of this force.

$$F_{stic} = \frac{3\pi\mu}{32(x_v + x_{v0})^3} \cdot \frac{dx_v}{dt} D_i^4 \left(1 - X^4 + \frac{1 - 2X^2 + X^4}{\ln(X)}\right) \quad (4.25)$$

where  $X$  is defined as a ratio of outer diameter to inner diameter  $X = \frac{D_o}{D_i}$ . In the equation 4.25, stiction force depends on the velocity of the valve opening and the distance separating both surfaces which cannot be considered zero since in such case the first term of the equation would approach infinity. As a result, a certain minimum separation value has to be identified ( $x_{v0}$ ). This value can be considered as a measure of the height of the surface asperities of the adjacent faces and strongly influences the overall level of stiction force generated during valve opening.

**Shim valve friction** The slit through which hydraulic fluid can pass during the opening of the shim valve requires tilting the stack of discs. Due to transversal forces, this tilting motion is accompanied by sliding between discs which are resisted by frictional forces because of the normal force at the surface of the disc. Friction between discs, demonstrates itself in form of hysteresis in the P/Q characteristic in such a way that during the opening of the valve, the stack has a higher stiffness than during closing (see figure 4.10). The frictional force created with the mechanism described above depends on

the normal force generated at the surface of each of the discs which for a given diameter of the valve will depend on the stiffness of the complete stack.

In order to reproduce hysteresis in the P/Q relationship with the existing mechanical model (see figure 4.1), different models of friction have been considered and their performance has been compared with the experimental data described in section 6.2.1 as well as in [25]. It has been observed that any model that involved viscous frictional behavior did not match the measured data. Experimental data also did not show any behavior that would suggest the effect of static frictional force.

It was hypothesized that despite lubrication, the transversal motion between discs is small enough and slow enough to be confined entirely to the boundary lubrication regime of Stribeck's curve where frictional forces are exerted directly at the asperities. Advanced dynamic models of friction that are capable of capturing such phenomena as stiction, rate dependency and viscous friction and aim at reproducing the friction in the wide range of lubrication regimes (e.g. LuGre or Bliman and Sorine) often perform poorly at such low displacements [90]. On the other hand, Dahl's friction model primarily aims at modeling the behavior of the friction which is resulting from contacting asperities and their elastic and plastic compliance, prior to actual sliding motion. When the relative displacement between surfaces is large enough and sliding does occur, Dahl's friction becomes a simple dry, Coulomb friction. However, a characteristic feature of Dahl's friction is that due to the elastic deformation of asperities, after unloading, part of the relative displacement returns to the original configuration (see fig 4.2). As a result, Dahl's friction model was implemented as in eq. 4.26. As demonstrated in section 6.2.3, the application of this friction mechanism allows for an accurate representation of the valve opening and closing characteristics.

$$\frac{dF}{dx_v} = \sigma_0 \left(1 - \frac{F}{F_c} \cdot \text{sgn}(\dot{x}_v)\right)^\alpha \quad (4.26)$$

**Valve opening** When the force  $F_{\Delta p}$  exceeds the preload force of the spring element, the valve opens. Opening of the valve creates an orifice that is facilitating the flow of the fluid. Due to the fact that in the case of the intake valve, oil can flow around the outer and inner circumference of the disc, the area of the orifice is calculated differently for both valves: for shim valve eq. 4.27 (see figure 4.1a) is used for the intake valve eq. 4.28 (see figure 4.1b) is used.

$$A_{fs} = x_v \cdot \pi D_d \quad (4.27)$$

$$A_{fi} = x_v \cdot \pi (D_d + D_i) \quad (4.28)$$

Pressure drop over an orifice of a given area due to dependency on multiple side factors

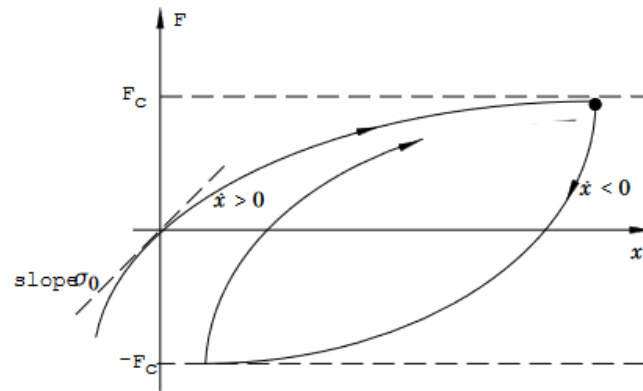


Figure 4.2: Friction force in the function of displacement according to Dahl's friction model [90]

such as valve geometry and flow conditions is not a trivial problem. The most commonly used approach for addressing this problem has been a formulation involving discharge coefficient as in equation 4.29 which is convenient from the perspective of subsequent parameter identification [71, 121, 20].

$$Q = C_q A_f \sqrt{\frac{2\Delta P}{\rho}} \quad (4.29)$$

In order to capture a correct characteristic at different values of Reynolds number, the discharge coefficient depends on flow number  $\lambda$  as in equation 4.31. However, it has been observed that in practice, due to the complex geometry of the valves of the shock absorber, the flow number is relatively high, meaning that for the majority of operating conditions of valves, they remain within a turbulent flow regime. This further simplifies parameter identification because according to the relation from eq. 4.30, for flow values above the critical value, the discharge coefficient is virtually constant.

$$C_q = C_{q,max} \cdot \tanh\left(\frac{2\lambda}{\lambda_{crit}}\right) \quad (4.30)$$

$$\lambda = \frac{D_{Hyd}}{\nu} \sqrt{\frac{2\Delta P}{\rho}} \quad (4.31)$$

**Additional valve flow paths** As discussed in 2.5, passive valves often incorporate a small additional orifice at the first shim disc that is influencing the low flow rate part of the P-Q valve characteristic (see figure 4.3). This part of the valve is represented in the model by a parallel (to the valve opening flow) flow path that is governed by the equation 4.29 but with an assumption of constant value of the discharge coefficient (assuming a turbulent flow regime). The value of  $C_q$  differs significantly from the one used for the

flow created by the valve opening therefore, its valve has been established experimentally based on the separate flow-bench experiment (see figure 4.4a).



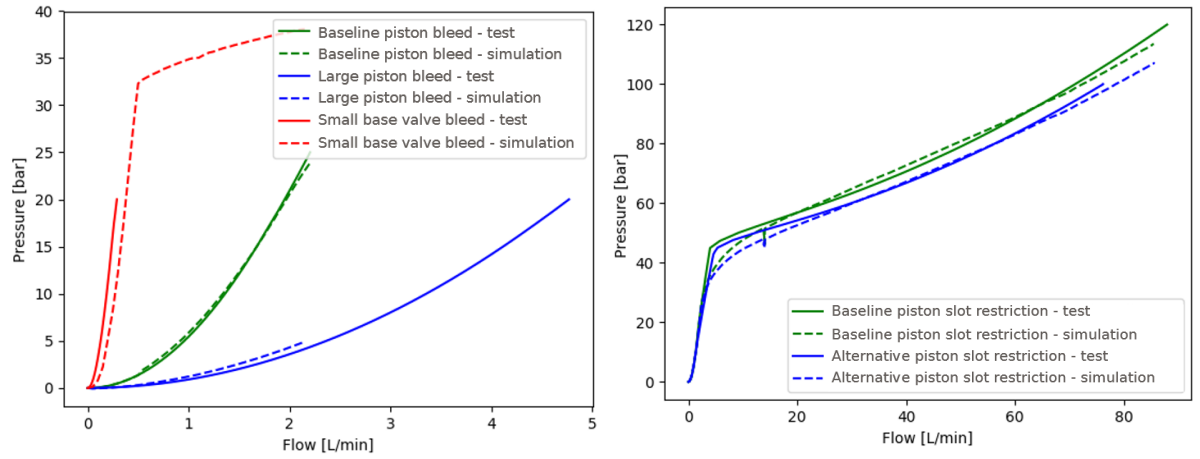
Figure 4.3: View of the purposefully introduced slot that influences the low flow rate part of the P/Q curve (valve bleed)

Apart from the purposefully introduced open orifices in the valve, inevitably certain leakages are always present between rebound, compression, third and reserve chambers. Although many authors include those leakages in their models (e.g. in [111]), due to difficulties in characterization as well as the fact that the flow behavior is similar to the valve bleeds, in the proposed model these leakages were not considered. This simplifies the model and reduces the number of input parameters.

Conversely, to the valve bleeds, the high flow rate area of the P-Q characteristic can be influenced by the restriction that is created by the main slots of the piston and base valve. This can only have an influence at high flow rates but due to the wide range of the possible valve characteristics, this restriction is also taken into account. The flow is governed by the same approach as in the case of the valve bleed although with a different value of the discharge coefficient that was calibrated only at the very high flow rate part of the P-Q characteristic (see fig. 4.4b).

## 4.5 Top mount

In order to reproduce the dynamic behavior of the top mount vibroisolator, a rheological rubber bushing model developed for Altair MotionView Multi-body simulation package has been used [2] (also known as "AutoBushFD"). It originates from the rheological model incorporating Bouc-Wen hysteretic restoring force formulation described in [89] (radial bushing model) and [116]. This model is capable of reproducing dynamic stiffness



(a) Restriction through the bleed slot (low flow rates) (b) Restriction through the main slot (high flow rates)

Figure 4.4: Verification of the discharge coefficient values performed based on the flow-bench test results

and loss angle dependency on amplitude, frequency as well as on preload. Non-linear load-deflection characteristic is included using an empirical approach by higher order polynomial approximation of the measured static response. The schematic layout of the model has been shown in figure 4.5. Reaction force resulting from this bushing formulation is described by equation 4.37 which depends on effective stiffness  $K$  and damping  $C$  as well as nonlinear static load deflection curve  $F_{LD}$  which is a function of the input displacement  $X$ . Effective stiffness and damping are derived in eq. 4.36 and 4.35 based on the values of state variables  $y$  and  $\dot{w}$  which are adjusted with set of scaling coefficients  $(c_0 q_0 q_1 q_2 k_0 p_0 p_1 p_2)$ . Values of two internal states are obtained from the ordinary differential equations 4.34 and 4.33. For the dynamic force estimation, filtered excitation (denoted by  $x$ ) is used according to eq. 4.32.

$$\dot{x} = \dot{X} - Rx \quad (4.32)$$

$$\dot{y} = \frac{1}{c_1}(c_1\dot{x} + k_1(x - y) - k_0y) \quad (4.33)$$

$$\dot{w} = \frac{1}{(c_0 + c_2)}(c_2\dot{x} + k_2(x - w)) \quad (4.34)$$

$$K = k_0(p_0 + p_1|y|^{p_2}) \quad (4.35)$$

$$C = c_0(q_0 + q_1|\dot{w}|^{q_2}) \quad (4.36)$$

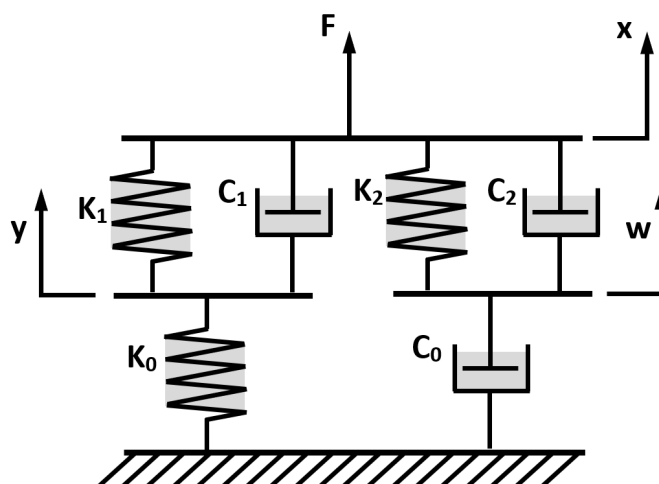


Figure 4.5: Schematic layout of the AutoBushFD [2]

$$F = Ky + C\dot{w} + F_{LD}(X) \quad (4.37)$$

## 4.6 Rod friction

As discussed in section 2.3, the frictional forces generated by the shock absorber between rod and tube assembly can have a significant negative impact on ride, handling as well as noise-related aspects of the automotive suspension. Despite significant resources devoted by the damper suppliers to reducing friction force, often it is still a daunting problem. Friction forces depend strongly on the side forces exerted by the shock absorber bearings. For that reason, effects related to the frictional forces are most pronounced for the MacPherson type of shock absorber strut, because at this design particularly high bending moments are transferred via rod. In other mounting conditions, shock absorbers bending moments are much lower (generated by the coil-spring and mounting bushing rotations and non-axialities) and therefore the impact of the friction is much lower, however, it should still be taken into account when high-frequency rod vibrations are analyzed.

Due to the significance of damper friction forces in the vehicle dynamics domain, the experimental procedures dedicated to characterizing it are well established. The most widely used method for determining the friction force is to measure the damper force at such a low velocity that other forces originating from the hydraulic layout of the damper are negligible. This approach is convenient but due to velocity constraints doesn't allow to capture of the complete friction force behavior. Another strategy to separate the friction force is to decrease the damping force by removing the passive valve restrictions. This allows for the measurement also at the higher velocities. Exemplary friction force characteristics have been shown in figure 4.6.

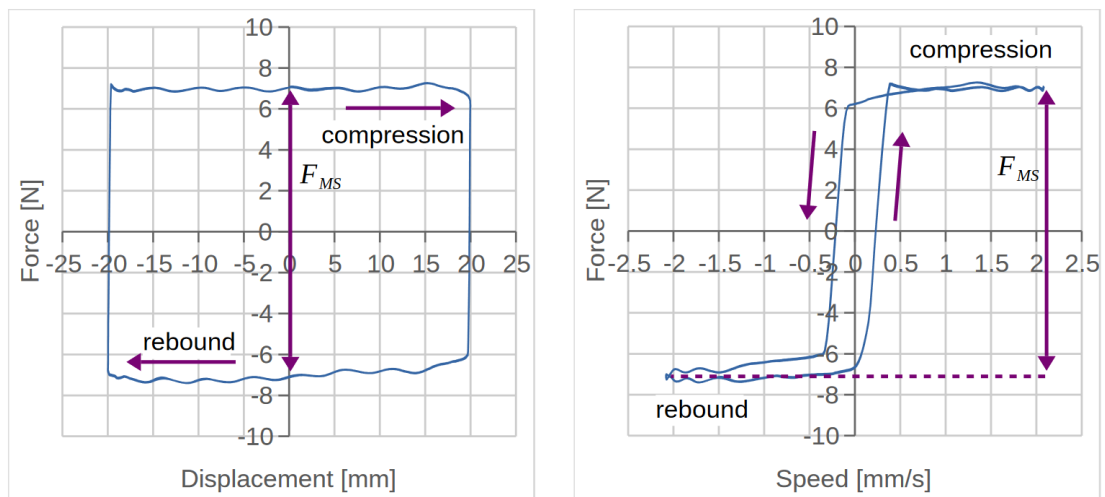


Figure 4.6: Exemplary friction force-displacement and force-velocity graph for the piston sliding bearing surface [72]

Frictional forces in the shock absorber originate at three separate sets of adjacent surfaces (indicated in figure 4.7):

- piston bearing (steel - PTFE sliding bearing)
- rod guide bearing (steel - PTFE sliding bearing)
- oil sealing (steel-rubber)

Friction forces originating from sliding at bearing surfaces (at rod guide and piston) are highly dependent on the side loads whereas the oil sealing behavior remains similar regardless of the shock absorber bending. Since in the considered cases, the side loads exerted on the shock absorber are low, for the sake of model simplicity, frictional forces from all the surfaces are included as one combined frictional force.

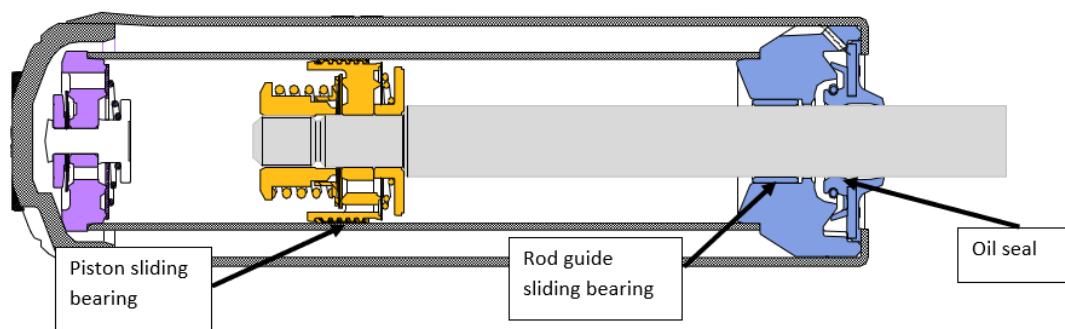


Figure 4.7: Surfaces at which the friction force is induced at double tube design (courtesy of Tenneco Automotive Eastern Europe Sp. z o.o.)

For each of the considered contact areas, the oil film is present between the sliding surfaces. Together with the fact that the rod movement in relation to the rest of the damper might occur at high rates and amplitudes, the model of the friction should take

into account various lubrication regimes, as captured by Stribeck's curve. It is characterized by high static friction force due to physical contact at the level of surface asperities. After the relative motion is initiated the friction force decreases due to the increased oil film but only up to a certain point at which the friction is only generated by hydrodynamic forces created by lubrication which are increasing proportionally to the velocity of the relative motion.

As demonstrated in [72] a formulation that captures the aforementioned behavior is a variant of the LuGre model (Lund Grenoble) proposed in [27]. It is able to combine the stiffness behavior captured by the Dahl model with the Stribeck effect. The model is visualized as the bending of a set of bristles that act as a spring element. Using this approach the force can be represented by equation 4.38.

$$F_{r\mu} = k_b \cdot z_b + s_1 \frac{dz_b}{dt} + s_2 \Delta v \quad (4.38)$$

where  $k_b$  is representing the stiffness of the bristles,  $z_b$  is the average bristle deflection,  $s_1$  the bristle microscopic damping coefficient governed by equation 4.39,  $s_2$  the viscous friction coefficient and  $\Delta v$  the relative velocity.

$$s_1 = c_{comp} \cdot \exp\left(\frac{-\Delta v}{vd}\right)^2 \quad (4.39)$$

where  $c_{comp}$  is a parameter controlling damping for the tangential compliance and  $vd$  is a velocity threshold. Further, the bristle deflection  $z$  is captured by equation 4.40 whereas the Stribeck effect is reproduced by  $g(\Delta v)$  function in equation 4.41.

$$\frac{dz}{dt} = \Delta v - k_b \cdot \frac{|\Delta v|}{g(\Delta v)} \cdot z \quad (4.40)$$

$$g(\Delta v) = F_c + (F_s - F_c) \cdot \exp\left(\frac{|\Delta v|}{a_s}\right)^{\alpha_s} \quad (4.41)$$

here  $F_c$  is the Coulomb friction force,  $F_s$  the static friction force and  $a_s$  the Stribeck constant. At large deflection,  $F_c$  is a dominant parameter that can be easily established from the standard measurement procedures as shown in figure 4.6.

## 4.7 Study of alternative valve modeling techniques

The reasoning behind some of the decisions made regarding the valve modeling techniques for the proposed model might not be immediately clear to the reader. This subsection aims at indicating the effects that some of the valve-level physical phenomena have on the characteristics of the semi-active shock absorber and therefore it serves as an additional justification for including these parts of the numerical model.

### 4.7.1 Impact of the valve stiction forces

As demonstrated in the subsequent subsection 6.5.1, one of the key sources of the disturbance that is contributing significantly to the rod vibration is the opening (and to a lesser extent closing) of the passive valves. During the opening of the valves two, flat, adjacent surfaces that are submerged in the hydraulic medium have to separate. When the rate of the separation is high enough, additional stiction force will be exerted on the valve. This additional force might contribute negatively to an event that by itself, is already causing undesired dynamic rod accelerations. Since stiction forces are induced always at the onset of the valve opening, in an idealized case, this should happen when the shock absorber force direction is changed. However, due to the hysteresis caused by the damper compliance valve openings and closings are offset as indicated in the force-velocity and force-displacement graphs in figure 4.8. In the force-velocity graph, stiction force demonstrates itself as an instability in the characteristic at the time when the valve is opening (see figure 4.9a). When the stiction force is not taken into account the transition in the damping force resulting from valve opening is always smooth (see figure 4.9b).

In terms of force-velocity graphs, contrary to the intake valve opening, neither experimentally nor numerically obtained force signals do not show any significant instabilities resulting from the shim stack valve opening. The main reason of this behavior is that the stiction forces resulting from the shim stack valve opening are lower due to the much lower velocity of the valve opening (see table 4.1). As a result, the stiction force is included in the model only for the intake valves.

Table 4.1: Maximum opening velocity of the valves registered during damper level test simulation

Valve name	Velocity [mm/s]
Piston rebound	2.4
Base valve intake	192
Piston intake	154
Base valve compression	4.7

### 4.7.2 Impact of the valve level friction

One of the characteristic features of the semi-active shock absorbers (operating in the triple tube layout with one, unidirectional active valve) are more restrictive passive valves. The reason for this is that the electronically controlled valve only influences bypass flow that is present on top of typical flow paths present in the passive damper. In order for this bypass flow to take the desired effect, flows through the passive valves have to be sufficiently low. A consequence of this higher restrictiveness of the valve is the higher stiffness of the shim stack and together with that, the higher axial force exerted

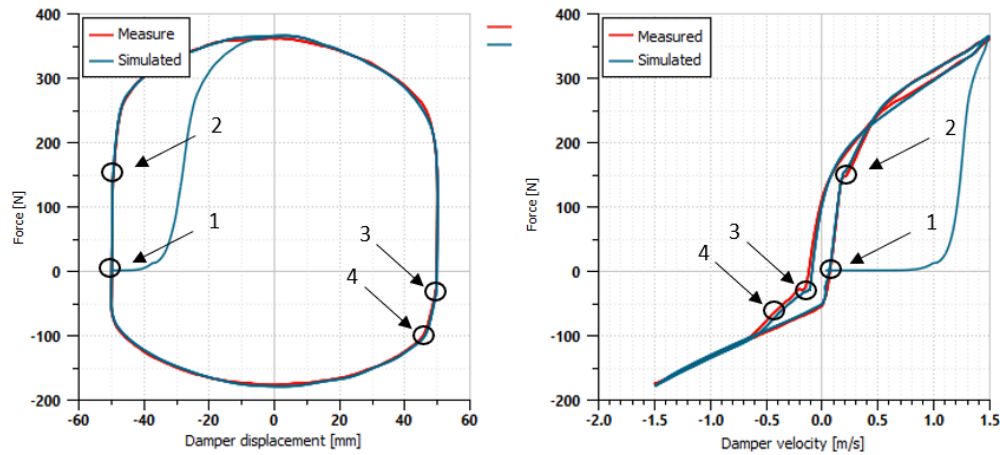


Figure 4.8: Location of the valve openings in relation to the force-displacement and force-velocity graphs of the damper, where:

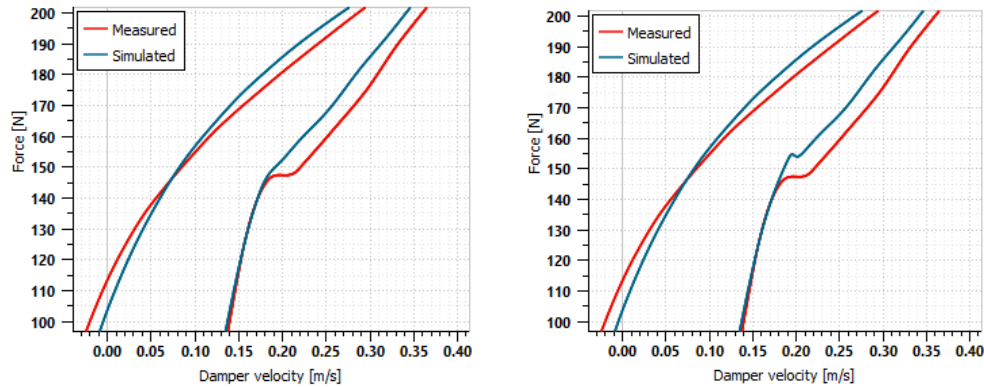
1. the start of piston rebound valve opening
2. the start of base valve intake valve opening
3. the start of piston intake valve opening
4. the start of base valve compression valve opening

between the shim stacks. This inevitably leads to higher frictional forces at the valve level as described in 4.4. Increased friction introduces hysteresis to the flow-pressure drop characteristic of the valve and at the damper level can demonstrate itself as a crossing of the curve in the force-velocity graph. This characteristic is also present in some passive dampers (e.g it is observed and described in [47]), but due to the relatively low impact of friction in passive dampers, this phenomenon has not been reproduced in high-frequency models of shock absorbers so far.

Using model calibrated, on the force-velocity graphs, effect of the valve friction can be clearly observed in figure 4.10 at the rebound stroke of the damper (focus at the right column) as a crossing between damper acceleration and deceleration curves. Due to the relatively low valve opening of the compression valve, at this direction of the damper stroke, friction effects are not observed. On the other hand intake valves of the damper don't produce frictional forces due to the lack of relative motion of the valve during the opening.

## 4.8 Conclusion

Based on the survey of the current state of knowledge in terms of numerical modeling of the shock absorbers (performed in chapter 3) general guidelines for the developed model have been established and subsequently specific modeling approach was proposed. An important goal was to assemble and develop a model that on one hand can reproduce



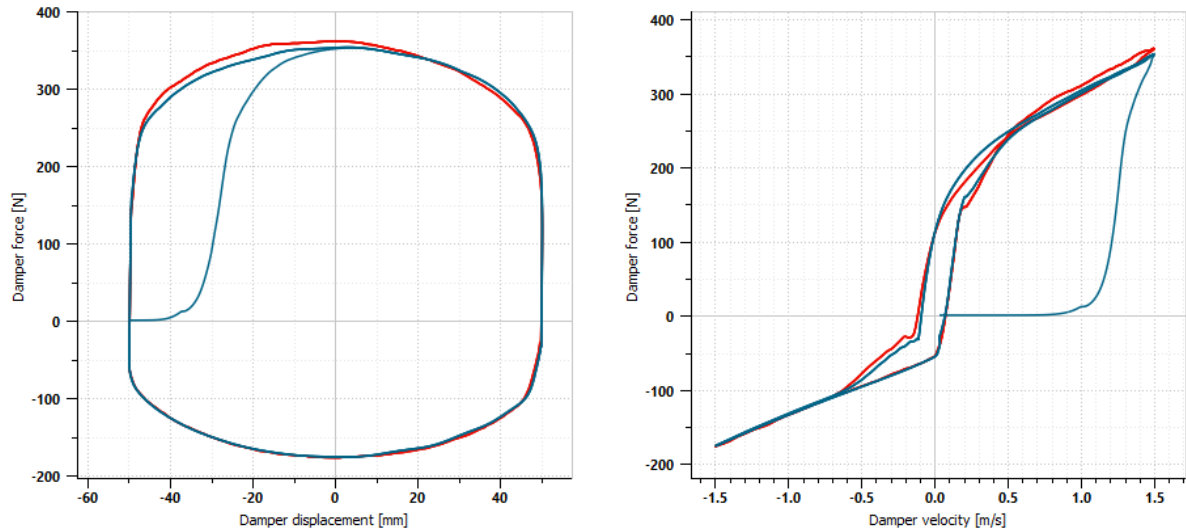
(a) Simulation performed without the valve stiction force

(b) Simulation performed with the valve stiction force

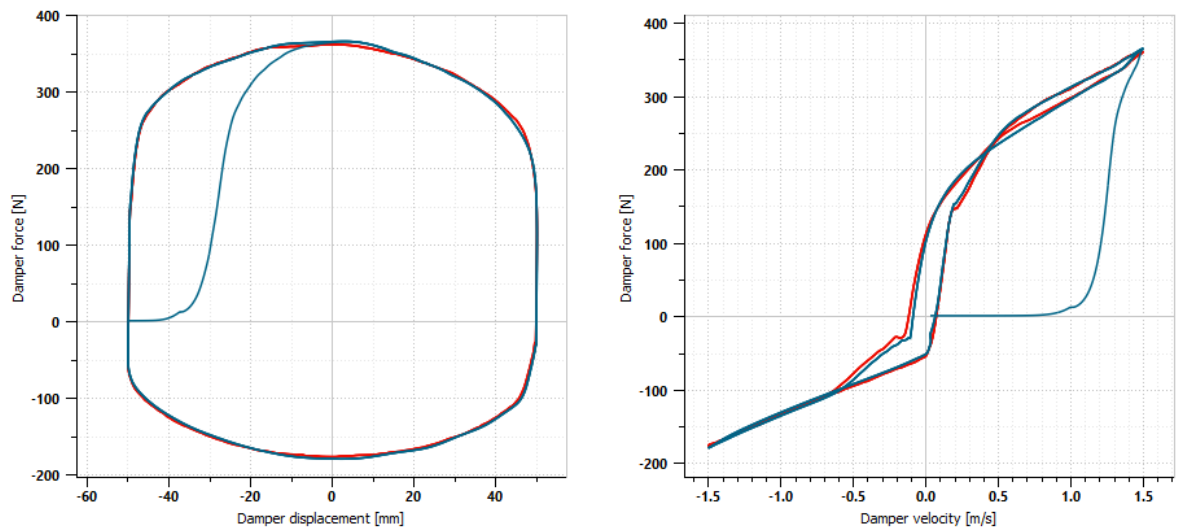
Figure 4.9: Impact of stiction force on the force-displacement and force-velocity curves from damper level testing

the dynamic behavior of the shock absorber that is relevant to the vehicle dynamics performance as well as to the noise-related issues (methodology of measuring and assessing these aspects was discussed in paragraph 2.7) and on the other hand, the complexity of the model cannot constrain its practical application in the realities of the automotive industry.

A model presented in this chapter allows calculating forces exerted on the shock absorber's rod that results from the relative movement of the tube. From the damper displacement signal, volumetric changes are related to the pressure differential according to the equation in 4.2, taking into consideration compliance, as in section 4.3. The relation between flow and pressure differential is calculated based on the mechanical valve model described in 4.4. From the calculated pressure differentials, the force present at the rod is obtained with eq. 4.1. The set of equations resulting from the described approach is solved using Simcenter Amesim variable step integrator. Apart from the forces resulting from the pressures in the compression and rebound chambers, rod forces are affected also by friction, induced at damper sliding bearing and sealing surfaces which is reproduced with equations 4.38-4.41. At the mounting point, the damper dynamics are impacted by top mount force which is captured by the submodel described in section 4.5. When combined, the above subsystems constitute a model with 105 input parameters.



(a) A simulation performed without the valve friction



(b) A simulation performed with the valve friction

Figure 4.10: Impact of friction on the force-displacement and force-velocity curves from damper level testing

# Chapter 5

## Parameters estimation methodology

The value and knowledge gained from the simulation depend not only on the quality of the model but also on the ability to provide realistic values of its parameters. As described in the chapter 4, the proposed model requires 105, distinct input parameters. Since the parameter identification may be required to be performed each time a new design of subsystem is analyzed, in the realities of the automotive industry, this part often becomes a limiting factor when it comes to the practical application of simulation tools. Therefore, (in accordance with the formulated goals of the project) a clear parameters calibration procedure has to be proposed.

Each new considered design will first have to be characterized with the values taken from the documentation. These parameters do not require any additional characterization procedure, therefore the only challenge is related to managing the engineering documentation. Most of the parameters related to the geometrical description of the model fall into this category. The second group includes parameters that cannot be easily derived from documentation but since their value remains approximately the same regardless of the considered design, they should be characterized only once for the scope of the applicable designs. Good examples of this type of parameter are discharge coefficients for different restrictions as well as shim valve friction parameters. The fact that these parameters are considered to be design invariant is a simplification, however, in the course of the model preparation, it has been established that the cost of characterization of their values (which would have to be performed specifically for each design) is not justified by the added value brought by their accurate representation for given design. The last group includes parameters that for a given design of shock absorber are not easily estimated based on the design documentation and heavily impact the dynamic behavior of the damper therefore they require a separate calibration procedure since it has to be performed for each specific design. There are three main groups of such parameters, which are related to valve stiffness, damper compliance, and top mount dynamic characteristics. All parameters of the model have been listed in table 5.1. The last column

of this table provides a code indicating which method of defining the parameter value should be used. The methods are defined as follows:

- **D** - Design-based parameters - the values of parameters in this group can be established entirely based on technical documentation without any complex measurement or simulation procedure.
- **F** - Fixed valued parameters - the values of parameters in this group, based on the literature study or experimental measurement have been established. For the purpose of the practical application of the developed simulation methods, these parameters should be adjusted only in the case of significant design changes.
- **C** - Calibrated parameters - the values of parameters in this group have to be established based on one of the proposed calibration procedures (described in subsequent sections).
- **T** - Test parameters - the values of these parameters solely depend on the test conditions.

## 5.1 Theoretical introduction

### 5.1.1 Parameter estimation

The goal of the model calibration procedure for the deterministic models can be defined as an attempt to improve the characterization of the input parameter values, by maximizing agreement between simulation output and experiment target [36]. It is often referred to as parameter estimation, identification or tuning. This procedure of adjusting the input parameter values can be performed to achieve two types of goals [51]:

- estimate and therefore learn the real values of the physical parameter used in the model (usually referred to as calibration),
- improve the model response without physical meaning so that is a better surrogate for the physical process.

Despite this classification, in many cases, both goals are being pursued at the same time. An important challenge for the model calibration methods regardless of its objective is the fact that the computer model always contains a certain level of imperfection with regard to the physical phenomena it is designed to reproduce. If the level of model imperfection (discrepancy) is high enough it can compromise the calibration process and lead to biased parameters and simulation results. To address this challenge, multiple approaches have been proposed that aim to capture the hidden error of the model as well as the experimental data [46, 98, 45, 86]. One of the most commonly used approaches is the Bayesian calibration framework proposed in [76] by Kennedy and O'Hagan which demonstrated that the wrong estimation of input parameters can be mitigated by application of discrepancy function that represents the inherent error of the model and provided

data. Another challenge that model calibration procedures face is related to the problem of establishing the identifiability of the parameters, since if the noise present in the experimental data is higher than the impact of the parameter value over the simulation results, the calibration cannot be performed [65].

### 5.1.2 Optimization

Regardless of the specific method chosen to address the problems of model discrepancy and parameter identifiability, in the majority of model calibration cases, the procedure involves an optimization problem. In the case of simple problems, the least-square method is often adopted. More advanced methods involve Kriging, particle swarm [51], genetic algorithms [75] or other optimization methods. For model calibration procedures used in this dissertation, the genetic algorithm was selected as a primary optimization tool. This computational technique is inspired by the process of natural selection. It utilizes principles of mutation, inheritance, crossover, and selection to influence the search for the optimal solution. Thanks to those intuitive concepts it is relatively easy to adjust how exploratory the algorithm will be. This allows genetic algorithms to be effective at exploring even large and complex optimization spaces [75, 56]. Since genetic algorithms usually do not make use of any problem-specific knowledge, with simple encoding they can be versatile and easy to apply for a wide range of problems, particularly given the rich library of ready-to-use applications in various programming languages. Unfortunately, high versatility and reliability at complex problems come at the cost of low performance due to being relatively, computationally expensive. This is however mitigated to a certain degree by the fact that due to the iterative (population-based) character of the optimization processes, genetic algorithms are easy to parallelize. Due to the popularity of this optimization technique, there are many variants of genetic algorithms. Regardless of the considered parameter estimation method, for the optimization procedures used in this dissertation, steady-state parents selection, single-point crossover and random mutation together with elitism were used as applied on the Python Scripting Language Library "PyGAD" [60].

## 5.2 Parameter estimation methods used in this dissertation

Due to the complexity of the considered system of the semi-active damper, the numerical model involves a relatively large number of input parameters. Some of them are easy to be determined based on the engineering documentation while others can only be obtained by means of measurements or advanced numerical simulations. The complete list of the

parameters used in the model has been provided in table 5.1. Based on the measurement capabilities, each parameter in that list has been classified as such that can be accurately defined based on design documentation or as such that has to be determined in another way. The most challenging parameters are related to the mechanical system of the valving, overall damper compliance as well as dynamic properties of the top-mount.

As described in the introduction, the problem of parameter estimation can be approached in two different ways. The first method (studied in chapter 6) aims at defining parameters based on the measurements or simulations of the isolated subsystems. This approach is the most common since it allows for the simulation of the system that doesn't exist prior to the simulation, only separate subsystems have to be characterized. However, since the parameterization is performed in an isolated environment for each part of the model, the influence of the measurement method inaccuracies can distort the results.

Apart from the regular parameter estimation procedure used at the level of isolated subsystems in calibration approach 1 (see chapter 6), the second proposed method described in chapter 7, utilized results of the variance-based (Sobol) model sensitivity analysis [113, 26, 103]. The goal of the sensitivity analysis is to quantify the influence of the input parameter over the selected results of the simulation. By incorporating this information into the parameter calibration procedure, the risk of calibrating parameters with low identifiability is reduced. Additionally, the optimization algorithm can use a better quality of the feedback information regarding the response for a given parameter change [95]. Direct usage of the Sobol indices within the parameter estimation procedure is not straightforward and creates challenges related to computational cost. A detailed description of the sensitivity-based parameter estimation procedure can be found in section 7.1.

Table 5.1: Summary of all the input parameters used in the model

	no.:	Symbol	Description	Type
Geometrical data	1	$M_{rod}$	Mass of the rod assembly (including all the components rigidly attached)	D
	2	$D_{PT}$	Inner diameter of the pressure tube	D
	3	$D_R$	Outer diameter of the piston rod	D
	4	$V_b$	Volume of the third tube chamber	D
	5	$l_{c0}$	Length of the compression chamber at damper initial position	D
	6	$l_{r0}$	Length of the rebound chamber at damper initial position	D
Oil properties	7	$K_{oil}$	Bulk modulus of the oil	F
	8	$\rho_{oil}$	Density of the oil	F
	9	$\nu$	Kinematic viscosity	F
	10	$P_{sat}$	Oil saturation pressure	F
	11	$P_{vap}$	Oil vaporisation pressure	F
	12	$\chi$	volumetric gas content of the emulsion	D
	13	$\Gamma$	Polytropic index	F
	14	$aa$	Initial pressure	D
	15	$aa$	Temperature	T
Third tube	16	$E$	Young modulus	F
	17	$\nu$	Poisson's ratio	F
	18	$r_o$	Outer radius of the third tube	D
	19	$r_i$	Inner radius of the third tube	D
Top mount	20	$R$	The cutoff frequency related to a first order filter that acts on the input X	C
	21	$P_0$	Scale factor for stiffness	C
	22	$P_1$	Scale factor for stiffness	C
	23	$P_3$	Scale factor for stiffness	C
	24	$Q_0$	Scale factor for damping	C
	25	$Q_1$	Scale factor for damping	C
	26	$Q_3$	Scale factor for damping	C
	27	$K_0$	Represents the bushing rubber stiffness	C
	28	$K_1$	Represents the bushing rubber stiffness	C
	29	$K_3$	Rubber stiffness at high velocities	C
	30	$C_0$	Produces the roll-off observed in the experimental data at low velocities	C
	31	$C_1$	Accounts for the relaxation of the bushing impact force	C
	32	$C_3$	Represents the viscous damping observed at large velocities	C
	33	$X_{Static}$	The static force response of the bushing	C

	no.:	Symbol	Description	Type
Piston shim stack valve	34	$D_d$	Outer diameter of the valve disc	D
	35	$D_i$	Outer diameter of the valve slot	D
	36	$C_{q,max}$	Discharge coefficient at turbulent flow regime	F
	37	$\lambda_{crit}$	Critical flow number	F
	38	$A_{bleed}$	Flow area of the valve bleed	D
	39	$C_{qb}$	Discharge coefficient of the bleed flow	F
	40	$A_{slot}$	Flow area of the valve slot	D
	41	$C_{qs}$	Discharge coefficient of the slot flow	F
	42	$m_v$	Mass of the valve moving part	D
	43	$c_v$	Valve damping	F
	44	$\sigma_0$	Dahl's friction stiffness coefficient	F
	45	$F_c$	Coulomb (dynamic) friction coefficient	F
	46	$\alpha$	Dahl coefficient controlling shape of the stress-strain curve	F
	47	$F_{preload}$	Valve stiffness preload	F
	48	$a$	First stiffness approximation coefficient	C
	49	$b$	Second stiffness approximation coefficient	C
50	$c$	Third stiffness approximation coefficient	C	
51	$d$	Fourth stiffness approximation coefficient	C	
Piston intake valve	53	$D_d$	Outer diameter of the valve disc	D
	54	$D_i$	Outer diameter of the valve slot	D
	55	$D_c$	Inner diameter of the valve slot	D
	56	$D_h$	Inner diameter of the intake valve disc	D
	57	$C_{q,max}$	Discharge coefficient at turbulent flow regime	F
	58	$\lambda_{crit}$	Critical flow number	F
	59	$A_{slot}$	Flow area of the valve slot	D
	60	$C_{qs}$	Discharge coefficient of the slot flow	F
	61	$m_v$	Mass of the valve moving part	D
	62	$c_v$	Valve damping	F
	63	$F_{preload}$	Valve stiffness preload	D
	64	$a$	First stiffness approximation coefficient	C
	65	$b$	Second stiffness approximation coefficient	C
	66	$c$	Third stiffness approximation coefficient	C
	67	$d$	Fourth stiffness approximation coefficient	C
	68	$x_{v0}$	Initial valve separation distance for the stiction force calculation	F

	no.:	Symbol	Description	Type
Base valve shim stack valve	69	$D_d$	Outer diameter of the valve disc	D
	70	$D_i$	Outer diameter of the valve slot	D
	71	$C_{q,max}$	Discharge coefficient at turbulent flow regime	F
	72	$\lambda_{crit}$	Critical flow number	F
	73	$A_{bleed}$	Flow area of the valve bleed	D
	74	$C_{qb}$	Discharge coefficient of the bleed flow	F
	75	$A_{slot}$	Flow area of the valve slot	D
	76	$C_{qs}$	Discharge coefficient of the slot flow	F
	77	$m_v$	Mass of the valve moving part	D
	78	$c_v$	Valve damping	F
	79	$\sigma_0$	Dahl's friction stiffness coefficient	F
	80	$F_c$	Coulomb (dynamic) friction coefficient	F
	81	$\alpha$	Dahl coefficient controlling shape of the stress-strain curve	F
	82	$F_{preload}$	Valve stiffness preload	F
	83	$a$	First stiffness approximation coefficient	C
	84	$b$	Second stiffness approximation coefficient	C
85	$c$	Third stiffness approximation coefficient	C	
86	$d$	Fourth stiffness approximation coefficient	C	
Base valve intake valve	87	$D_d$	Outer diameter of the valve disc	D
	88	$D_i$	Outer diameter of the valve slot	D
	89	$D_c$	Inner diameter of the valve slot	D
	90	$D_h$	Inner diameter of the intake valve disc	D
	91	$C_{q,max}$	Discharge coefficient at turbulent flow regime	F
	92	$\lambda_{crit}$	Critical flow number	F
	93	$A_{slot}$	Flow area of the valve slot	D
	94	$C_{qs}$	Discharge coefficient of the slot flow	F
	95	$m_v$	Mass of the valve moving part	D
	96	$c_v$	Valve damping	F
	97	$F_{preload}$	Valve stiffness preload	D
	98	$a$	First stiffness approximation coefficient	C
	99	$b$	Second stiffness approximation coefficient	C
	100	$c$	Third stiffness approximation coefficient	C
	101	$d$	Fourth stiffness approximation coefficient	C
	102	$x_{v0}$	Initial valve separation distance for the stiction force calculation	F
Friction	103	$F_c$	Coulomb friction force	C
	104	$F_s$	Static friction	C
	105	$k_b$	LuGre bristles stiffness	F

# Chapter 6

## Parameters calibration study – approach 1

The goal of this chapter is to establish the level of accuracy of the results obtained with the proposed model when the values of parameters are calibrated based on the measurements performed on isolated test benches. For this purpose, experimental measurement and model calibration analysis were performed separately for each of the considered subsystems: valves (section 6.2), damper structure (section 6.3, for compliance-related parameters) and top-mount (section 6.4).

After parameters identification for isolated subsystems was done, the quality of the assembled model of the complete system of the modular assembly was assessed (in section 6.5) based on the comparison of the results obtained from simulation and measurements of the damper performance (force-velocity and force-displacement curves) as well as damper dynamical tests (mono-sine and noise excitation tests).

### 6.1 Description of the design used for the calibration exercise

In order to assess the quality of the proposed model and calibration procedure, the design of the semi-active shock absorber that is featured for the rear suspension of the SUV class of a passenger car model was used (an overview of the design can be seen in figure 6.1) However, in order to estimate the quality of the model and parameterization process under various design cases, the comparison is performed using one-factor-at-a-time experiment for the design features that might influence its dynamic behavior. As a result, each design feature is considered at two levels. The following design cases were considered:

- piston intake valve stiffness
- piston rebound shim valve stiffness

- base-valve intake valve stiffness
- base-valve compression shim valve stiffness
- active valve P/Q characteristic
- active valve current (see figure 6.2, considered at 3 levels)
- top mount stiffness
- precharge pressure level

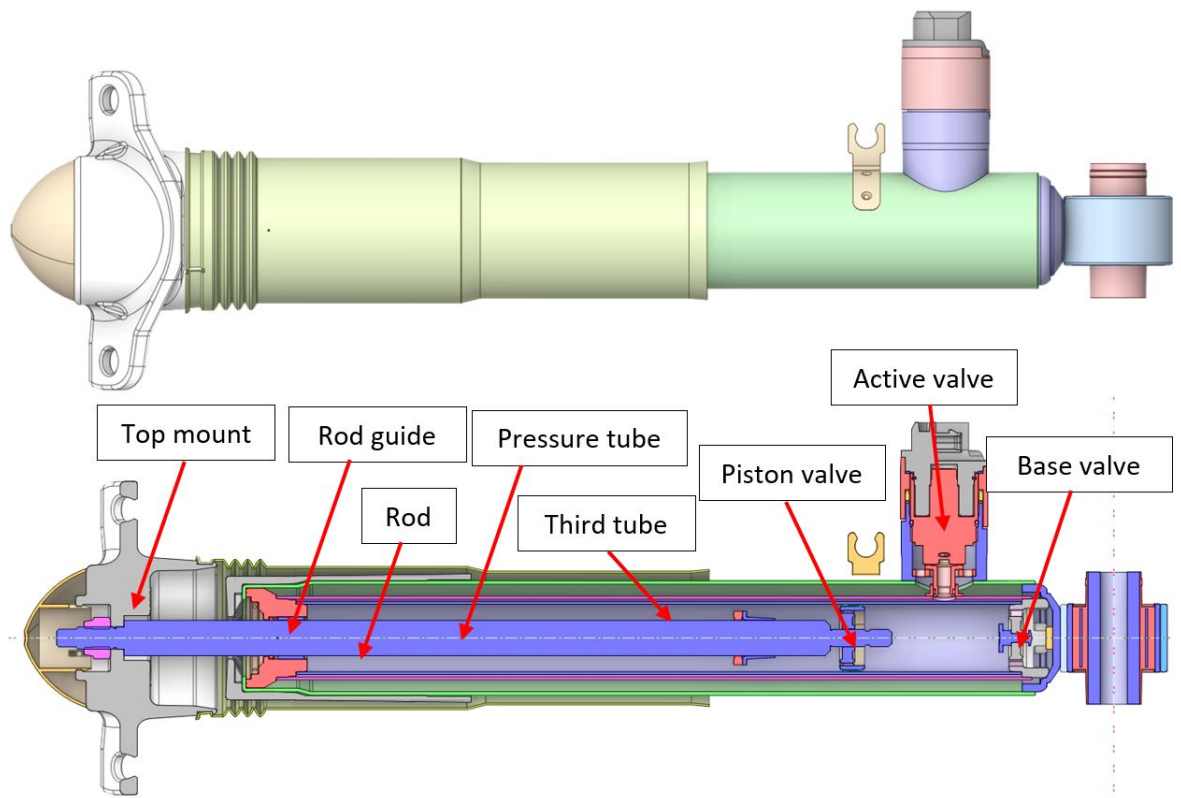


Figure 6.1: Overview of the sample of the semi-active shock absorber used for the model calibration studies

In order to facilitate an easy adjustment of the damper settings, a "take-apart" sample was used (which can be seen in fig. 6.15b at the test set-up). This design of the damper is facilitated with the threaded closing of the reserve tube which allows easy disassembly of the shock absorber. Regular production units are assembled by plastically deforming the reserve tube around the rod-guide (known as the roll-closing process).

## 6.2 Calibration of valves related parameters

The primary difficulty with the determination of the input parameters of the valve comes from having multiple valves active at any given point in time during shock absorber operation. For this reason, it is necessary to either measure directly the pressure in all the

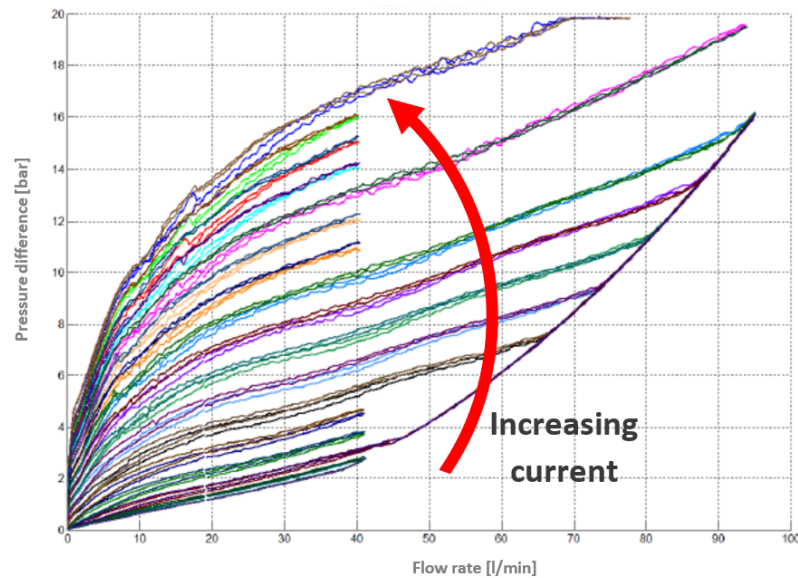


Figure 6.2: P/Q characteristic of the active valve used in the sample during model calibration studies (in relation to increasing current for the CES valve)

chambers of the damper or use external equipment (e.g. flowbench machine) which allows for the parameters identification of the individual valve (see section 2.7). The first method demonstrated in [109, 19] requires a specially designed shock absorber that is featured with internal pressure sensors. This approach is also difficult to apply with the semi-active dampers since the flow rate cannot be directly derived from the damper displacement. The second approach is limited to relatively low flow accelerations but allows for the complete isolation of the valve from the influences of other parts of the damper. The design of the test machine facilitates easy and quick measurement of the valve which makes it a practical tool in the process of the valve parameters characterization. Since the second approach is easier to apply within standard design development procedures, it was selected for the current comparison.

### 6.2.1 Experimental set-up and results

Due to the fact that the relationship between flow rate and the pressure drop at the valve is the primary characteristic used to establish parameters of the valve subsystem, a flow bench machine (described in 2.7) is used as an experimental test system. It allows for an accurate representation of the P-Q characteristic of the valve. The measurement procedure consists of mounting the sample in the test setup and inducing flow through the sample. The maximum flow rate which is achieved during the test was estimated based on the expected velocities of the damper. It is important not to induce an excessive flow rate (corresponding to damper velocity higher than 2 m/s) as such even could easily damage

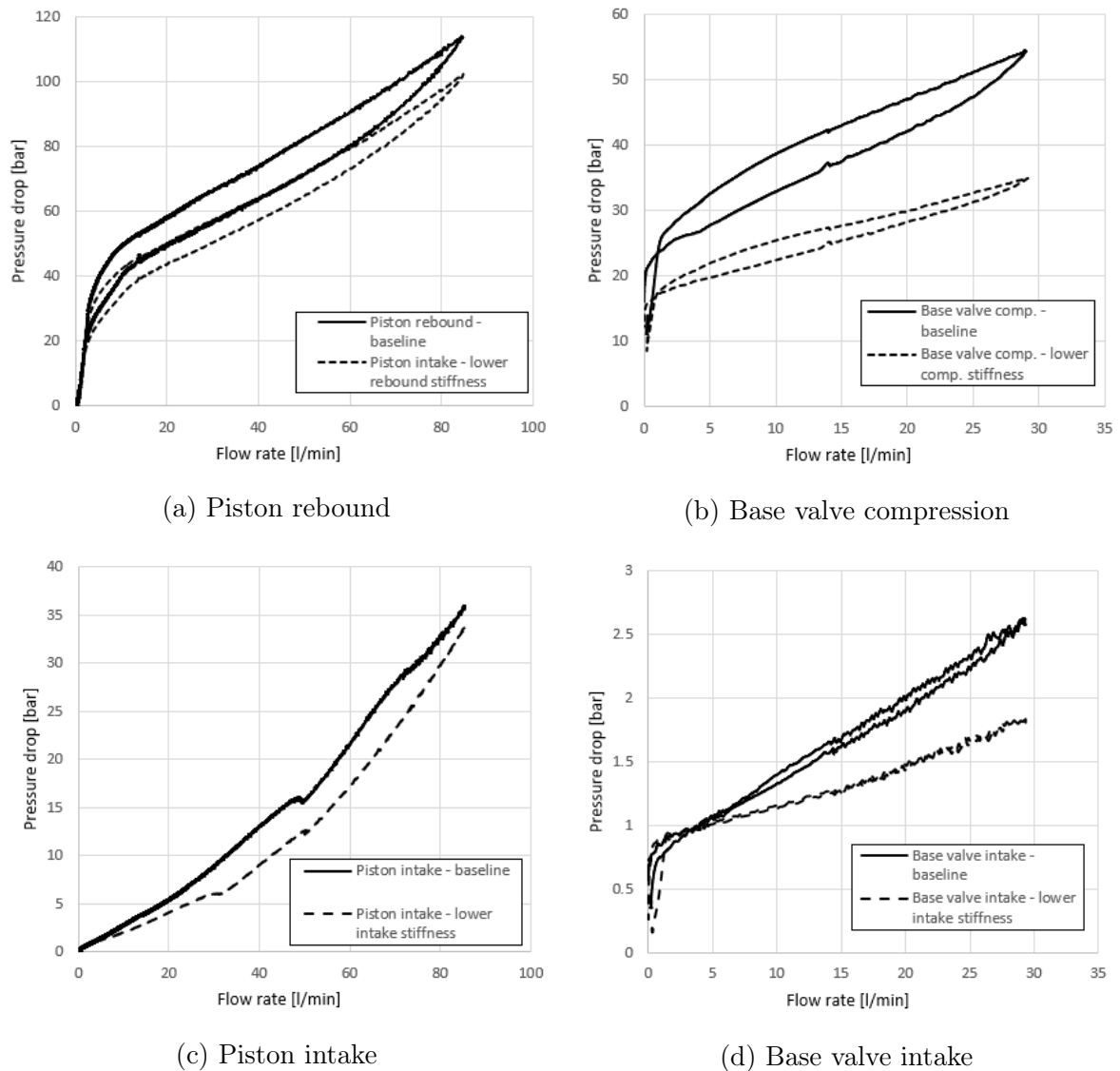


Figure 6.3: Relationship between flow-rate and the pressure drop for all the design cases considered in the model quality assessment, measured on the flowbench test set-up

the valve and corrupt the results. Shim stack at the rebound and compression direction have been tested up to the flow of 80 l/min whereas the intake side of the valve was tested only up to 30 l/min. This range covers the maximum flow rates during the expected conditions of the damper. For each of the considered valve settings, the measurement is performed after several initial flow cycles since the first few opening cycles of the valve may produce significantly different characteristics. Each valve is measured at least three times to ensure consistency of the valve behavior.

Results of the P-Q relationships measured for the considered cases can be observed in figure 6.3. In the case of the shim stacks, the influence of friction can be easily distinguished by the presence of hysteresis after the blow-off point (flow rate acceleration

and deceleration follow different paths, e.g. fig. 6.3a and 6.3b). In the case of piston intake measurements, local instabilities have been observed on the PQ graph. The exact source of those instabilities is not clear however it might be related to the stick-slip behavior at the interface of the disk and the guiding core. Those instabilities can have an influence on the dynamic characteristic at the damper level, however, since their origin is not fully understood, most likely the numerical model will not be able to capture that influence.

## 6.2.2 Estimation of the parameters of the valve model

Since the selected model includes a mechanical system of the valve, measured P-Q characteristics cannot be used directly in the model, instead, the parameters of the valve have to be established so that the model can recreate the measured relationship between flow rate and pressure drop. Most of the geometrical features of the valve model can be determined from the engineering documentation. Since the discharge coefficient can be estimated and fixed based on the existing knowledge in [83, 121, 18], the only remaining unknown parameters are the non-linear stiffnesses of the valves as well as parameters of the frictional effects at the interface of the shim stacks and stiction force initial gap. In order to calibrate the parameters of the model according to the measured relationship, a genetic algorithm has been employed. For each member of the algorithm, the flow test is simulated and the difference between measured and simulated pressure drop is calculated. The goal function is to minimize this difference as expressed by equation 6.1

$$J = \int_0^T |\Delta p_{test}(t) - \Delta p_{simulation}(t)| dt \quad (6.1)$$

A summary of the parameters being identified can be found in table 6.1 and the settings of the genetic algorithm can be found in table 6.2. Usually, a sufficient match can be obtained within the first 30-40 generations, although the width of the boundaries for each parameter greatly influences the rate of optimization.

Table 6.1: Parameters identified with the genetic algorithm at valve level

Parameter name	Lower limit	Upper limit
First stiffness approximation coefficient [-]	0	10 000
Second stiffness approximation coefficient [-]	0	100
Third stiffness approximation coefficient [-]	-10 000	0
Fourth stiffness approximation coefficient [-]	-100	0
Coulomb friction coefficient [-]	0.001	100
Contact stiffness [N/mm]	1	1e9

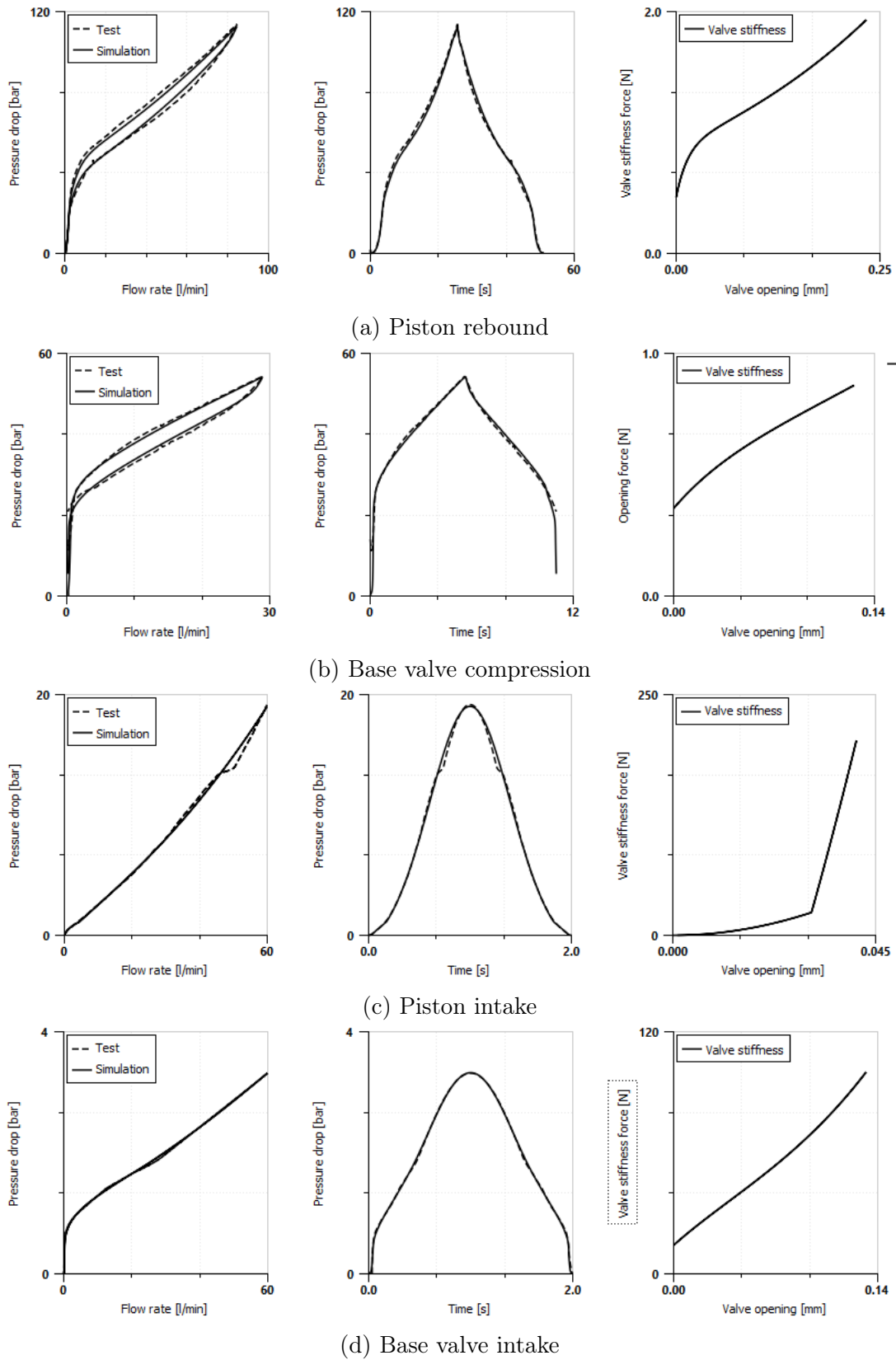
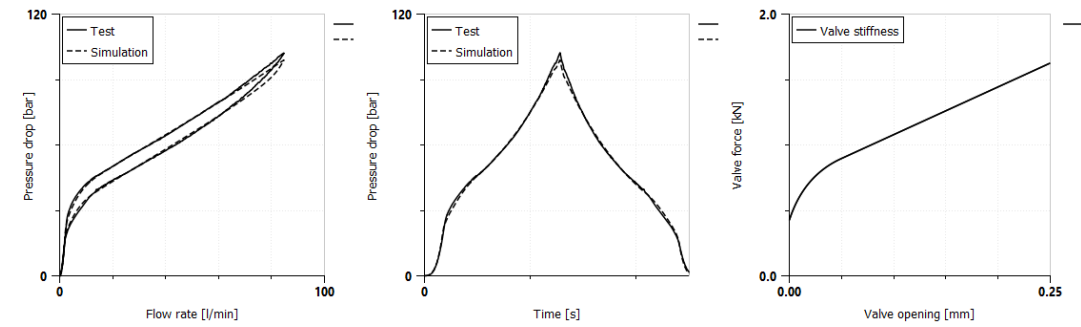
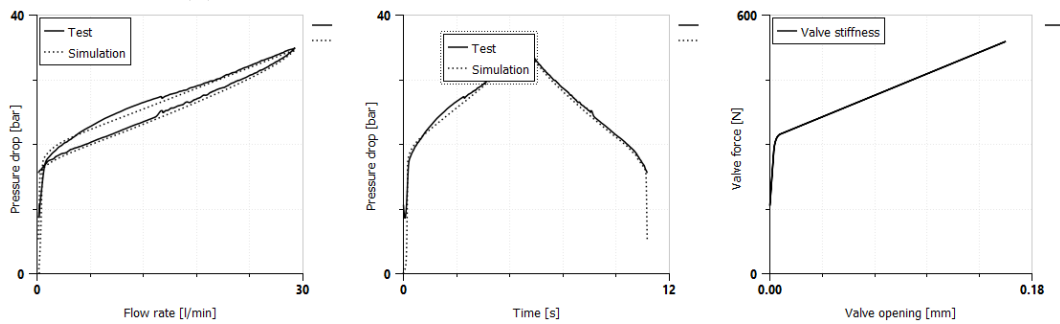


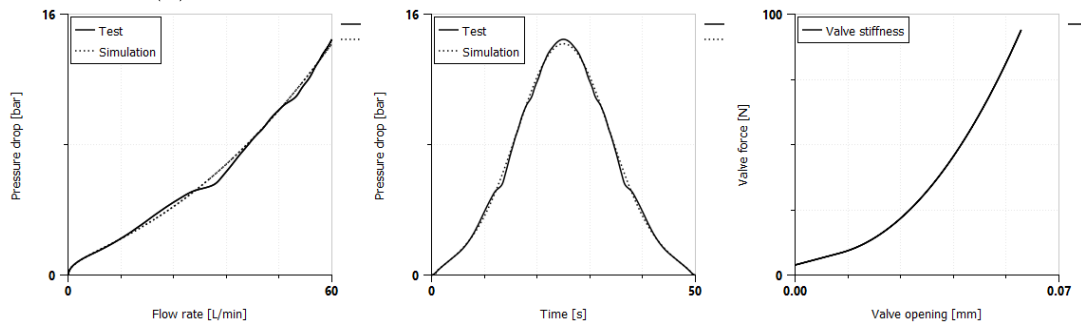
Figure 6.4: Result of the baseline design valves parameters estimation: Left column - P-Q characteristic, Middle column - comparison of the pressure, Right column - identified valve stiffness



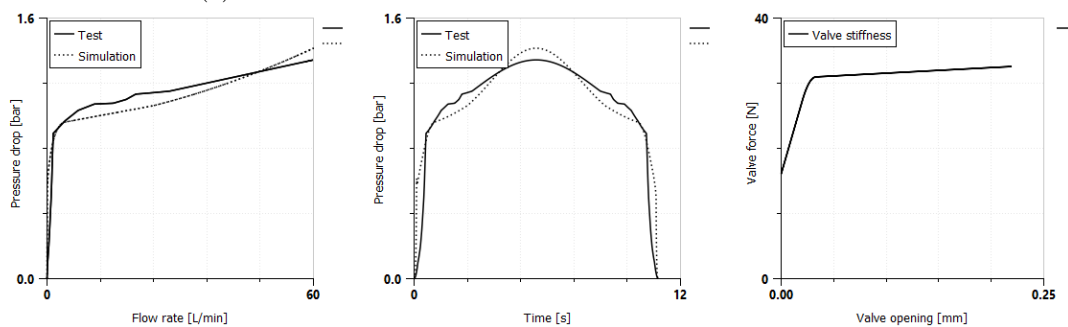
(a) Piston rebound modification - lower stack stiffness



(b) Base valve compression modification - lower stack stiffness



(c) Piston intake modification - lower intake stiffness



(d) Base valve intake modification - lower intake stiffness

Figure 6.5: Result of the alternative design valves parameters estimation: Left column - P-Q characteristic, Middle column - comparison of the pressure, Right column - identified valve stiffness

Table 6.2: Parameters of the genetic algorithm used for valves parameters identification

Parameter name	Value
Population size	50
Reproduction ratio	80
Number of generations	40
Mutation probability	10%

### 6.2.3 Results of the calibration process

The result of the measurement together with the pressure drop characteristics obtained from calibrated simulation are shown in figures 6.4 - 6.5. As can be observed in these figures, the relationship between flow rate and pressure drop for each valve has been accurately recreated by the model. The frictional effect at the valve level has also been recreated, however, due to the low flow acceleration of the test set-up attempt to calibrate the stiction force parameters was not successful.

As can be observed, in the figures showing the results of the parameter estimation, valve stiffness characteristic varies significantly between intake valves and shim valves. This often necessitates different approximation curves for valve stiffness. The frictional effect can be clearly observed in the shim valve designs while the intake valves (which in most cases, comprise of only a singular disk and a spring) show almost no hysteresis related to the friction.

## 6.3 Calibration of compliance related parameters

As mentioned in section 4.3, the amount of undissolved gas that made its way from the reserve chamber to other chambers of the damper, strongly influences the overall compliance of the emulsion and is difficult to estimate using an analytical approach. The bulk modulus of the pure oil (without the gas) can be obtained from the oil supplier's datasheet, however, due to environmental conditions (temperature, oxidation), it might vary from the specified values. Due to the above reasons, in order to use the model in practice, a model calibration procedure has to include a step for the estimation of parameters related to compliance. This can be performed on the fully isolated test set-up which is dedicated to the oil bulk modulus measurements or as described in [111] based on the measurements of the speed of sound in the oil, but in such cases, undissolved gas content might be not correctly represented in the sample. Due to this reason, it was proposed to perform the compliance-related parameter estimation based on the damper level measurement but in such conditions that expose the influence of the bulk modulus as much as possible, so that it is possible to use damper level results for the purpose parameters estimation. The overall damper compliance influences primarily the hysteresis

in the force-velocity graph (see fig. 2.12). Therefore the conditions of the damper level that allow for the best focus on the influence of compliance are when the damper is excited with high accelerations and low strokes because, in such circumstances, the hysteresis is particularly pronounced. Additionally, to further isolate the response that is sensitive to the damper compliance, the top mount is removed and the damper is rigidly mounted in the testing machine. It is also important that the valve's parameters which have to be present during this test, are accurately characterized. For that reason, the compliance parameter estimation has to be performed after the valves parameters calibration.

### 6.3.1 Description of the compliance estimation procedure

This subsection presents the procedure for the identification of gas content as well as oil bulk modulus parameters based on the damper-level experimental data with the use of the genetic algorithm. The damper level test set-up shown in figure 6.6 consisted of the shock absorber which was rigidly mounted at the rod whereas the entire lower assembly was attached to the electromagnetic servo-actuator. The displacement signal of the actuator together with the lower assembly of the damper was registered with the LVDT sensor whereas forces generated at the damper were measured using a strain-gauge-based force transducer. During the test, the sample was excited with the sinusoidal displacement signal with the constant stroke of 10mm (typically, for the performance characteristics measurements stroke of at least 70mm is used) and varying velocity from 0.4 to 2m/s. For each velocity, the damper was cycled multiple times. The results of the cycling were not averaged, but the complete signal was simulated during the calibration process. Compliance-related parameter estimation was performed using a genetic algorithm with optimization algorithm parameters as in table 6.3. The goal function for the genetic algorithm has been formulated according to the equation 6.2. The influence of the gas content over the force generated by the shock absorber in relation to the damper velocity can be observed in figure 6.7.

$$J = \int_0^T |F_{test}(t) - F_{simulation}(t)| dt \quad (6.2)$$

Table 6.3: Parameters of the genetic algorithm used for valves parameters identification

Parameter name	Value
Population size	40
Reproduction ratio	70
Number of generations	20
Mutation probability	8%

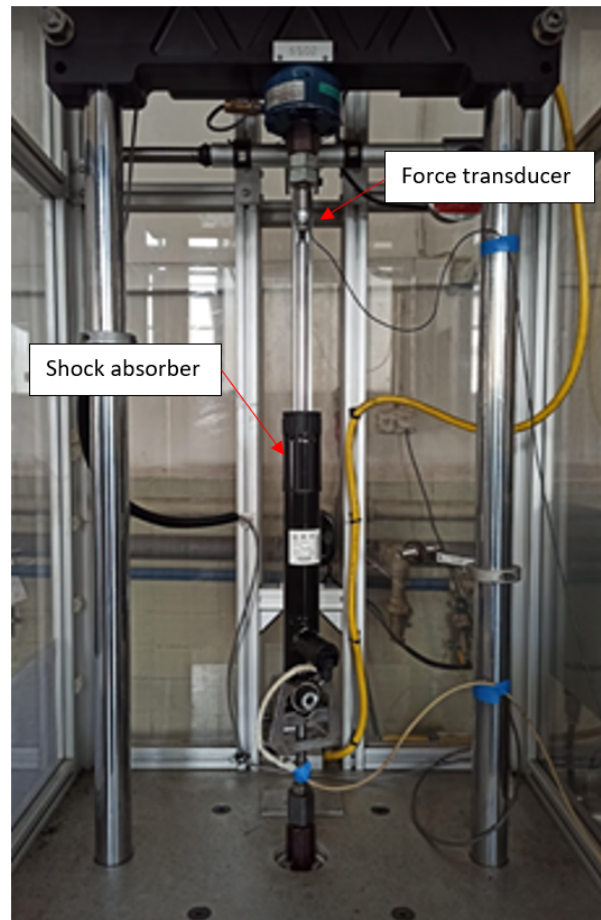


Figure 6.6: Experimental test set-up used for damper level tests

### 6.3.2 Results of the compliance estimation

Based on the performed parameter estimation process, it was established that the amount of the undissolved gas in the oil equals approximately 0.35% whereas the bulk modulus of the oil should equal 7.7kbar. Using those estimates as values of the model parameter, simulation results are compared with the measured force signals in figure 6.8 and for clearer comparison in figure 6.9 where only one cycle can be seen. As it can be observed in figures 6.7b, 6.8 and 6.9, the bulk modulus and gas content mainly influence the hysteresis in the force-velocity curve but the slope of the force-displacement graph during rebound stroke is also heavily affected.

## 6.4 Calibration of top mount related parameters

### 6.4.1 Description of the methodology

As indicated in section 4.5, the top mount dynamic behavior is represented with the AutoBushFD model available in Altair MotionView MBS package. Although this soft-

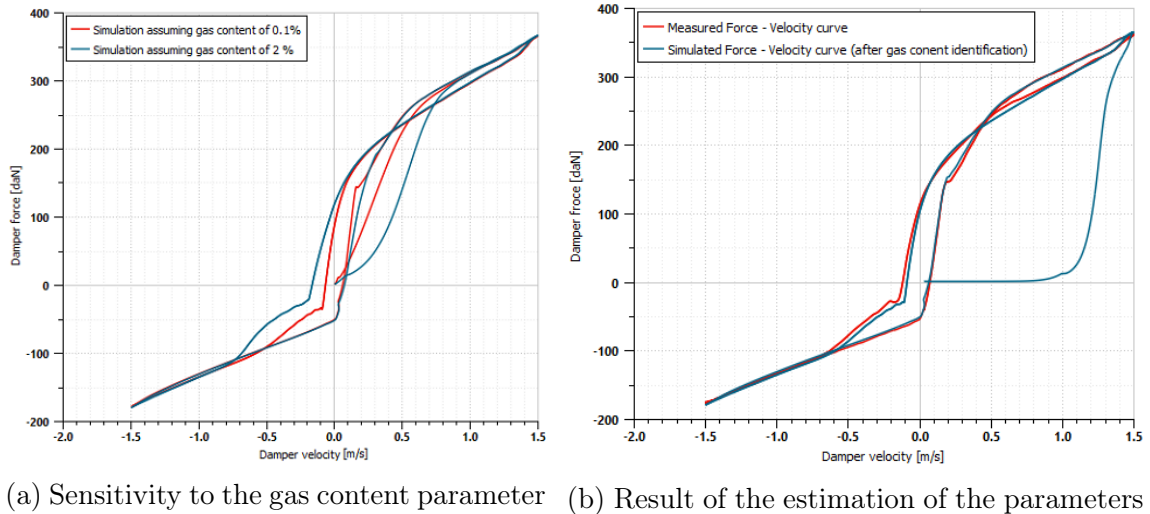
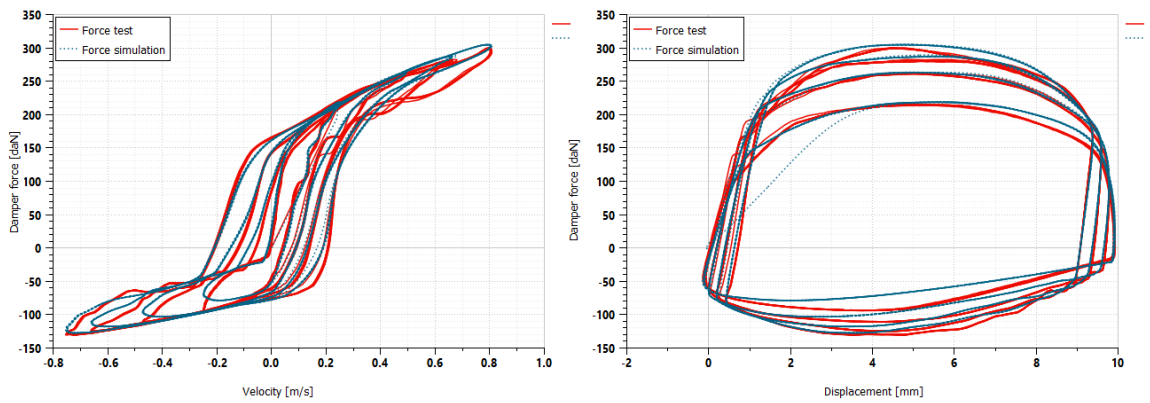
Figure 6.7: Impact of gas content over the shock absorber force-velocity characteristic<sup>2</sup>

Figure 6.8: Results of the compliance-related parameter estimation process - all acquired cycles

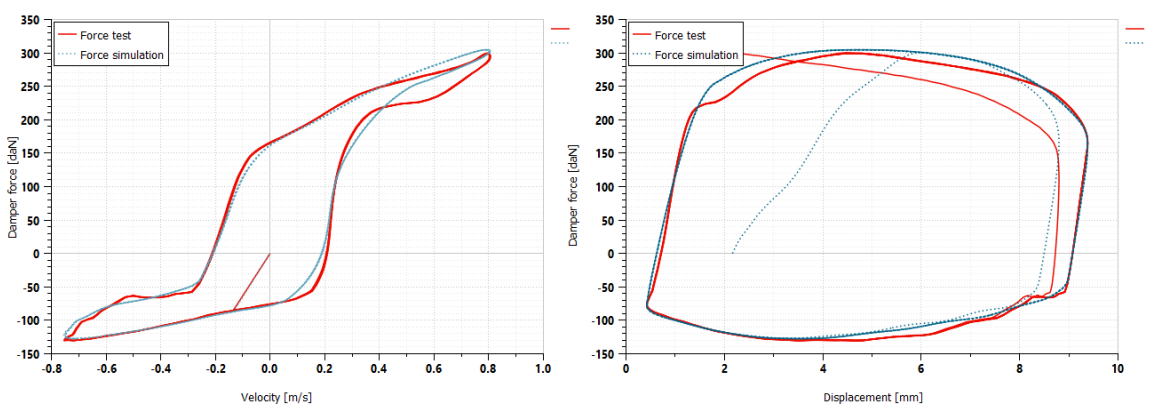


Figure 6.9: Results of the compliance-related parameter estimation process - one cycle

ware provides a ready-to-use environment for parameter identification, for practical reasons, it has been chosen to calibrate the parameters using a genetic algorithm. Such an approach might require more iterations but due to the highly exploratory character of

Table 6.4: Summary of the top mount model parameters and the limits used for the calibration process

Parameter name	Lower limi	Upper limit
R	1.0E-06	1000
P0	0.5	10
K1	0.1	20000
C2	0	10
C0	0	700
P1	-10	10
P2	0.01	2
Q1	-10	10
Q2	0.01	2
K0	0	10000
Q0	0.5	10
K2	0.1	100
C1	0	1000

the optimization algorithm, it is more reliable in providing a satisfactory level of model calibration. Additionally, this approach offers higher flexibility in the form of the data that can be used for the calibration, for instance, the training data can be supplied in the form of real measured time domain signals (this is the method used for this application) or synthesized based on the provided dynamic properties characteristics. Similar to previous subsystems, the calibration procedure was performed by comparing the time domain results of the simulation and test results. Minimization of a residual between these values constituted an objective function (see eq. 6.3). Parameters subject to the calibration procedure together with the bounding limits have been summarized in the table 6.4.

$$J = \int_0^T |F_{test}(t) - F_{simulation}(t)| dt \quad (6.3)$$

In terms of experimental data, for the considered top mount bushing designs the dynamic properties (dynamic stiffness and loss angle) in the function of frequency and amplitude were available from the external laboratory measurements. Additionally, time-domain random excitation data were also available. Experimental measurements of the dynamic properties of the bushing in the function of frequency usually require specialized testing machines and equipment which typically are not part of the shock absorber suppliers laboratory. Therefore, from the perspective of the future practical application of the developed simulation method, the necessity of obtaining such measurement results might be an important limiting factor.

## 6.4.2 Results of the calibration process

Results of the simulation performed with calibrated models of the top mount together with the experimental measurements results that have been used for this calibration procedure have been shown in figures 6.10a and 6.10b for the baseline design and in figures 6.11a and 6.11b for the alternative top mount design (higher stiffness design).

Dynamic properties have been measured at three amplitudes: 0.02 mm, 0.1 mm and 1 mm. Due to the limit of the excitation energy on the test machine, at higher amplitudes (1 mm) the dynamic properties were only measured up to  $\sim 20$  Hz. This is acceptable since under realistic loading conditions originating from the shock absorber operation it is unlikely that excitation would excite this level of signal power.

For both top mount design cases (that were part of the considered one-factor-at-a-time experiment), at lower amplitudes of excitation (0.02 mm), the dynamic stiffness is underestimated, while higher amplitudes (1 mm) are overestimated. In terms of the loss angle, although the simulated frequency dependency differs from the experimental measurements the nominal values remain close to the measured ones. The correct trend of the loss angle dependency on the amplitude is reproduced only at lower amplitudes.

Nonlinear, static load deflection curves (compared in figure 6.14) were not subject to the parameter calibration procedure but instead were directly derived from the experimental measurements. This simplifies the calibration procedure however any discrepancies in the obtained static characteristic might impact the quality of the calibration of the dynamic properties.

In order to confirm that the models have not been overfitted to the provided training data, verification tests and simulations have been also performed. Results of the comparison between test and simulation in both time domain and frequency domain have been shown in figures 6.12a and 6.12b for the baseline design and in figures 6.13a and 6.13b for the alternative design.

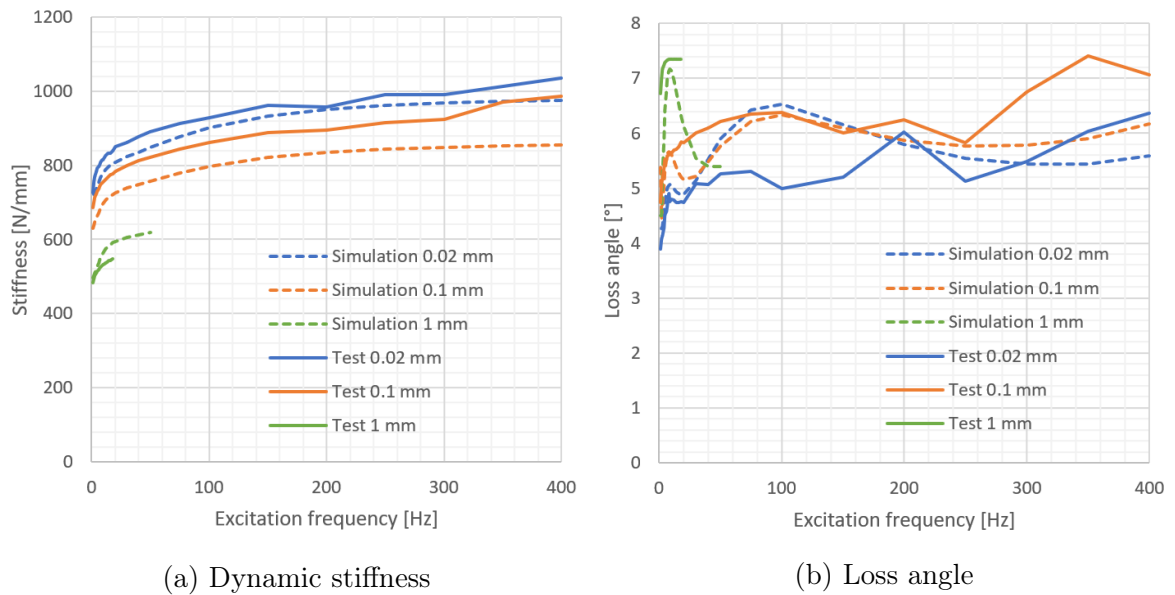


Figure 6.10: Dynamic properties in function of the frequency of the baseline top mount, obtained from the calibrated simulation and test results at different excitation amplitudes

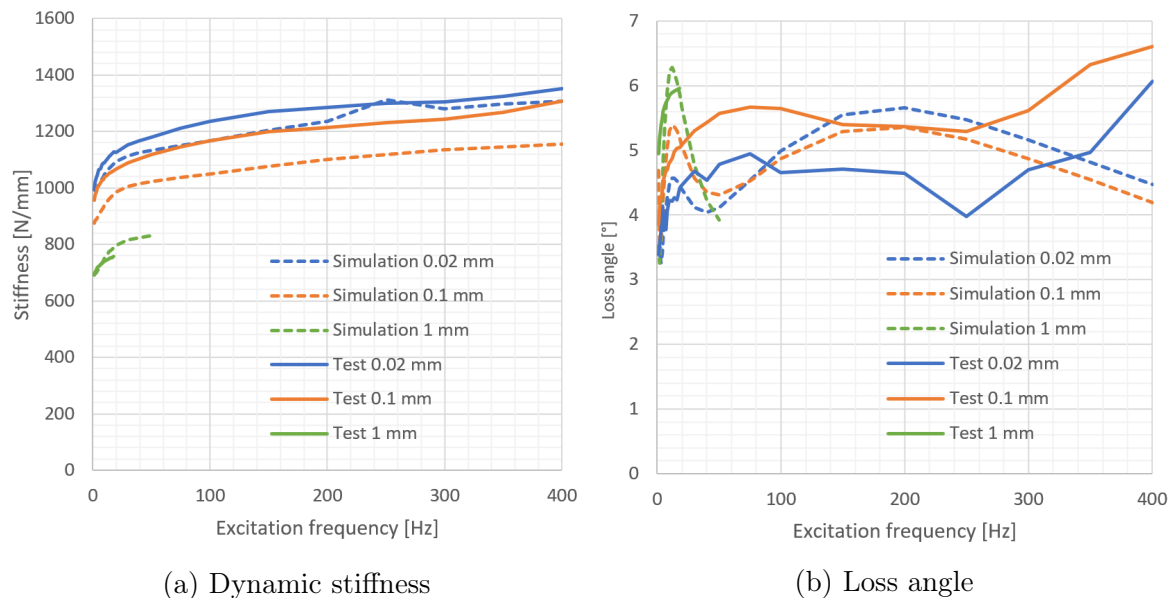
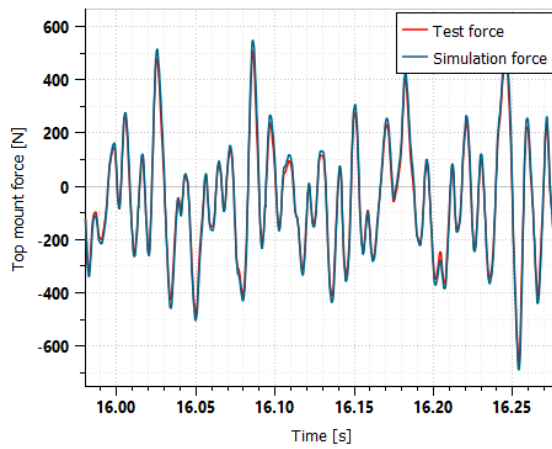
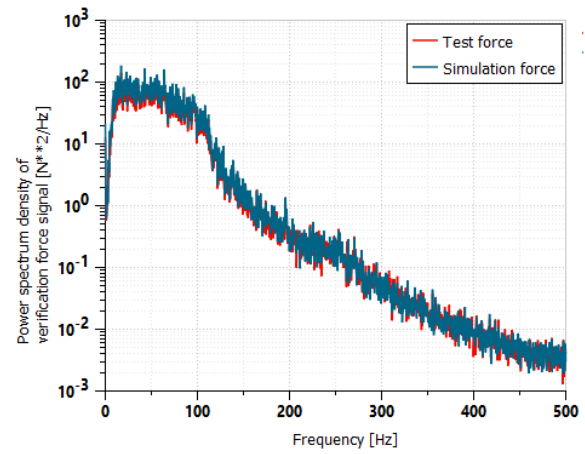


Figure 6.11: Dynamic properties in function of the frequency of the alternative design (high stiffness) top mount, obtained from the calibrated simulation and test results at different excitation amplitudes

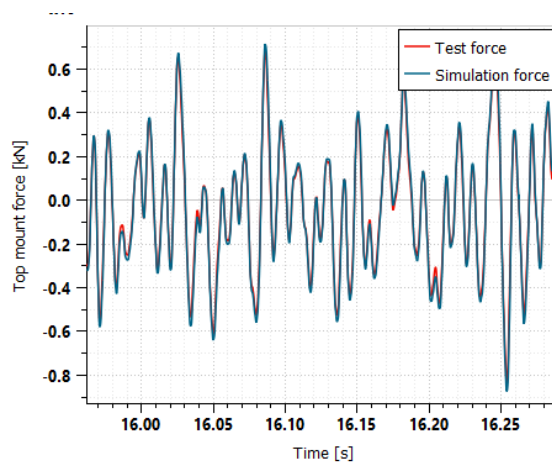


(a) Time domain force comparison

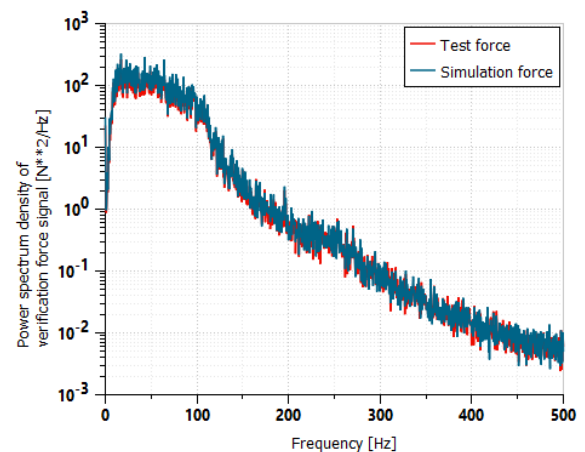


(b) Frequency domain comparison

Figure 6.12: Comparison of the baseline top mount force obtained from simulation and test under random verification excitation



(a) Time domain force comparison



(b) Frequency domain comparison

Figure 6.13: Comparison of the alternative design top mount force obtained from simulation and test under random verification excitation

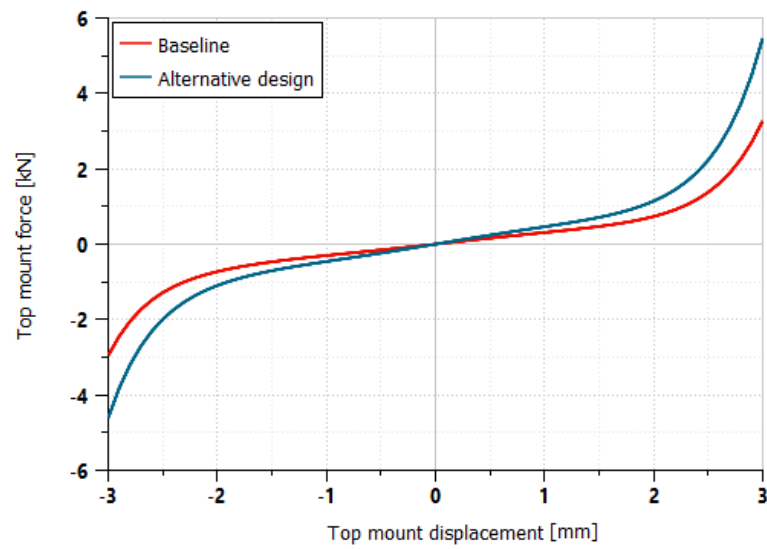


Figure 6.14: Comparison of static load-deflection characteristics ( $F_{LD}(X)$  in equation 4.37) for the baseline and alternative top mount designs

## 6.5 Assessment of the model quality based on experimental measurements

The main goal of the comparison described in this section is to establish the level of agreement between damper and module (shock absorber + top mount) level simulation and test results when the parameters of the model are characterized in an isolated manner (each subsystem separately).

For this purpose series of shock absorber and modular assembly tests were performed according to the standard procedure described in detail in section 2.7. These standard test procedures were performed on take-apart (disassemblable) samples of the design described in section 6.1, at the internal laboratory of the industrial partner company and included the following test:

- low-frequency shock absorber performance (curving tests) carried out using test set-up in figure 6.15a, according to the procedure described in section 2.7.1
- high-frequency time domain test using sine excitation (13Hz at 5mm amplitude) carried out using test set-up in figure 6.15b, according to the procedure described in section 2.7.3
- high-frequency, frequency domain using typical road excitation (see figure 2.15) carried out using test set-up in figure 6.15b, according to the procedure described in section 2.7.3

After the experimental measurements, each test has been recreated using the numerical model described in section 4 and parameters that were obtained from calibrations described in sections: 6.2, 6.3 and 6.4.

Due to the fact that during the physical experiment, the prescribed target excitation signal is always deformed to a certain degree by the dynamics of the test machine and control algorithm, for each test case, the true displacement signal has been measured. This registered displacement of the shock absorber tube was used as an input to the simulation. After the numerical analysis, the results are compared in subsequent paragraphs of this section.

Since a semi-active shock absorber is considered in this work, the results are presented including variation in the active valve current. As described in the section 2.4.3, the higher the electrical current supplied to the active valve, the higher the restriction to the flow created by that valve. This means that for given shock absorber excitation conditions (most importantly velocity), the flow through the passive shim valves is proportional (non-linearly) to the supplied current. As it can be observed in figures 6.17 - 6.19, this causes the high-frequency rod accelerations to be most pronounced at the high current signal. Due to a large number of the results combinations, the impact of the specific design changes is analyzed only at high current excitation.

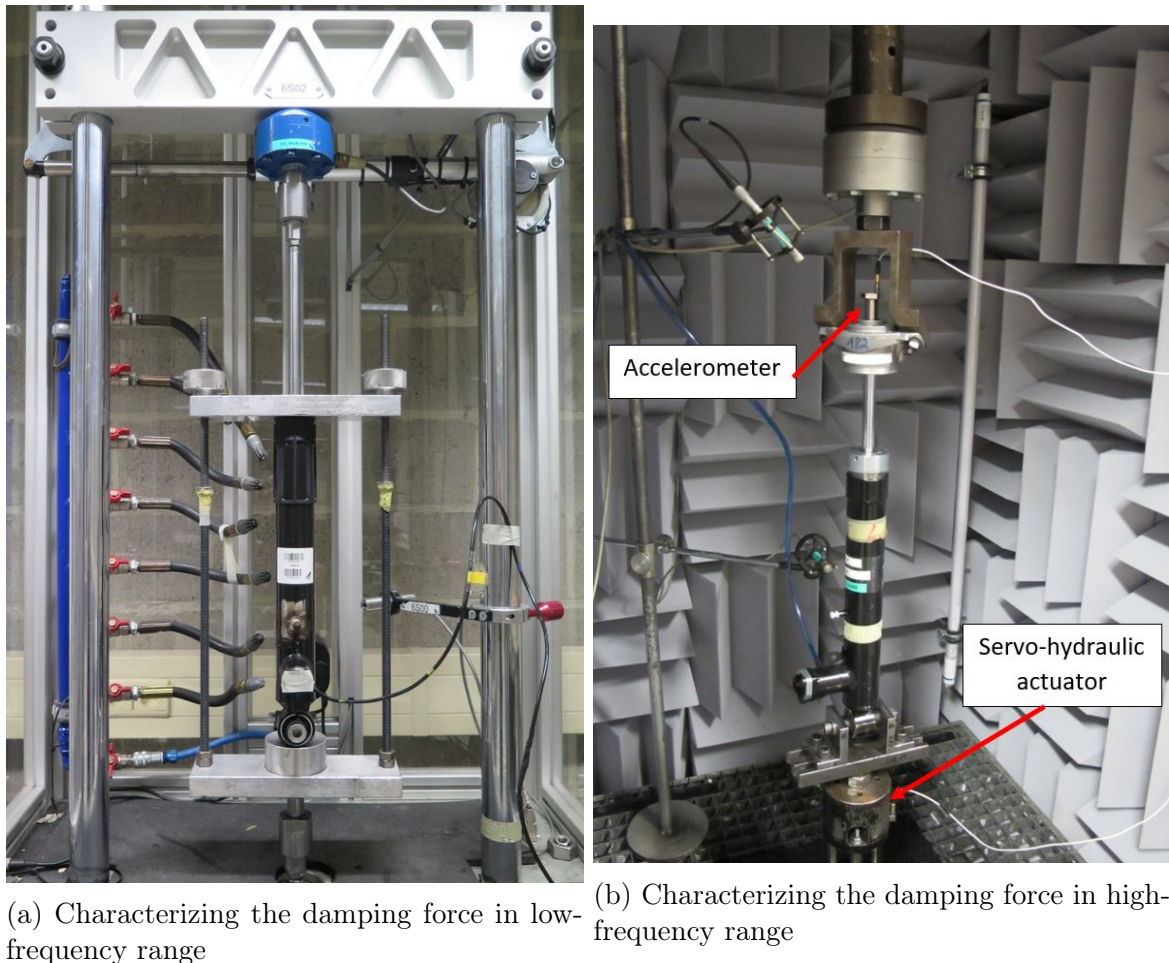


Figure 6.15: Test bench used for the experimental measurements

### 6.5.1 Results of the comparison

The first set of results allows for establishing how well, the numerical model is capable of reproducing the low-frequency behavior at large strokes of the damper (usually  $>50\text{mm}$ ). These are important characteristics since they impact directly the dynamic properties of the vehicle.

As demonstrated in figures 6.17, 6.18, 6.19, the model can accurately reproduce this part of the damper behavior. However, in the considered example, at higher excitation velocities ( $>1\text{m/s}$ ) and low flow through the passive shim valves, significant discrepancies can be observed (figures 6.17 and 6.18) in forces coming from the simulation and test. This can originate either from inaccurate active valve restriction or due to the base valve intake characteristics that are not measured correctly at large valve openings. Given that for the high current excitation, the mid-range velocities ( $0.5\text{m/s}$ ) are overestimated by the model, this discrepancy most likely originates from the active valve characteristics being distorted. However, due to good agreement between the test and simulation at high velocities and high current, it might be concluded that the discrepancy is not caused by

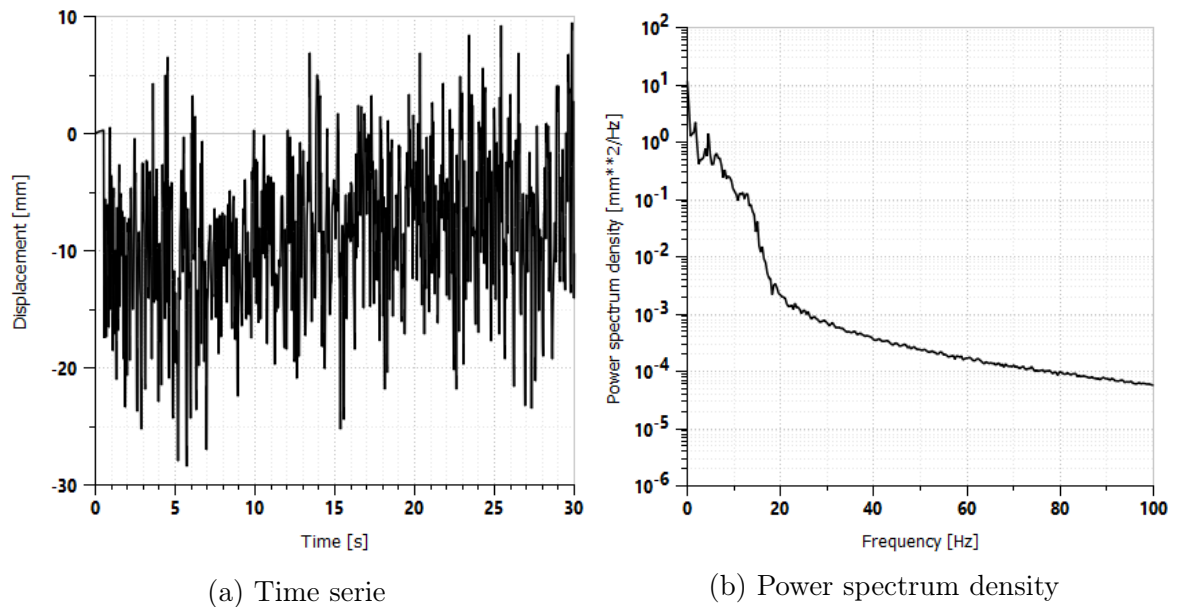


Figure 6.16: Random noise signal used as an excitation reproducing vibration of the wheel knuckle

the unaccounted-for leakage at the active valve.

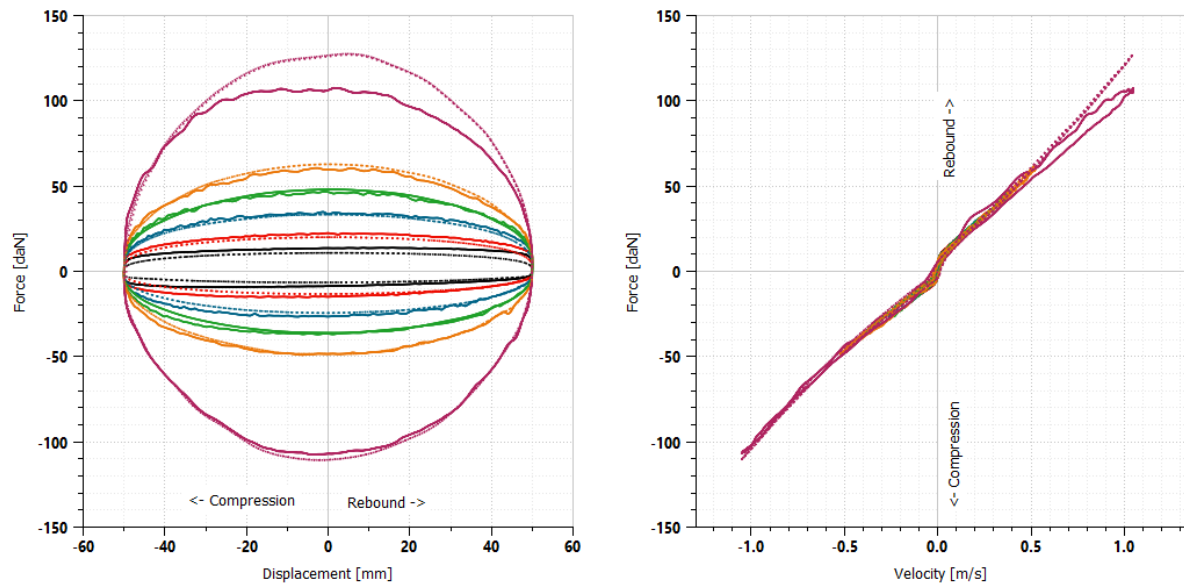


Figure 6.17: Curving test results at low active valve coil current (0.32A)  
Solid line: test results, dotted line: simulation results

The second type of experimental verification is oriented on measuring the shock absorber's rod acceleration during low-frequency excitation at a relatively low stroke (13Hz at 5mm amplitude) which typically corresponds to the unsprung mass natural frequency of the wheel (secondary ride mode). By analyzing the results in the time domain it is possible to observe rod vibrations caused by specific stages of the damper operation.

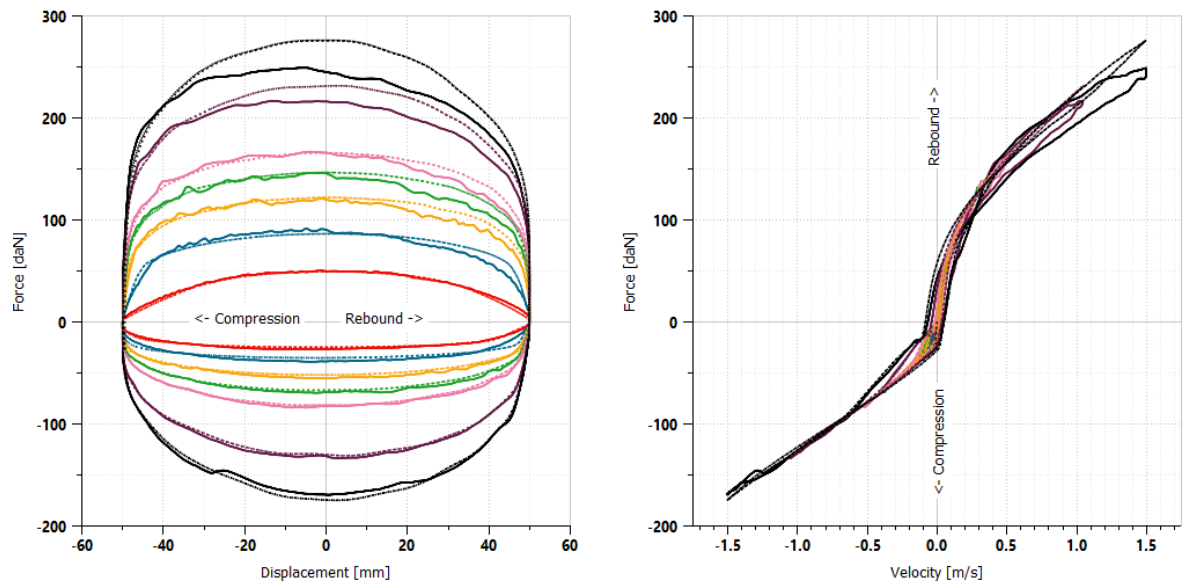


Figure 6.18: Curving test results at medium active valve coil current (0.9A)  
Solid line: test results, dotted line: simulation results

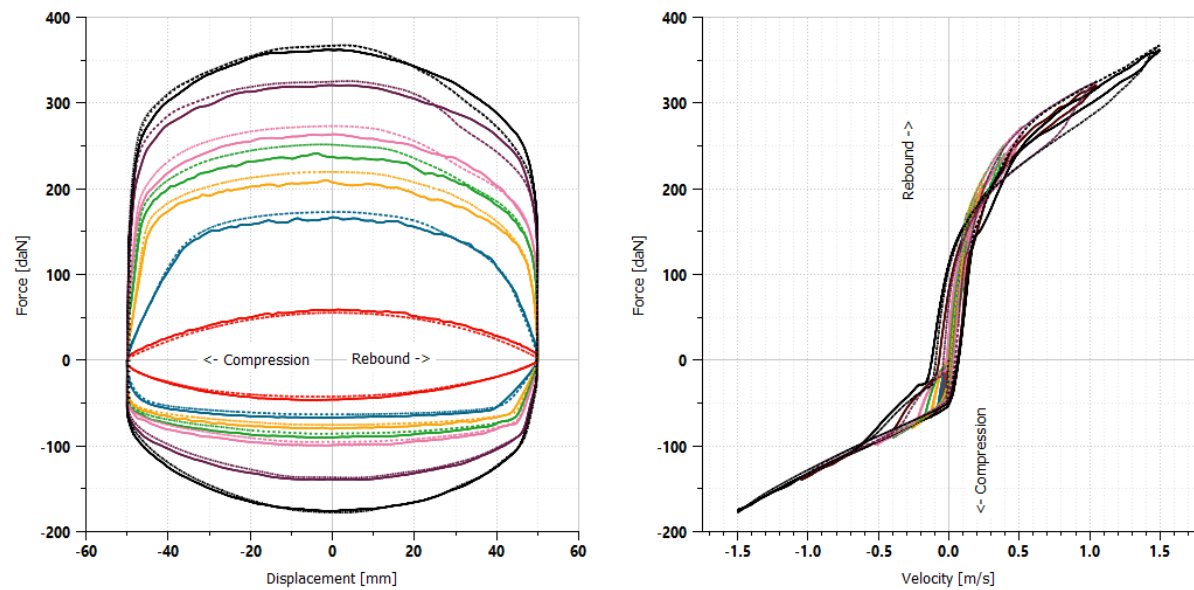


Figure 6.19: Curving test results at high active valve coil current (1.6A)  
Solid line: test results, dotted line: simulation results

At low active valve current, due to low flow through the active valves as well as the low influence of the compliance, all valves opening and closing happen at similar stages of the damper operation. For that reason, it is easier to observe the impact of the valves over the rod acceleration of the damper under a high active valve current (see fig. 6.20). In figure 6.20 rod acceleration together with passive valve openings can be visible. The first distinguishable disturbance in the rod acceleration (right before 1.06 s in fig. 6.20) originates from the closing of the piston intake valve. Later (at approximately 1.073 s), as

the damper is in the rebound stroke, the base valve intake opens abruptly. This induces a high level of vibration which attenuates up until the base valve intake closes. Right after the damper transitions to the compression stroke, the next distinguishable disturbance is caused by the piston rebound shim stack closing (1.100 s). Further at approximately 1.108 s during the compression stroke, the piston valve intake is opening. This causes a sharp acceleration peak of the rod. As it can be concluded from the above study, the main source of the high rod accelerations are openings of the intake valves. Due to the fact that shim valves are opening slowly, dynamic effects related to them are much lower.

In terms of comparison of the simulation and test results, for each of the active valves' current levels (see figures 6.20, 6.21 and 6.22 ) the effects of valves openings and closings are reproduced by the model. However, the magnitude of the estimated rod acceleration peaks noticeably differs from the measured values. The disturbance caused by the base valve intake is slightly underestimated by the calibrated model whereas the piston intake peak is substantially overestimated. This relation holds true for each of the active valve currents cases.

The comparison with the alternative top mount design in figure 6.23 shows a similar pattern when it comes to the rod acceleration between simulation and experiment. Since the alternative top mount design decreases the magnitude of the rod acceleration, the simulation results should also predict lower values. That is, however only for the base valve intake peak. The simulated piston peak opening, slightly increases which might indicate wrong parameterization of the piston intake valve. By analyzing figures 6.24 and 6.25 it can be concluded that increased pressure as well as changes to the active valve are not causing significant changes to the rod acceleration signal. This is also confirmed by the frequency domain signals in figures 6.32 and 6.33. On the other hand, both measurements, as well as simulation, show a high sensitivity of the piston intake peak to the intake valve stiffness (fig. 6.26). Most importantly, correct relations can be observed for both of these cases. For the piston rebound shim valve, the model is too sensitive to the change when compared with test results (figure 6.27). A highly consistent response of the simulation can also be observed in figures 6.28 and 6.29 where base valve intake and base valve shim stiffness changes were considered.

In terms of the high-frequency test of random noise excitation, the influence of the different active valve currents is captured by the simulation (see figure 6.30), however, the medium current (0.9A) is substantially overestimated by the model. For all the considered cases, the frequency range 100-300Hz which is important for the structure-borne noise is overestimated by the model. This issue can be clearly observed in figure 6.34 where simulation of piston intake with lower stiffness produces an artificial peak at approximately 200Hz, a similar effect but to a lower degree can be observed in figure 6.31 for alternative top mount design. Similarly, as in the time domain analysis, the impact of passive valve stiffness changes is captured with the proper trend by the simulation per-

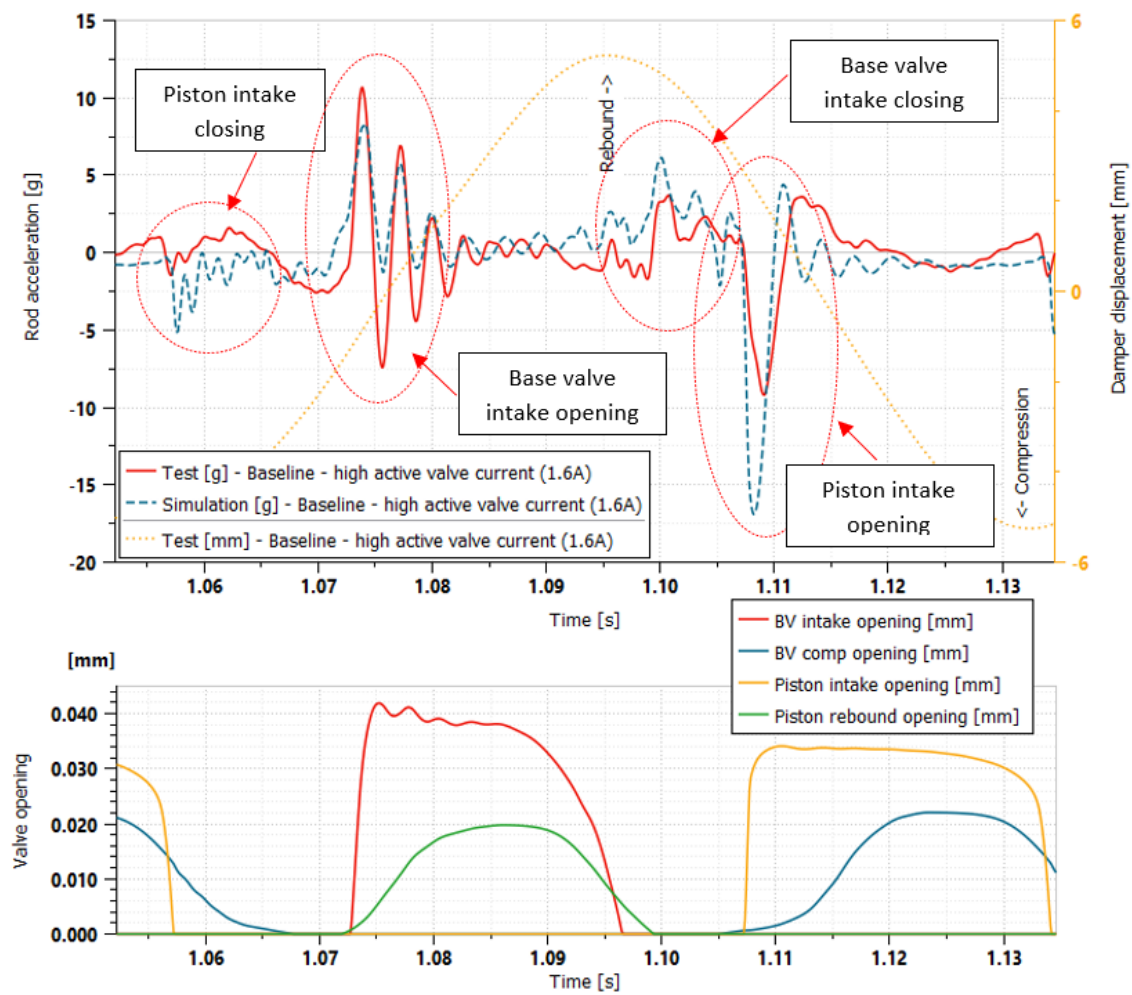


Figure 6.20: Comparison of the test and simulation results of the mono-sine test (13Hz excitation at 10mm of stroke) for high active valve current (1.6A)

formed under noise excitation but the magnitude of these changes is noticeably different from the measurements.

## 6.6 Conclusions

The goal of the exercise was to investigate how accurately the model which was calibrated using isolated test set-ups is capable of reproducing the results of standard experimental procedures that are used in the industry to assess various dynamic aspects of the shock absorber operation (as discussed in 2.7). In order to achieve that goal, as a first step, parameter calibration was performed for the critical parameter groups and different design configurations. The calibration process included:

- Experimental measurements of 8 different valve designs to derive their P/Q characteristic which was later reproduced using the isolated model. For each valve

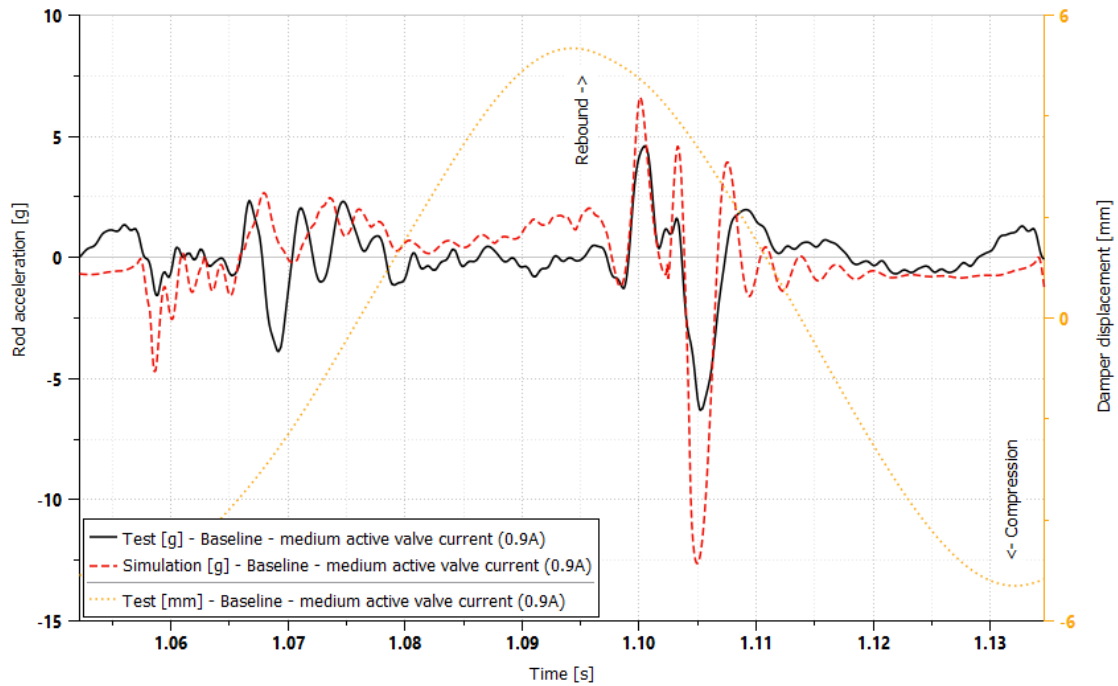


Figure 6.21: Comparison of the test and simulation results of the mono-sine test (13Hz excitation at 10mm of stroke) for medium active valve current (0.9A)

Table 6.5: Summary of the mono-sine test results comparison of the test and simulation

no.:	Design case	Active valve current [A]	Rod acceleration peak at rebound stroke			Rod acceleration peak at compression stroke		
			Simulated [g]	Measured [g]	Diff. [%]	Simulated [g]	Measured [g]	Diff. [%]
1	Baseline	1.6	8.1	10.7	23.7	-16.9	-9.2	-83.1
2	Baseline	0.9	-4.7	-1.3	-247.4	-12.6	-6.1	-105.0
3	Baseline	0.32	2.4	4.5	45.6	-2.3	-2.7	-15.5
4	Alternative top-mount design	1.6	6.9	8.3	17.0	-15.9	-10.9	-46.4
5	Increased precharge pressure	1.6	10.0	10.2	1.9	-16.6	-9.5	-73.7
6	Different active valve design	1.6	8.3	9.1	9.5	-16.3	-8.9	-83.6
7	Lower piston intake stiffness	1.6	7.7	10.9	29.6	-19.0	-12.3	-54.8
8	Lower piston rebound stack stiff.	1.6	8.6	10.7	19.6	-14.7	-9.6	-53.4
9	Lower base-valve intake stiff.	1.6	13.7	15.7	12.8	-16.1	-8.4	-92.1
10	Lower base-valve comp. stiff.	1.6	4.4	5.1	13.3	-15.7	-8.6	-83.2

measurement, the calibration procedure was performed (see section 6.2)

- Experimental measurement of the shock absorber assembly for the compliance-related parameter calibration (see section 6.3)
- Parameter calibration of two different designs of the top mount models (see section 6.4)

For the model quality assessment, 10 separate semi-active damper design configurations were measured using a low-frequency oriented test (detailed in section 2.7.1) and a

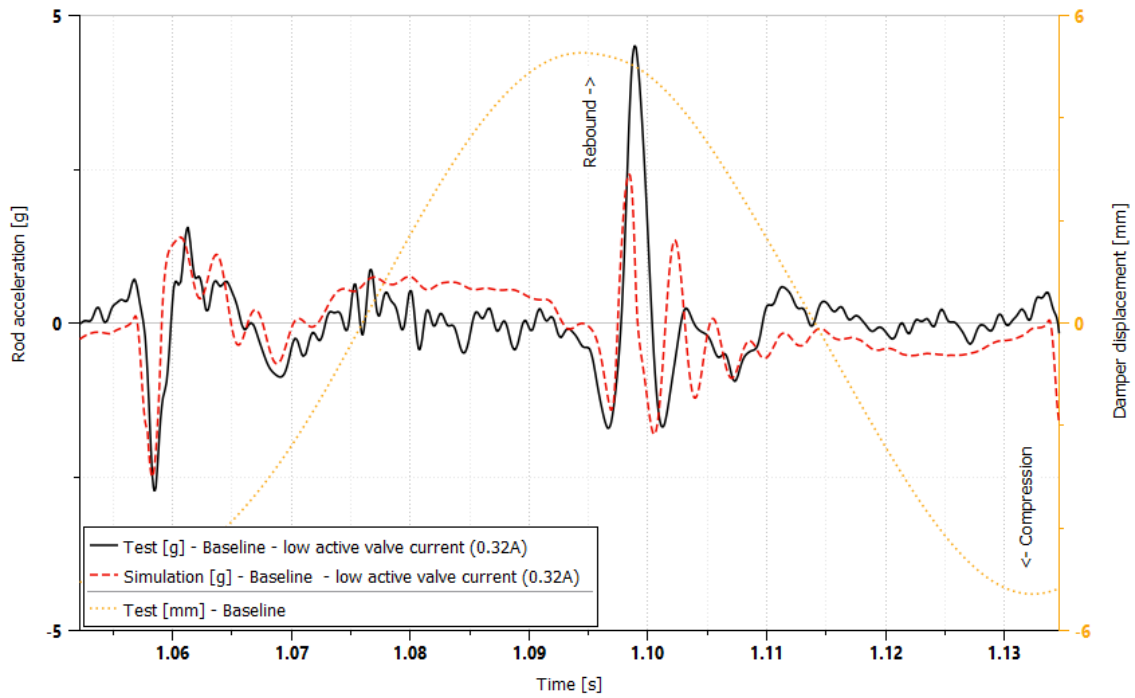


Figure 6.22: Comparison of the test and simulation results of the mono-sine test (13Hz excitation at 10mm of stroke) for low active valve current (0.32A)

Table 6.6: Summary of the random test results comparison of the test and simulation

no.:	Design case	Active valve current [A]	PSD of rod acceleration at 200Hz			PSD of rod acceleration at 300Hz		
			Simulated [dB]	Measured [dB]	Diff. [dB]	Simulated [g]	Measured [g]	Diff. [dB]
1	Baseline	1.6	-4.6	-7.6	3.0	-6.0	-5.2	0.9
2	Baseline	0.9	-5.4	-12.5	7.0	-8.8	-14.4	5.5
3	Baseline	0.32	-15.1	-16.2	1.1	-16.1	-19.3	3.2
4	Alternative top-mount design	1.6	-3.7	-6.1	2.4	-4.8	-5.2	0.4
5	Increased precharge pressure	1.6	-4.0	-7.5	3.5	-4.8	-6.2	1.4
6	Different active valve design	1.6	-4.6	-8.0	3.3	-6.1	-6.7	0.6
7	Lower piston intake stiffness	1.6	-1.9	-6.2	4.3	-6.3	-5.7	0.5
8	Lower piston rebound stack stiff.	1.6	-4.5	-7.3	2.7	-6.6	-5.4	1.2
9	Lower base-valve intake stiff.	1.6	-4.5	-6.9	2.4	-3.7	-3.1	0.6
10	Lower base-valve comp. stiff.	1.6	-4.9	-10.3	5.3	-8.1	-10.9	2.8

high-frequency test with two distinct excitation approaches (one for time domain analysis and one for frequency domain analysis, section 2.7.3). Each test has been recreated using the proposed model and parameters which were calibrated in this section.

**Conclusions regarding model assessment** From the perspective of assessing the quality of the calibrated model, the most important comparison is done for the rod acceleration since this is the quantity that is in most cases used for dynamic assessment

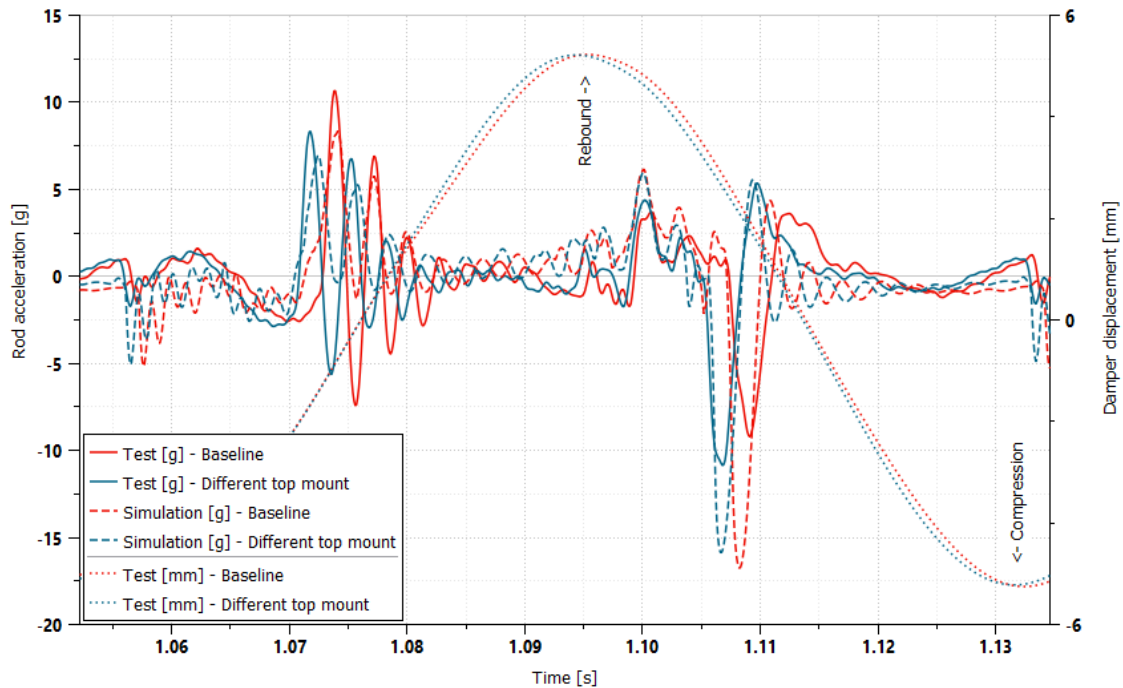


Figure 6.23: Comparison of the test and simulation results of the mono-sine test (13Hz excitation at 10mm of stroke) for baseline and alternative top-mount designs

purposes. Comparison of the experimental and simulation results of high-frequency tests which were done based on figures 6.20 - 6.37 and summarized in tables 6.5 and 6.6, indicates that the proposed model together with the calibration procedure is capable of reproducing the dynamic behavior of the semi-active shock absorber but in terms of nominal values of rod acceleration peaks, discrepancies are present. However, for nearly all the considered design cases, the trends in the rod acceleration peaks are reliably reproduced by the model. Similarly, when the results are analyzed in the frequency domain, as it can be observed based on the summary in table 6.6 in nominal terms, the model shows noticeable discrepancies in the frequency range of interest (0-500Hz) but the response to the design changes of the numerical model is correct. The most likely reason for these discrepancies in the peak values of the rod acceleration signals comes from the fact that the passive valves have been only calibrated at the static conditions. Additionally, inaccuracies may arise when tests are performed in an isolated manner due to the artificial conditions present in such circumstances. As an example, passive valves measured at the flow-bench machine do not include the realistic amount of undissolved gas content. This may negatively impact the quality of the calibration of the parameters. Given the observed quality of the model calibration and the deficiencies in the nominal values, the best application for the considered model and parameters estimation procedure is the comparative analysis approach. In future cases, newly developed designs should be compared with already tested and analyzed simulations to assess the risk of noise issues. In

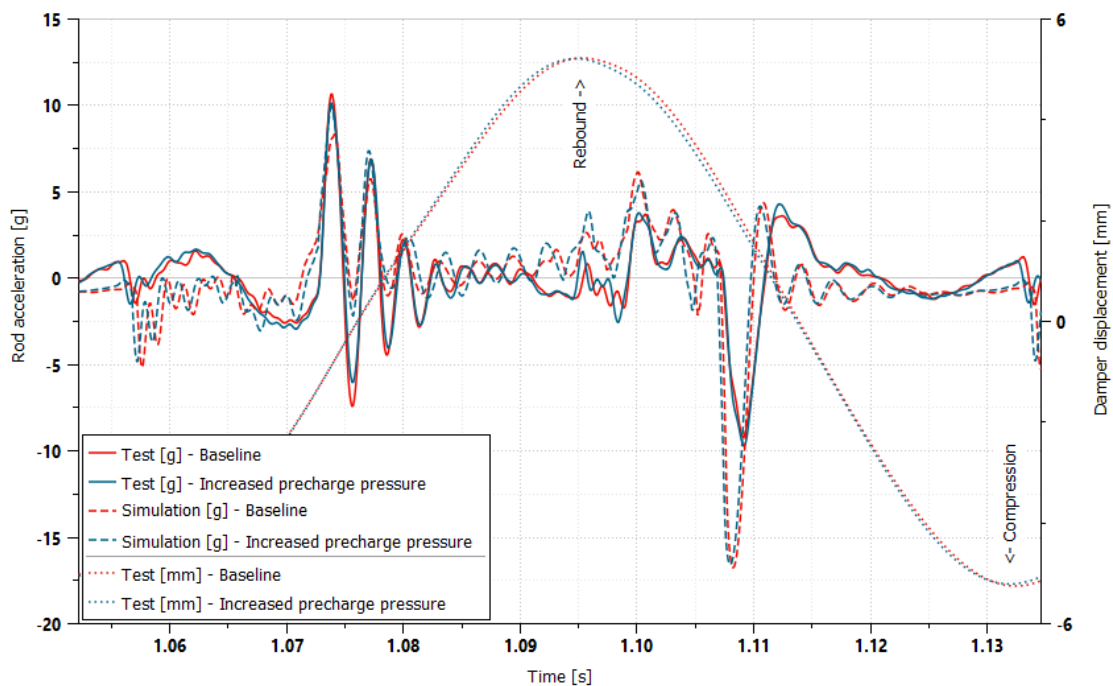


Figure 6.24: Comparison of the test and simulation results of the mono-sine test (13Hz excitation at 10mm of stroke) for baseline and increased precharge pressure (5 bar) scenario

terms of the low-frequency force comparison (performance test), despite the discrepancies at the high velocities and low active valve currents, the model predictions show overall good agreement with the experimental data.

**Conclusions regarding calibration process** Due to the detailed modeling techniques adopted for the model of the semi-active damper and therefore a large number of input parameters, the calibration process gains particular importance. As it can be observed based on the described procedures in this section (subsection 6.2 - 6.4) it involved multiple experimental measurements which have to be processed to be later used by the optimization algorithm. The overall process comprises multiple steps each requiring a different skill-set. From the perspective of practical application, such a chain of activities is difficult to introduce as a widely used engineering procedure. Although the model can be utilized using historical data or with theoretical values, a true assessment of the newly developed designs of subsystems requires a realistic characterization of its constituent parts. This can be achieved either by separate modeling tools or measurements and parameter calibration processes. As demonstrated in this section, each of the subsystems can be characterized using proposed methods but due to their complexity practical industrial implementation might pose organizational challenges. It is also emphasized that more sophisticated and accurate measurement and simulation methods are available for

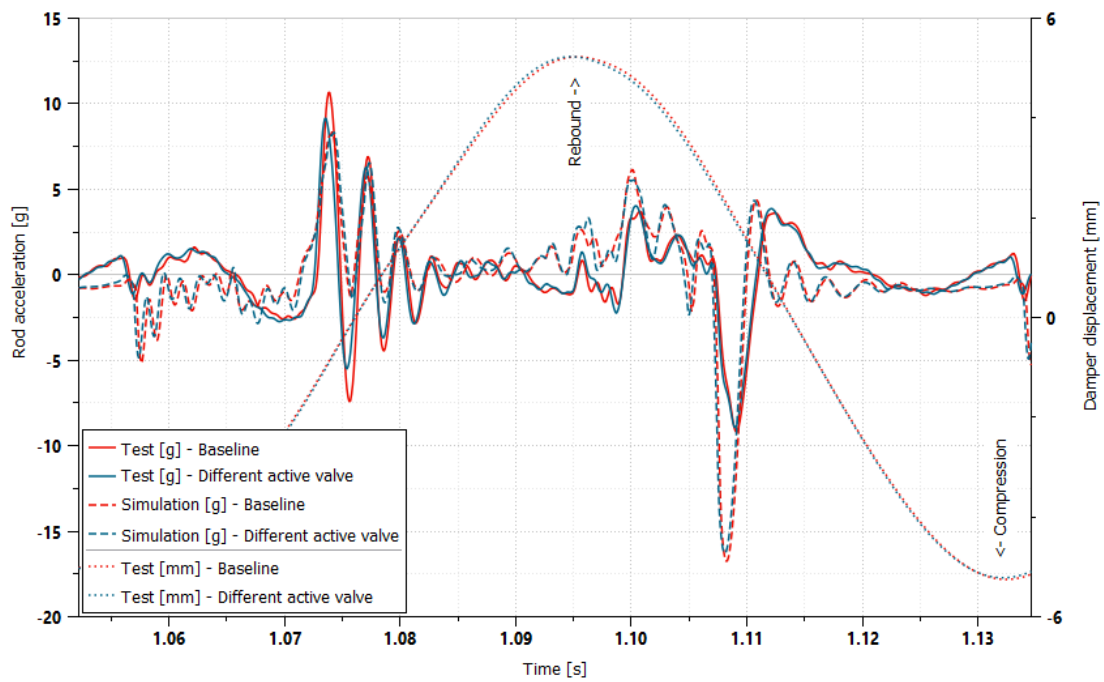


Figure 6.25: Comparison of the test and simulation results of the mono-sine test (13Hz excitation at 10mm of stroke) for baseline and different active valve designs

the parameter estimation process (e.g. pressure sensors placed in the damper chambers), however, the goal of this section was to observe the quality of the simulation when the proposed model is used with only the measurement methods that are currently available within the industrial environment.

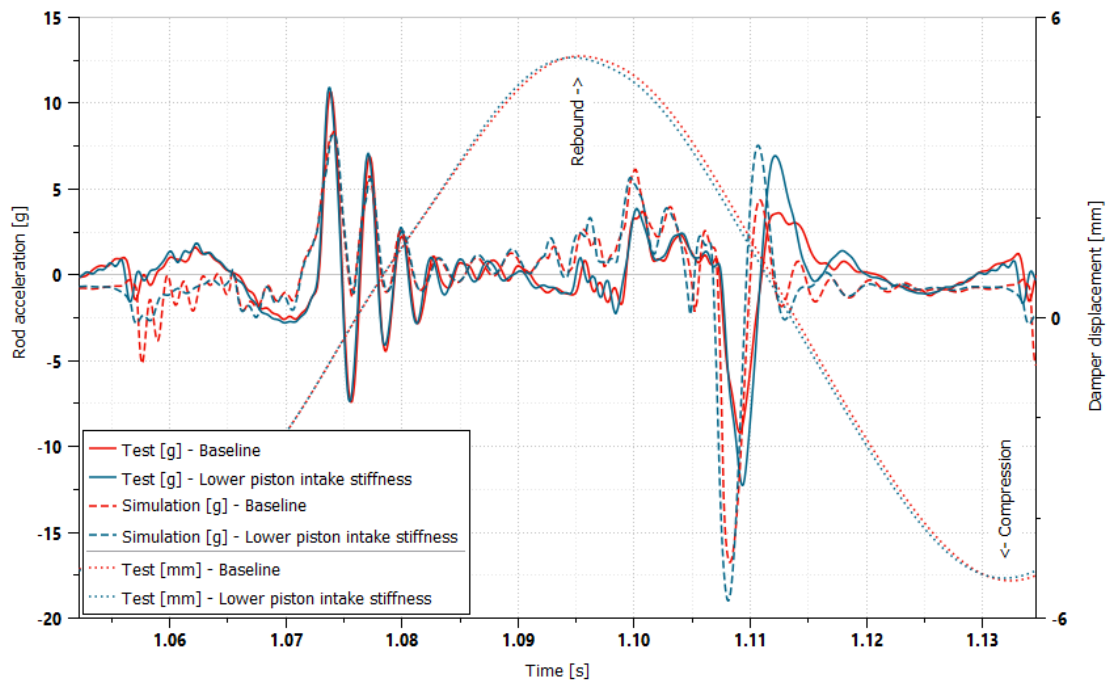


Figure 6.26: Comparison of the test and simulation results of the mono-sine test (13Hz excitation at 10mm of stroke) for baseline and lower piston intake stiffness (see fig. 6.3) designs

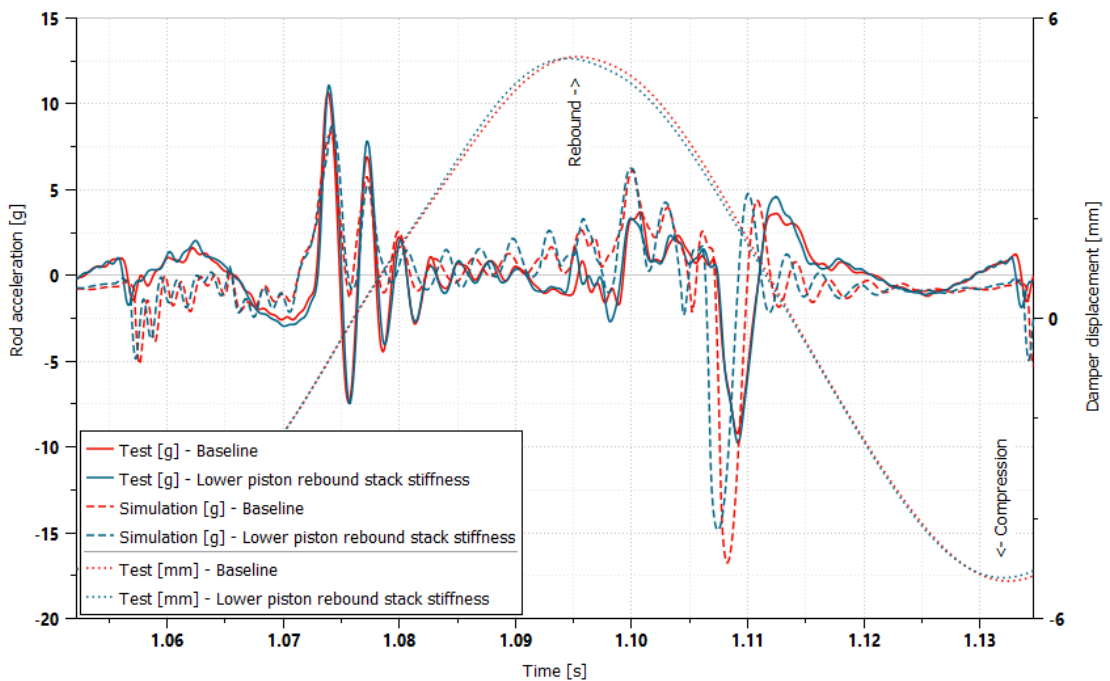


Figure 6.27: Comparison of the test and simulation results of the mono-sine test (13Hz excitation at 10mm of stroke) for baseline and lower piston rebound stack stiffness (see fig. 6.3) designs

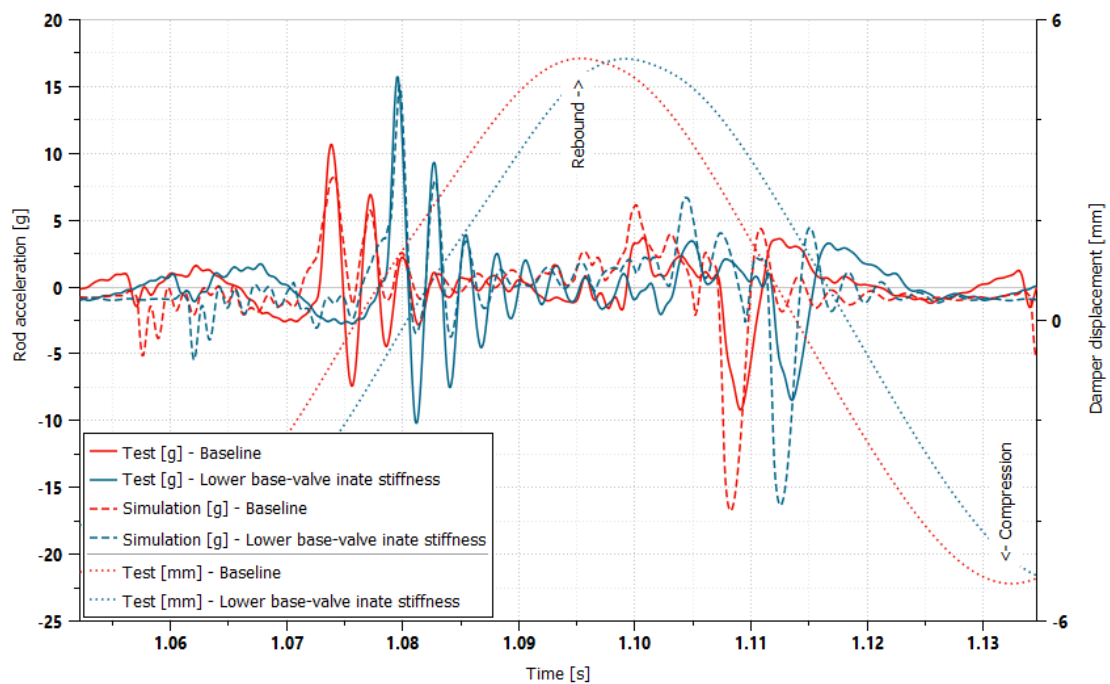


Figure 6.28: Comparison of the test and simulation results of the mono-sine test (13Hz excitation at 10mm of stroke) for baseline and lower base-valve intake stiffness (see fig. 6.3) designs

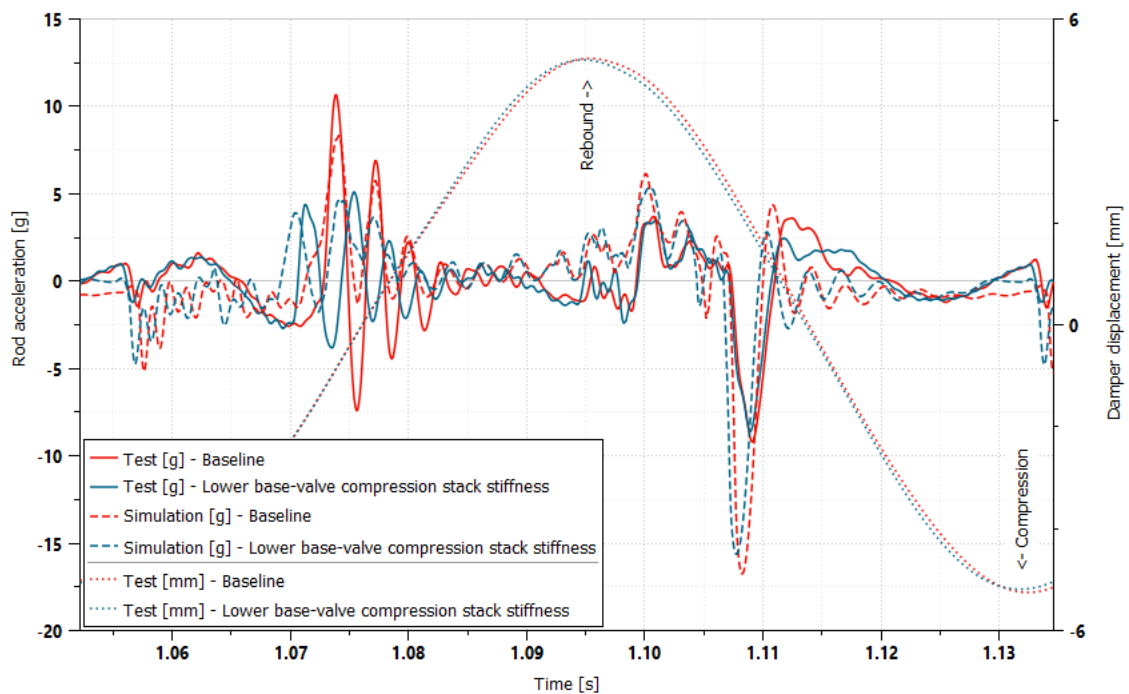


Figure 6.29: Comparison of the test and simulation results of the mono-sine test (13Hz excitation at 10mm of stroke) for baseline and lower base-valve compression stack stiffness (see fig. 6.3) designs

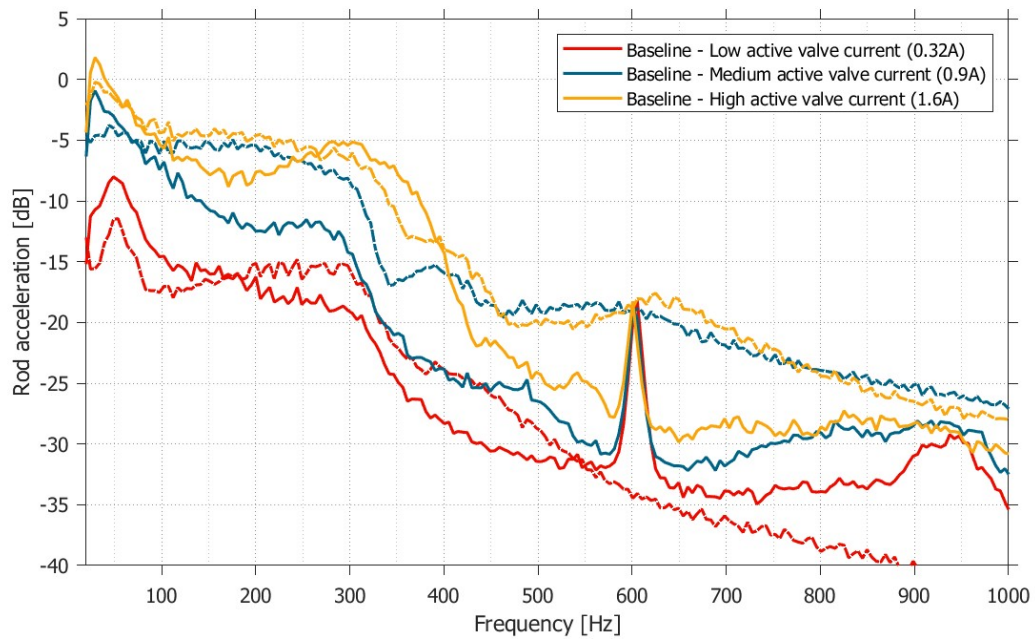


Figure 6.30: Comparison of the test and simulation of the random excitation signal test (see signal in fig. 6.16a and 6.16b) of different active valve currents

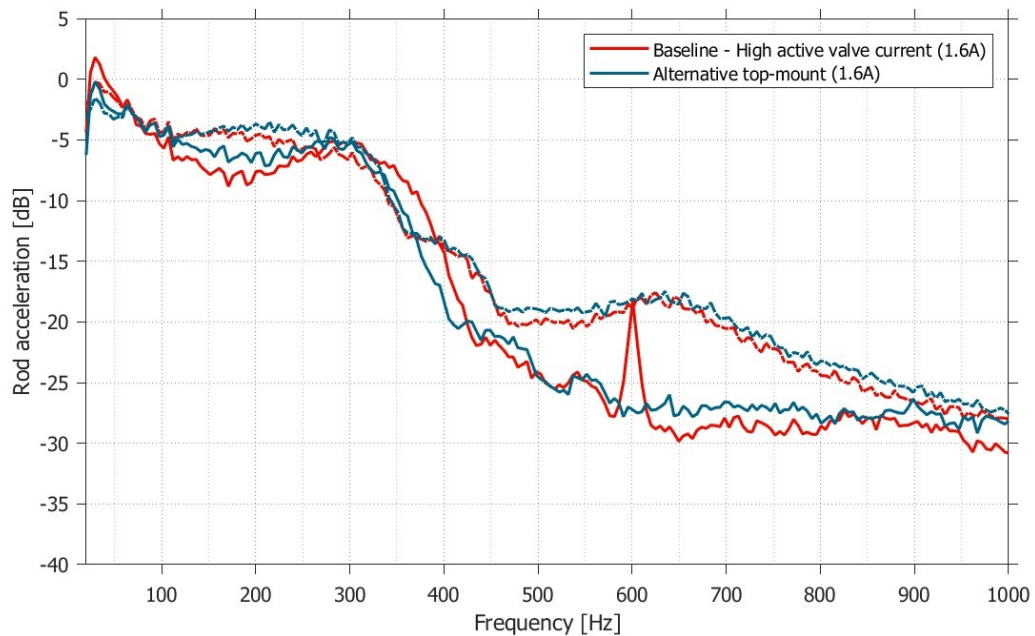


Figure 6.31: Comparison of the test and simulation of the random excitation signal test (see signal in fig. 6.16a and 6.16b) for baseline and alternative top-mount designs

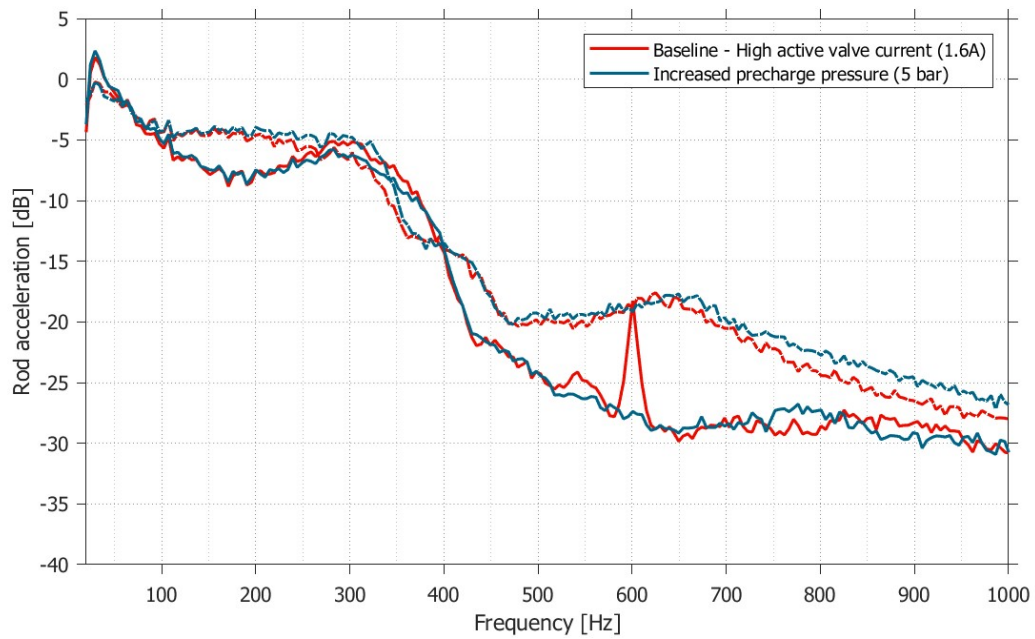


Figure 6.32: Comparison of the test and simulation of the random excitation signal test (see signal in fig. 6.16a and 6.16b) for baseline and increased precharge pressure (5 bar) scenario

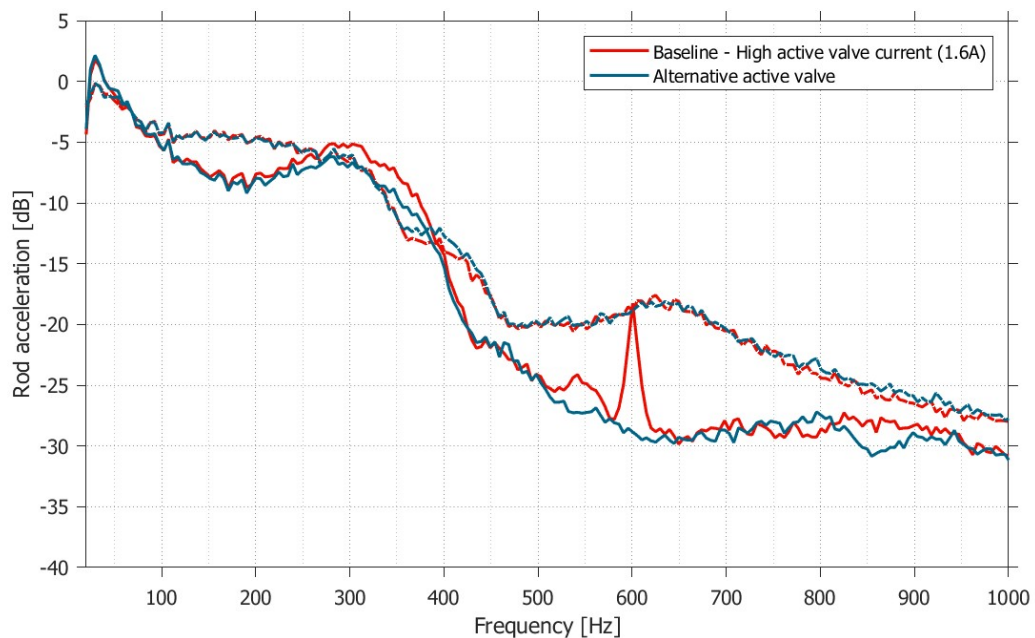


Figure 6.33: Comparison of the test and simulation of the random excitation signal test (see signal in fig. 6.16a and 6.16b) for baseline and different active valve designs

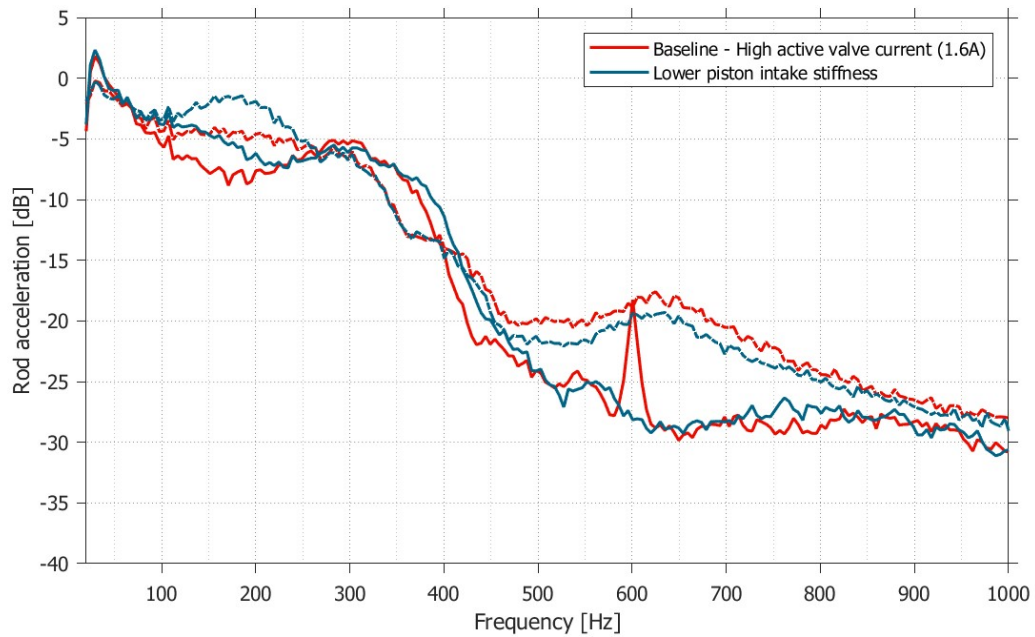


Figure 6.34: Comparison of the test and simulation of the random excitation signal test (see signal in fig. 6.16a and 6.16b) for baseline and lower piston intake stiffness (see fig. 6.3) designs

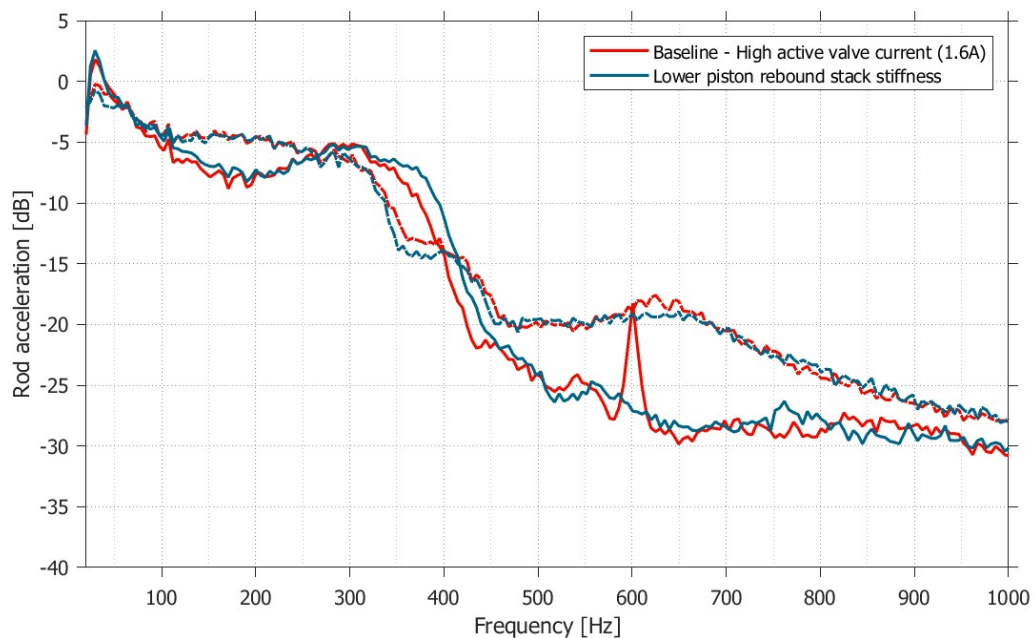


Figure 6.35: Comparison of the test and simulation of the random excitation signal test (see signal in fig. 6.16a and 6.16b) for baseline and lower piston rebound stack stiffness (see fig. 6.3) designs

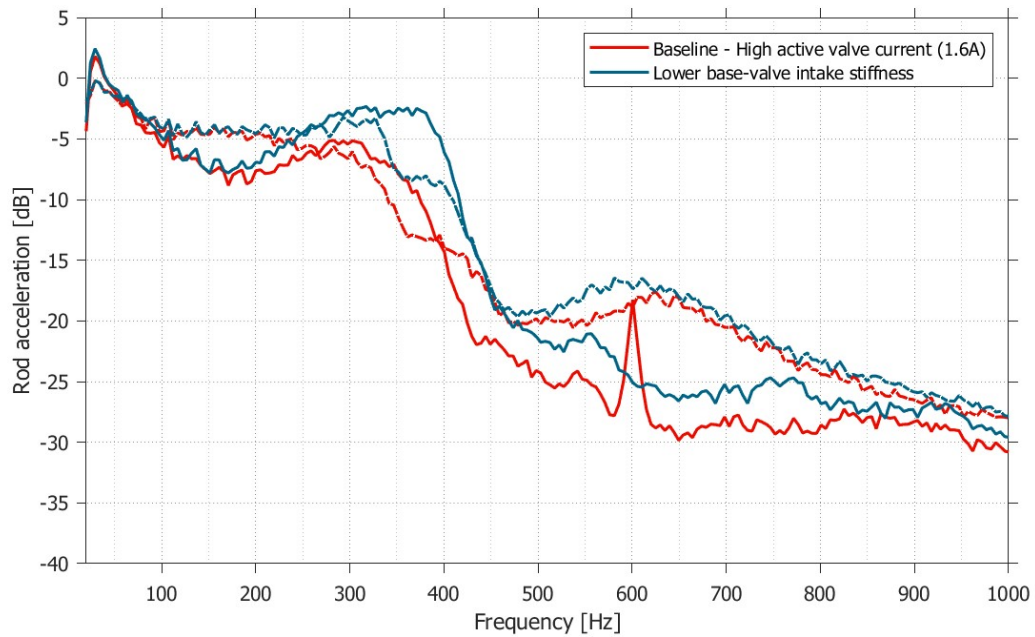


Figure 6.36: Comparison of the test and simulation of the random excitation signal test (see signal in fig. 6.16a and 6.16b) for baseline and lower base-valve intake stiffness (see fig. 6.3) designs

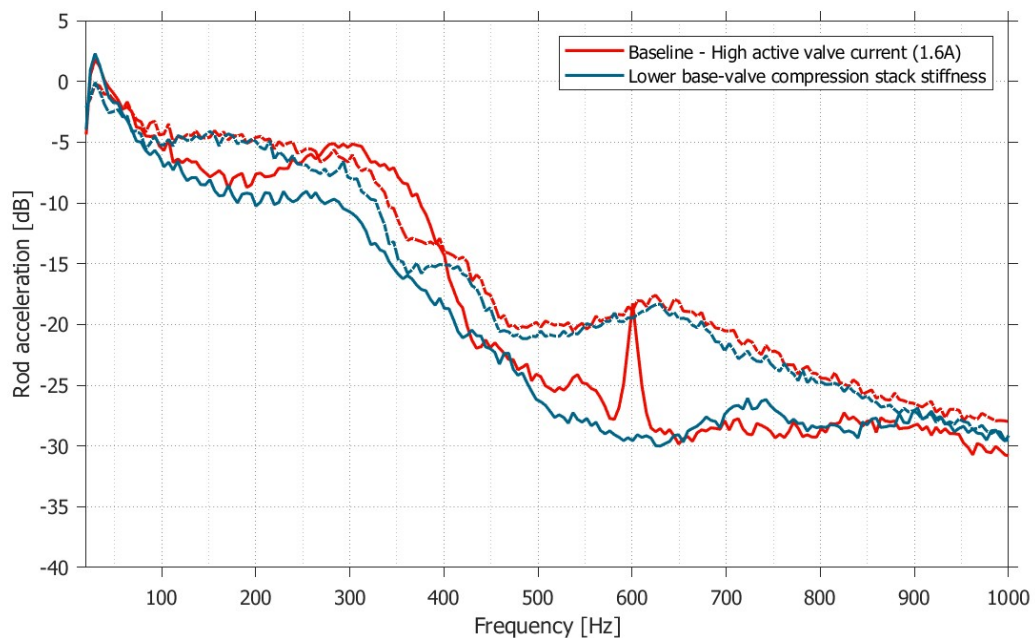


Figure 6.37: Comparison of the test and simulation of the random excitation signal test (see signal in fig. 6.16a and 6.16b) for baseline and lower base-valve compression stack stiffness (see fig. 6.3) designs

# Chapter 7

## Parameters calibration study – approach 2

As demonstrated in the previous chapters, the proposed damper model together with parameter calibration performed on isolated subsystems can be considered a useful tool that allows to assess the dynamic behavior of the semi-active shock absorber. However, due to the multiple measurements and separate parameter estimation algorithms, this process of parameter calibration is relatively complex if considered a standard industrial procedure. Additionally, due to the measurement inaccuracies at subsystem levels, in absolute terms, simulated results often do not match the measured rod acceleration values.

Therefore, in order to simplify the characterization process, an alternative approach has been proposed and described in this chapter. The main idea behind it is that all the unknown parameters are calibrated at the shock absorber level based on the damper level test. This might seem like a not useful approach when compared to the previous method since in order to use the model for a specific design, a physical sample has to be available and a regular test has to be performed. This takes away the ability to model specific designs that are not yet produced. However in practice, as a result of such a model calibration approach, a digital twin (an idea introduced by the Industry 4.0 concept) of the considered design is created.

For industrial applications, the digital twin approach can offer a wide range of practical advantages. The main benefit comes from the fact that one training signal test can be used to calibrate the model which is later used to reproduce multiple test scenarios. Secondly, given the large number of designs being developed, utilizing easy-to-use calibration procedures, a library of the subcomponents could be built over time and used in the future to decrease the need for physical test-based calibration [57]. Moreover, by using the digital twin concept, the model becomes the extension of the DAQ (data ac-

quisition system) system since it allows in-depth analysis of the physical quantities that influence the dynamic behavior (opening and closing of the valves, pressure distribution, and inertia of different components).

Despite many advantages, the proposed method creates its own challenges. It attempts to simplify the parameter calibration process in terms of experimental testing however this is achieved at the cost of increased computational difficulty since all the unknown parameters are calibrated at the same time. To address this challenge, multiple parameter estimation strategies that are designed for the identification of a large number of parameters have been considered and compared. Significant improvement has been observed using the sensitivity-based parameter estimation method (method has been described in the section 7.1) [133].

In order to assess the accuracy and computational cost of this approach, an experiment has been performed and based on the results, a sensitivity-based parameter estimation study was performed. The same sets of parameters have been considered as in the previous calibration approach: valve stiffnesses, oil compliance parameters (bulk modulus and gas content), and dynamic parameters of the main vibroisolator (top mount). Due to the fact that damper and module level tests closely share the test set-up and both are very common and easy to perform the digital twin parameter estimation approach has been split into both levels in such a way that the damper level test is used for the sensitivity based calibration of the valves and compliance while the module level test is used for the top mount calibration using regular genetic algorithm. In both cases, the primary quantity that is used to construct the goal function is the damper force.

Validation of the obtained parameters is performed by using a pseudo-random excitation test signal and analysis of the damper force. This comparison is done to confirm that the model has not been overfitted. However, from the perspective of the practical application of the digital twin concept the most interesting verification is done by comparison of how well the model which was calibrated at the damper level using force measurements is able to reproduce the rod acceleration measurements during standard high-frequency tests of the shock absorber.

Sensitivity based parameters estimation procedure described in this section has been performed using the same semi-active damper design as in chapter 6, however, samples of the shock absorber were different (samples produced approximately 2 years after the samples used in chapter 6) therefore some design features have changed and direct comparison between those result sets is not possible.

## 7.1 Sensitivity-based parameters estimation procedure

A parameters estimation procedure performed on the complete assembly of the shock absorber requires conducting a comparison of experimental measurements and numerical simulation of the shock absorber under the same conditions, especially in terms of excitation (training signal). Usually, the test is run according to the theoretical target damper position signal which due to inaccuracies of the control system differs from the actual position achieved by the testing machine. Therefore actual position signal is registered during the test and sent as an input to the model. After the numerical results are available, both force signals (numerical and experimental) are compared by calculating the difference. The result of this operation becomes a residual signal. By integrating the absolute value of this residual signal, the total error between the test and simulation can be obtained. This becomes a goal function that the optimization algorithm attempts to minimize by adjusting the values of the parameters that are subject to the estimation. However, when multiple parameters are used, the optimization hyperspace can become very complex and some parameters that are being estimated can have a weak influence over the goal function, whereas other parameters tend to dominate the residual signal. As a result, the parameter identification procedure can require a large number of iterations. Additionally, the risk related to such a situation is that good agreement between the simulation and the experiment may be achieved even with not physically correct values of the parameters. The sensitivity-based parameter estimation approach is an attempt to mitigate these problems and make the overall process more robust.

The key principle behind the sensitivity-based approach used for the parameter estimation procedure is that it takes advantage of the fact that not all the considered parameters are influencing the residual signal at the same time. This is particularly true for the case of the semi-active shock absorbers where different passive valves are active at different operating stages of the damper (e.g. compression, rebound, different active valve flows). The sensitivity-based approach described in this chapter attempts to decompose a singular large optimization problem into a number of smaller ones, each having its own goal function that is focused only on the regions of the residual signal that are relevant for the considered parameters.

In order to quantify when each of the parameters is influencing the residual signal, the value of the first-order Sobol index is used. For this, a sensitivity analysis has to be performed for each time point of the training signal. With a large number of parameters, this itself might become a computationally demanding problem. However, in many cases, based on the physical relations, certain parameters can be grouped a priori by the range of their effect on the dynamic response of the damper. In the case of shock absorbers, all the parameters related to the specific valve can be safely assumed to have an impact on the residual signal roughly at the same time. By grouping the parameters and deriving

combined Sobol indexes, the computation required to perform the sensitivity analysis can be greatly reduced. After sensitivity signals for each of the groups are available, goal functions can be derived by scaling the residual signal with the corresponding sensitivity signal as represented in eq. 7.1.

$$J(i) = \int_0^T I_i(t) \cdot |F_{test}(t) - F_{simulation}(\Theta_i, t)| dt \quad (7.1)$$

where  $I$  is the value of the sensitivity signal and  $\Theta_i$  is the  $i$ -th set of parameters.

From the perspective of the computational cost, an additional challenge arises from the fact that in order to calibrate each of the parameters group using a regular optimization algorithm (e.g. genetic algorithm, as used in other cases), each group requires separate iterations which means the amount of computation would multiply by the number of groups. Given the fact that for each iteration a complete damper model of the shock absorber is used, it was proposed to synchronize optimization algorithms for each group. Using genetic algorithms, this can be achieved in such a way that at each member of the population, each algorithm contributes part of the chromosome to the main optimization engine. When all the parts of the chromosome are available the iteration is performed and the fitness is evaluated separately for each group. Such an approach demonstrated using pseudocode 1 allows to computationally maintain only one optimization process. This, however, from the perspective of the singular genetic algorithm, due to higher-order sensitivities across different parameters causes the simulation to lose its deterministic character. Although such side effects of synchronizing the sub-algorithms might be confusing to the genetic algorithm, it has been demonstrated in [133], that utilizing sensitivity scaling is improving the rate and quality of the obtained parameter characterization.

## 7.2 Description of the parameter estimation procedure

In order to facilitate easy implementation of the developed model into the industrial design processes, the parameter estimation procedure should allow for the characterization of all the relevant parameters using simple, standard experimental methods. However, identifying all the unknown parameters related to the damper as well as to the top mount would make the procedure unacceptably computationally expensive. For that reason, it has been proposed to perform parameter estimation based on the two types of the test, one at the shock absorber level and one at the assembly with the modular components (most importantly top mount). Both tests are similar and can be easily performed on the same test rig.

For both tests, the training signal (displacement excitation applied at the lower mount of the damper) must cover a wide range of the typical conditions in which the shock

---

**Algorithm 1** Pseudocode of concurrently performed, sensitivity-based genetic algorithms

---

```

for each parameter_group g:
    Initialize population:  $P_g \leftarrow \text{RandomIndividuals}()$ 
endfor
Combine chromosomes of all the individuals in population:  $P \leftarrow \text{Combine}(P_{g1}, P_{g2}, \dots, P_{gn})$ 
Run simulation for each individual to obtain result:  $R \leftarrow \text{Simulations}(P)$ 
for each parameter_group g:
    Evaluate fitness:  $F_g \leftarrow \text{Fitness}_g(R)$  // fitness function uses its group's sensitivity signal
endfor
Initialize best solution:  $I_{\text{best}} \leftarrow 0$ 
while (given number of generations is reached)
    for each parameter_group g:
        Perform parents selection:  $P_g \leftarrow \text{Selection}(P_g, F_g)$ 
        Perform crossover:  $P_g \leftarrow \text{Crossover}(P_g, F_g)$ 
        Perform mutation:  $P_g \leftarrow \text{Mutation}(P_g, F_g)$ 
    endfor
    Combine chromosomes of all the individuals in population:  $P \leftarrow \text{Combine}(P1_g, P2_g, \dots, Pn_g)$ 
    Run simulation for each individual to obtain result:  $R \leftarrow \text{Simulations}(P)$ 
    for each parameter_group g:
        Evaluate fitness:  $F_g \leftarrow \text{Fitness}_g(R)$ 
    endfor
    Save best solution in population:  $I_{\text{best}} \leftarrow \text{Fitness}(R)$  // fitness function without sensitivity signal
endwhile

```

---

absorber is envisioned to operate, with appropriate resolution. On the other hand, if the training signal is too long, the optimization procedures will be unnecessarily extended in time. Based on the review of the damper vibration levels caused by the typical road excitation, a sinusoidal signal that covers the following characteristics has been defined (see figure 7.1):

- 3 level of stroke: 50 mm, 30 mm and 10 mm
- 4 levels of excitation velocity: 0.25 m/s, 0.5 m/s, 0.75 m/s, 1 m/s.

In order to characterize the parameters under different active valve settings, the entire training signal is repeated at 3 levels of the active valve current: 0.32 A, 0.9 A and 1.6 A. During all the tests, the temperature of the sample has been controlled and remained in the range between 28-35°C.

**Module level test** Module level test has been proposed as an easy-to-implement alternative to the regular measurement of the dynamic characteristics of the top mount vibro-isolator. For that purpose, the mounting tool has been featured with the LVDT position sensor which was attached rigidly via adapter to the piston rod. This allowed for the registering of the displacement signal of the piston rod in relation to the top mount housing (the entire test set-up can be seen in figure 7.3b whereas the top mount mounting tool together with the LVDT sensor is shown in 7.2). The force has been captured with the strain gauge-based load cell rated for measurements up to 1kHz. During the test, displacement training signal (shown in 7.1) was prescribed to the actuator which was rigidly

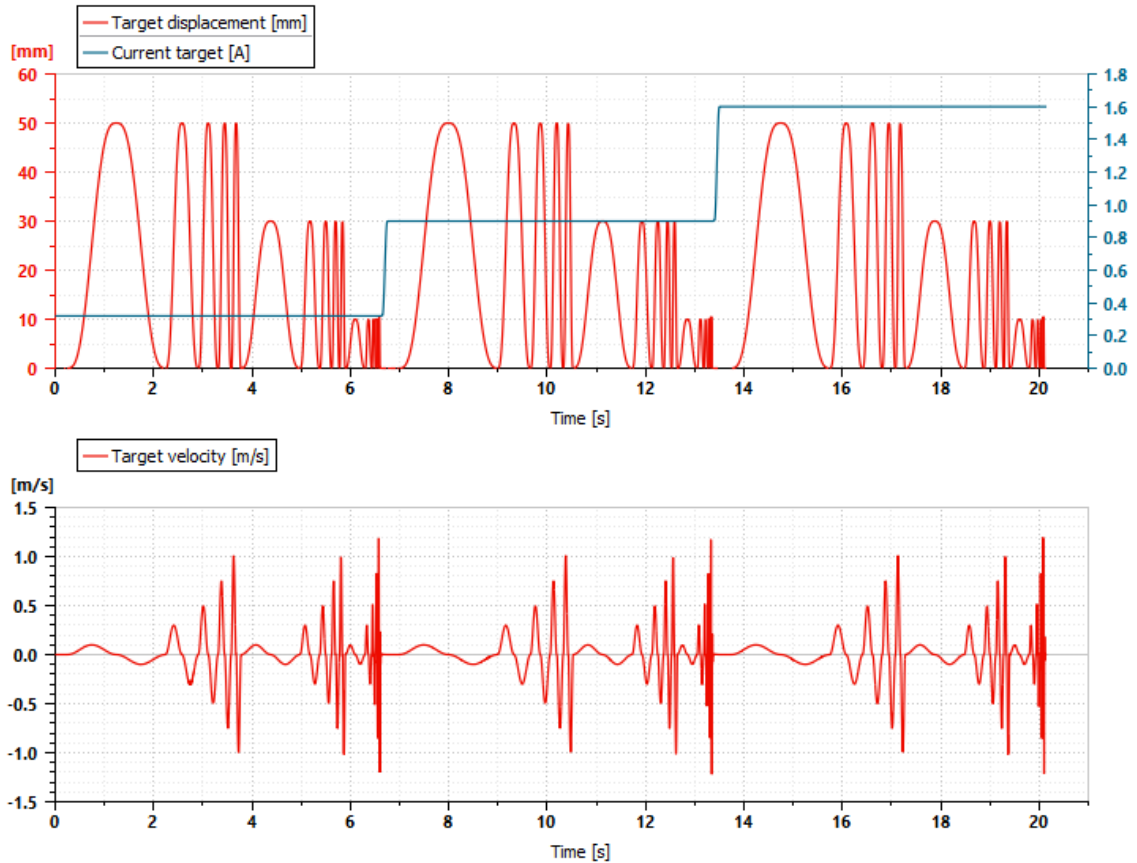


Figure 7.1: Training excitation signal used for the sensitivity-based parameter calibration procedure

attached to the lower mount of the damper. As a result of the actuation and dynamic response of the shock absorber, the piston rod has also been excited. By having the rod position signal as well as force measurement it is possible to employ regular parameter estimation procedures to establish values of the top mount model parameters. The genetic algorithm has been used as an optimization algorithm with the same parameters as in the parameters calibration method 1 (see table 6.4 for the limits set to the parameters during calibration). In order to reduce the problem size of the parameter calibration, the static curve has been approximated based on the force-displacement characteristic, with the 5th-order polynomial using the least square curve fitting approach. The resulting approximation can be observed in figure 7.4b.

**Shock absorber level test** The experimental test set-up used for the calibration (which can be seen in fig. 7.3a) of the damper level parameters (valves and compliance related) in principle does not differ from the standard layout used for the performance measurements (as described in section 2.7). However, since the results have to be analyzed also at a higher frequency range, it is important to ensure that the sensors are capable of properly capturing this higher frequency content (up to  $\sim 700\text{Hz}$  compared to  $< 100\text{Hz}$

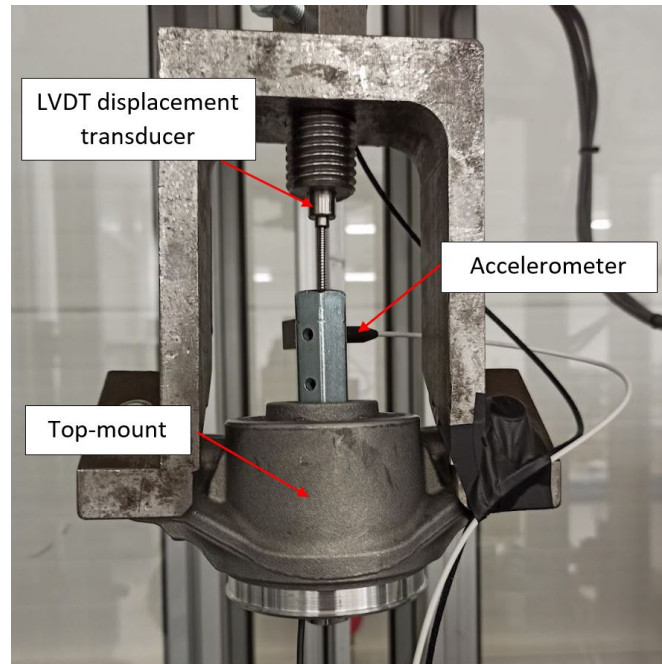


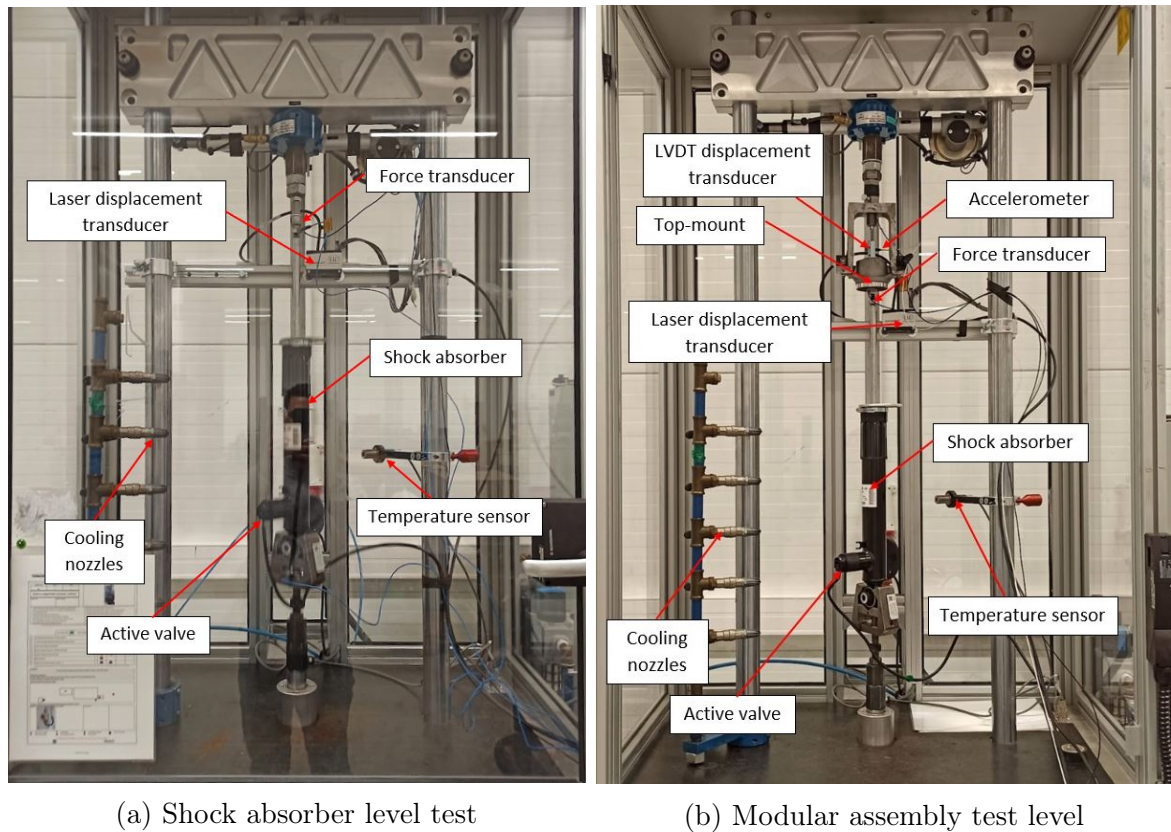
Figure 7.2: Overview of the tooling used during the module level calibration test to register displacement of the rod in relation to the top-mount housing

for the typical performance-related test of the shock absorber). For that reason, during the experimental measurements used for this calibration procedure, an additional strain-gauge-based load cell, as well as a laser displacement sensor (Micron-epsilon IDL1900-100, both suited for measurements at, at least 1kHz), were used. The same excitation and verification signals were used during the module-level test, see figure 7.1.

As discussed in earlier paragraphs, a sensitivity-based approach has been used as a parameter estimation method. However, due to the fact that the impact of the compliance-related parameters overlapped with valve level sensitivities, this group of parameters has been considered without the sensitivity scaling approach. The parameter estimation procedure was performed using a genetic algorithm implemented within the Python Scripting Language library: PYGAD [60].

### 7.3 Results of the calibration process

**Top mount parameters estimation** The goal of the module level test and calibration described in this section was to estimate the parameters of the top mount model using a test set-up that is easily accessible at the testing facility of the shock absorber suppliers. The results of this calibration exercise can be observed in figure 7.4a where the measured force is compared with the response of the calibrated model. In terms of dynamic characteristics of the calibrated top mount model, results can be observed in figures 7.5a and 7.5b. Component-level test data were not available for the samples used



(a) Shock absorber level test

(b) Modular assembly test level

Figure 7.3: Test bench used for the experimental part of the sensitivity-based parameter estimation procedure

for the model calibration described in this section. Furthermore, since the samples might significantly differ from those used for the previous parameters estimation approach (described in section 6.4), it was not possible to obtain test data for the model calibration verification at the component level. However, the final verification of the module-level model calibration, in the form of the rod acceleration measurements and simulation results should serve as an indication whether the top mount model calibration is sufficient since any inaccuracies in the top mount model would inevitably impact the modular-level simulation results.

**Shock absorber parameters estimation** Since the shock absorber level parameters are estimated using a sensitivity-based approach, the first step was to carry out the variance-based sensitivity analysis. Each group of the parameters (corresponding to each of the passive valves) was assigned input values within provided ranges generated using a low-discrepancy Saltelli sampler [26, 103]. For the sensitivity analysis, each group has been analyzed considering 32 parameter combinations which for 4 groups resulted in 320 runs of the simulation. In the current experiment, the damper parameters related to the compliance (undissolved gas content and bulk modulus of oil) were assumed to

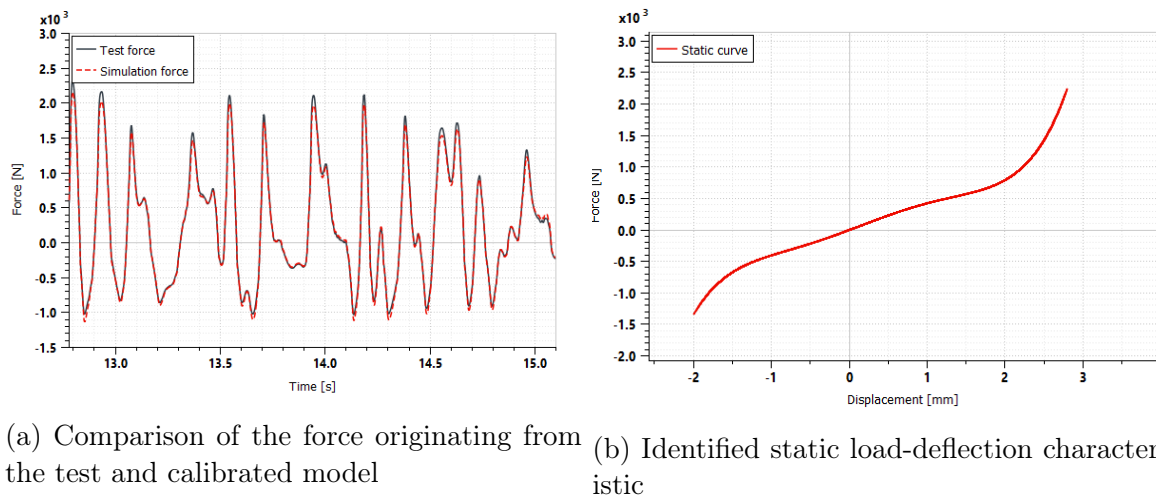


Figure 7.4: Results of the top mount model calibration

have a uniform impact on the results with respect to time, and therefore they were not included during the sensitivity analysis. After all the cases have been simulated, at each time point, global, first-order Sobol indices have been established using variance-based sensitivity algorithm [113, 104] implemented within SALib python scripting language library [70, 73].

The resulting sensitivity signals were shown in figures 7.6a and 7.6b and as it can be observed each of the valves at a certain point in time has a significant impact on the results (high sensitivity values). Due to high restriction, shim stacks are usually considered dominant in terms of impacting the damping forces whereas the impact of the intakes valves tends to be regarded as insignificant. By investigating the correlation between valve opening and values of sensitivities (shown in figures 7.6c and 7.6d) it can be observed that when the shim valves (base valve compression and piston rebound) are opening they indeed dominate response from the damper, however when shim valves are closed, naturally the intake valves become more important. Given the fact, that the intake valves open earlier than the shim valves (at high stroking velocities) there are many damper operating stages that can be used to calibrate them. For semi-active dampers similar conditions appear under low current at the active valve. In such a case, the bulk of the flow is directed via intake valves and active valves. This also presents a good opportunity for the parameter estimation algorithm to calibrate the parameter of the intake valves.

After sensitivity signals were obtained it was possible to construct the goal functions according to the equation 7.1. As discussed in 7.1 each group of parameters is calibrated using a separate genetic algorithm. All algorithms are launched at the same time and synchronization is realized by the fact that the calculation engine is designed in such a way that it can only start the simulation when all the parts of the chromosome are

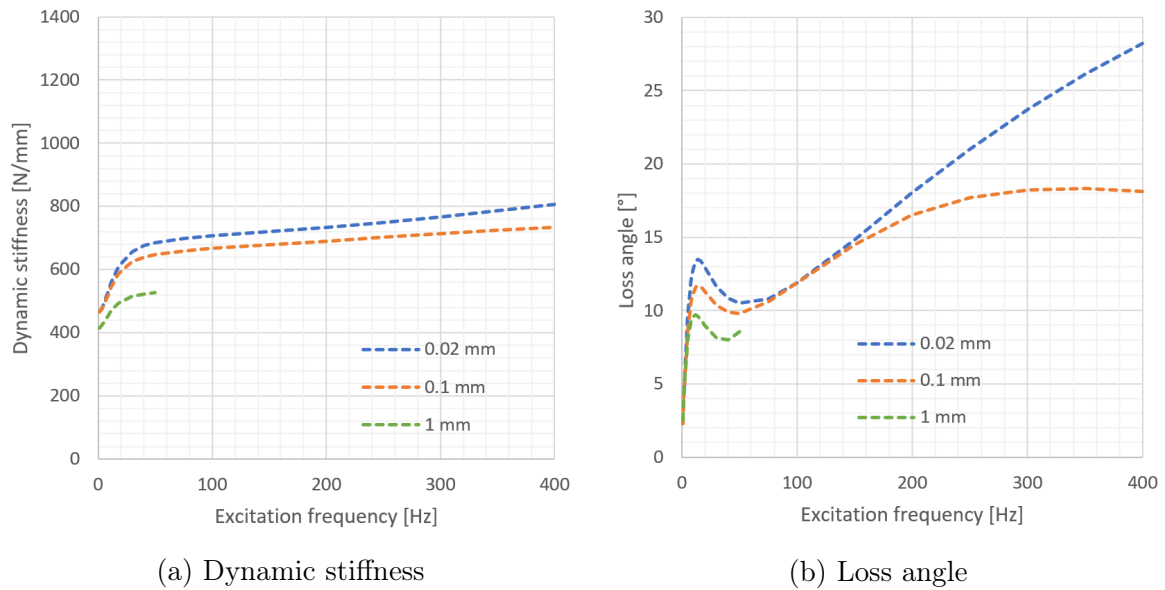
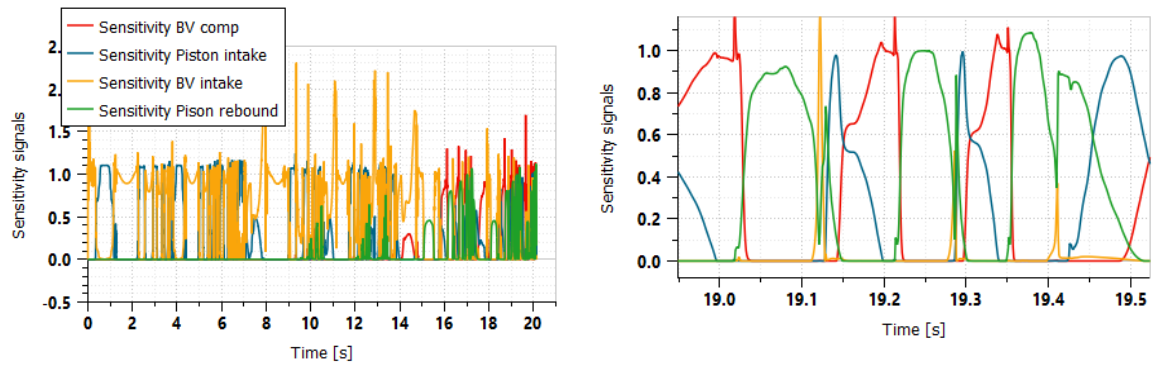


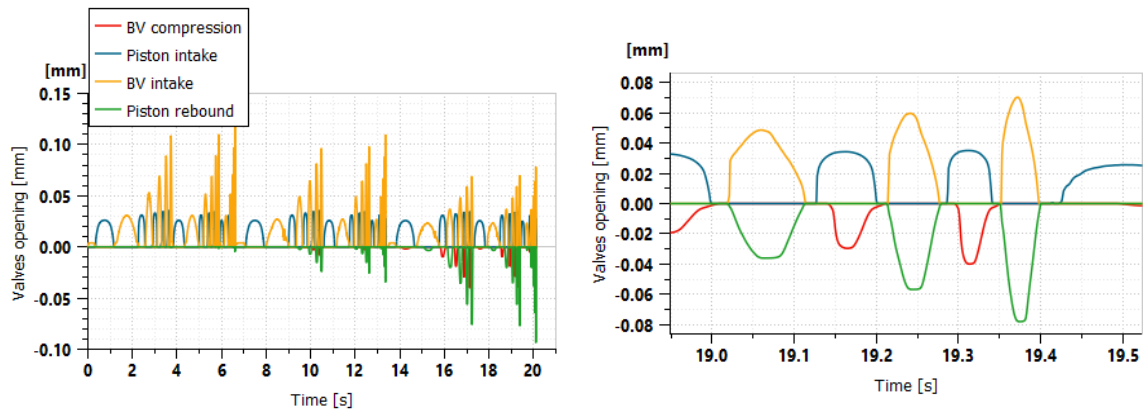
Figure 7.5: Dynamic characteristics obtained from the calibration top mount model simulation at different excitation frequencies and amplitudes

provided by each of the genetic algorithms. The progress of each of the optimization algorithms has been shown in Figure 7.7. Because the sensitivity-scaled residual impulse is significantly lower than the complete residual (non-scaled) different scales have been used for the comparison of the progress of the optimization algorithm. The best match in terms of complete (non-scaled residuals) has been obtained for the 2639-th iteration. Time-domain comparison of the force signal obtained from this iteration with the test data has been done in figures 7.9a and 7.9a. The same set of data was used to prepare the comparison of the force-displacement characteristic in figure 7.10.

Despite a good level of agreement between experimental and simulation force signals, several noticeable discrepancies can be observed. The first discrepancy occurs at low current and high excitation velocities. Since these conditions are related to high, dynamic flows through the active valve, these inaccuracies can be attributed to the simplified method of representing the active valve (look-up-table approach) which is not able to capture the dynamic behavior of the active valve. The second discrepancy takes place at high frequencies (high velocities at low strokes) at the beginning of the compression stroke. This shape of the force-displacement curve is characteristic of the aeration of the compression chamber during rebound stroke. This might originate from two reasons. The first is high restriction at the base valve rebound (intake) direction which is accompanied by too-low reserve chamber pressure. The second potential reason for this type shape of force-displacement characteristic might be excessive sloshing in the reserve chamber which causes the base valve to suck an oil-gas emulsion during rebound stroke. The third type of noticeable discrepancy (which can be observed in figure 7.10) is related to the forces



(a) Sensitivity signals - overview of the complete training signal (b) Sensitivity signals - focus on the high force range



(c) Valves opening - Overview of the complete training signal (d) Valves opening - Focus on the high force range

Figure 7.6: Sensitivity signals (first-order Sobol index) and valves opening of the different passive valves. For clarity, the opening of the intake valves has been plotted with a negative sign

generated at the end of the rebound stroke. This area of the graph depends on frictional forces at the valve level which is excessive at low and mid-stroke under high active valve current. However, when the current is decreased (0.9A) at the same strokes, the frictional forces are underestimated by the model. Despite these minor inaccuracies, the overall reproduction of the measured force by the model is good. This is not surprising since that was a goal of the optimization algorithm. The first check that allows confirming that the good model performance in terms of force signal is not a result of the overfitting is done by comparing the results of simulation performed under random noise simulation (see fig 7.8a and 7.8b) which is different from the one used during calibration. In this case, the level of agreement between the experimental results and simulation is also satisfactory.

**Combined model** An important practical value of the considered parameters estimation method is the ability to use the calibrated model to analyze the dynamic properties of the modular assembly. For this reason, the most interesting outcome of the model cal-

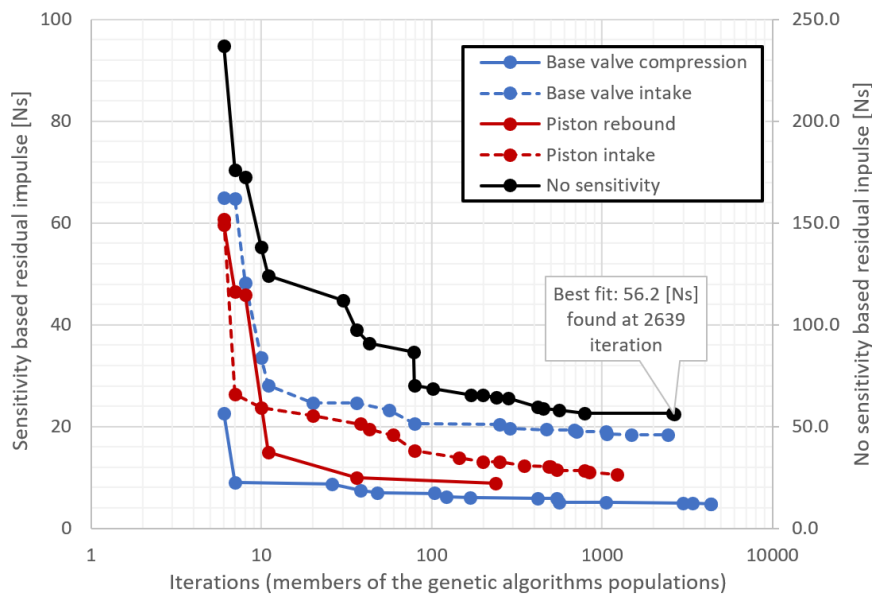


Figure 7.7: Improvements in reduction of the residual between simulation and training force signal across the iterations for each of the concurrent genetic algorithms

ibration exercise described in this section is the assessment of how well the module level model (which was calibrated at the damper level) together with calibrated top mount (using approach from section 7.2) is able to reproduce measured rod acceleration signal at high-frequency tests.

For the sinusoidal excitation test (see subsection 2.7.3), results of this comparison have been shown in figures 7.11, 7.12 and 7.13. Despite the relatively high noise level present in the experimental results, the simulated rod acceleration signal closely follows the test data. Two main acceleration peaks resulting from the opening of the intake valves are much closer in terms of nominal value to their experimental counterparts (table 7.1) than those obtained from the model calibrated using the first approach (section 6.5, see figures 6.22, 6.21, 6.20 and table 6.5). Similarly, for the tests of the shock absorber excited with the noise signal and analyzed in the frequency domain, the model is able to accurately reproduce the noise profile at each of the active valve conditions in the frequency range below 500Hz (figure 7.14 and table 7.2). Above this frequency, experimental data show an abnormally elevated level of rod vibration which most likely originated from the imperfect mounting structure which was used to assemble LVDT and acceleration sensors. By comparing these results with those obtained from the previous calibration approach (section 6.5 figure 6.30 and table 6.6), it can be observed that the current method provides a noticeable better representation of the rod vibrations measured during the test.

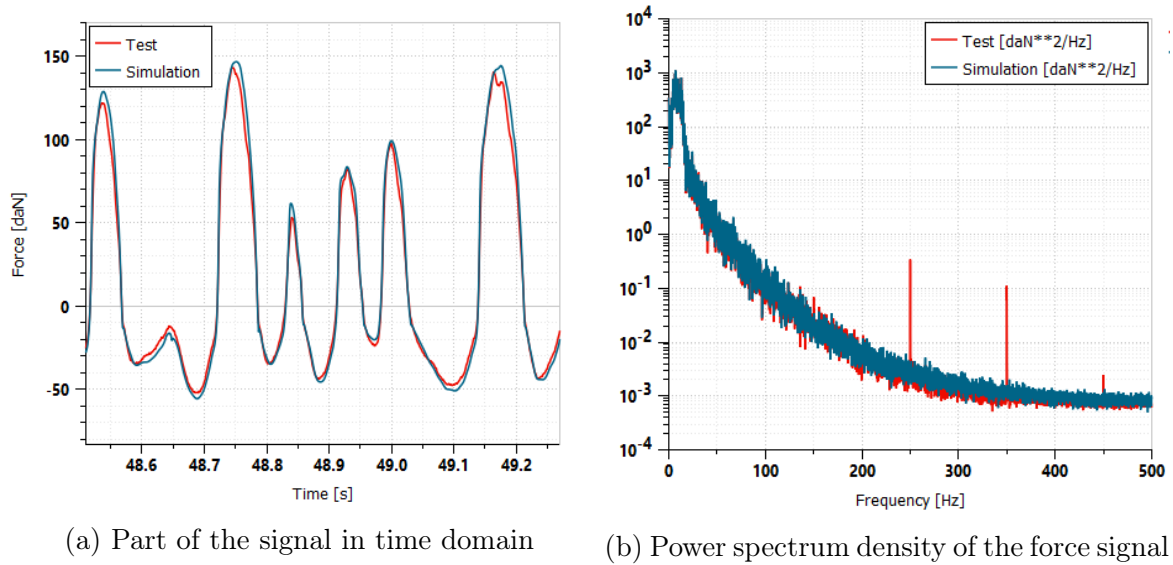


Figure 7.8: Comparison of the force signal obtained from the test and calibrated model of shock absorber assembly under verification signal excitation

Table 7.1: Summary of the mono-sine test results of the test and simulation

no.:	Active valve current [A]	Rod acceleration peak at rebound stroke			Rod acceleration peak at compression stroke		
		Simulated [g]	Measured [g]	Difference [%]	Simulated [g]	Measured [g]	Difference [%]
1	1.6	15.8	17.9	11.8	-9.1	-9.9	-7.2
2	0.9	7.7	10.0	23.6	-6.4	-7.6	-15.8
3	0.32	2.1	2.8	24.6	-3.5	-5.2	-32.2

Table 7.2: Summary of the random test results of the test and simulation

no.:	Active valve current [A]	PSD of rod acceleration at 200Hz			PSD of rod acceleration at 300Hz		
		Simulated [dB]	Measured [dB]	Difference [dB]	Simulated [dB]	Measured [dB]	Difference [dB]
1	1.6	-7.5	-7.6	0.1	-7.0	-5.6	1.4
2	0.9	-11.6	-10.4	1.2	-18.9	-14.5	4.3
3	0.32	-17.4	-15.8	1.5	-23.4	-19.1	4.4

## 7.4 Conclusions

The alternative parameter calibration procedure described in this chapter was proposed as an answer to concerns related to the industrial applicability of the standard parameter calibration methods described in chapter 6 which is done on the subsystems level. Due to the fact that the method proposed in this chapter operates on the level of the complete

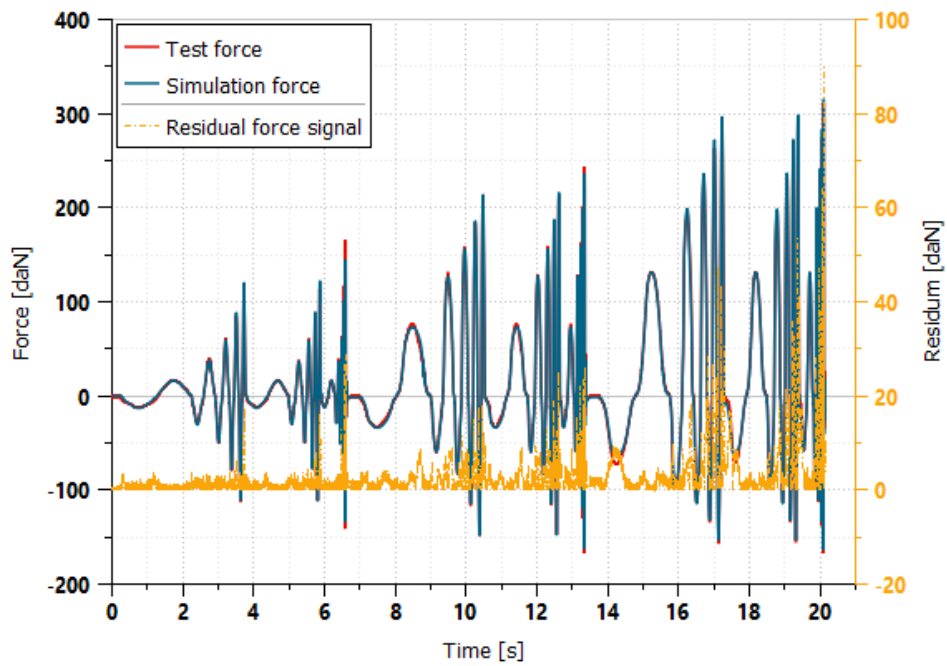
damper and module assembly, the overall amount of testing activities and handling of experimental data is reduced. This comes at the cost of a more complex parameter calibration procedure but if robust optimization methods are employed, this part is more easily automated. From the perspective of the design engineer (who is considered a future user of the developed methods) result of this procedure becomes effectively a digital twin of the considered design.

The digital twin concept helps streamline the complex development lifecycle in multiple ways. First of all, a calibrated model (digital representation) of a product brings flexibility when it comes to verification scenarios because, after the experimental tests required for model calibration, a digital twin can be used for verification of various testing specifications (performance, NVH related problems, control algorithms, extreme loading scenario predictions) without additional physical samples. Secondly, with the digital twin concept, the analysis of the damper behavior brings much richer insight into the results, because the model allows to easily track various physical quantities (not only force or acceleration but also flow rates, pressures, valve opening, etc.). However, above all, the digital twin concept provides design engineers with the ability to rapidly analyze the consequences of potential design changes. This is especially relevant in situations when the environment for storing the digital twin data is established and maintained.

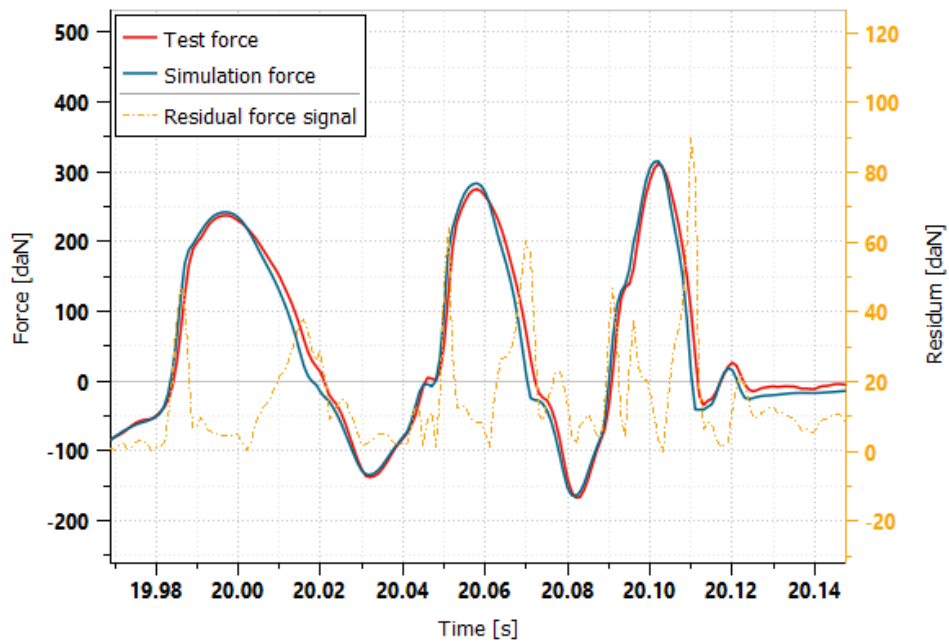
As has been discussed, the application of the digital twin concept can bring significant benefits to the designing process teams but in order to utilize these advantages, the quality of the underlying model and parameter values have to be confirmed. The most important physical quantity used for the verification is rod acceleration. As can be observed in figures 7.11 - 7.13, even though the parameter estimation was performed based on the damper force, the module level rod accelerations are well reproduced for both sine (summary table 7.1) and random (summary table 7.2) signal excitation.

Based on the comparison with the previous model calibration procedure (chapter 6 results summary in table 6.5 and 6.6), it can be concluded that the procedure described in this section allows for a more accurate reproduction of the rod acceleration during the high-frequency test for both sine and random noise excitation. Better quality of the calibration can be attributed to more diverse excitation conditions when using an assembled system for the calibration test. In particular, valve characterization using a flow-bench test machine allows for capturing only static flow conditions. Another reason for the better quality of the model calibration when using assembled damper is the lack of tooling and measurement system influence which is inevitable with the application of the isolated test system.

Since the shim valves are primary passive valves used to control the damping force exerted by the shock absorber the role of the intake valves might be underestimated. This might create concern regarding the identifiability of these valves. However, the sensitivity study showed that each of the passive valves at specific actuation conditions has a significant influence over the damper force and therefore can be calibrated.



(a) Overview of the complete training signal



(b) Focus at the high force cycles

Figure 7.9: Comparison of the force signal obtained from the test and model after parameters have been calibrated with sensitivity-based parameters estimation procedure

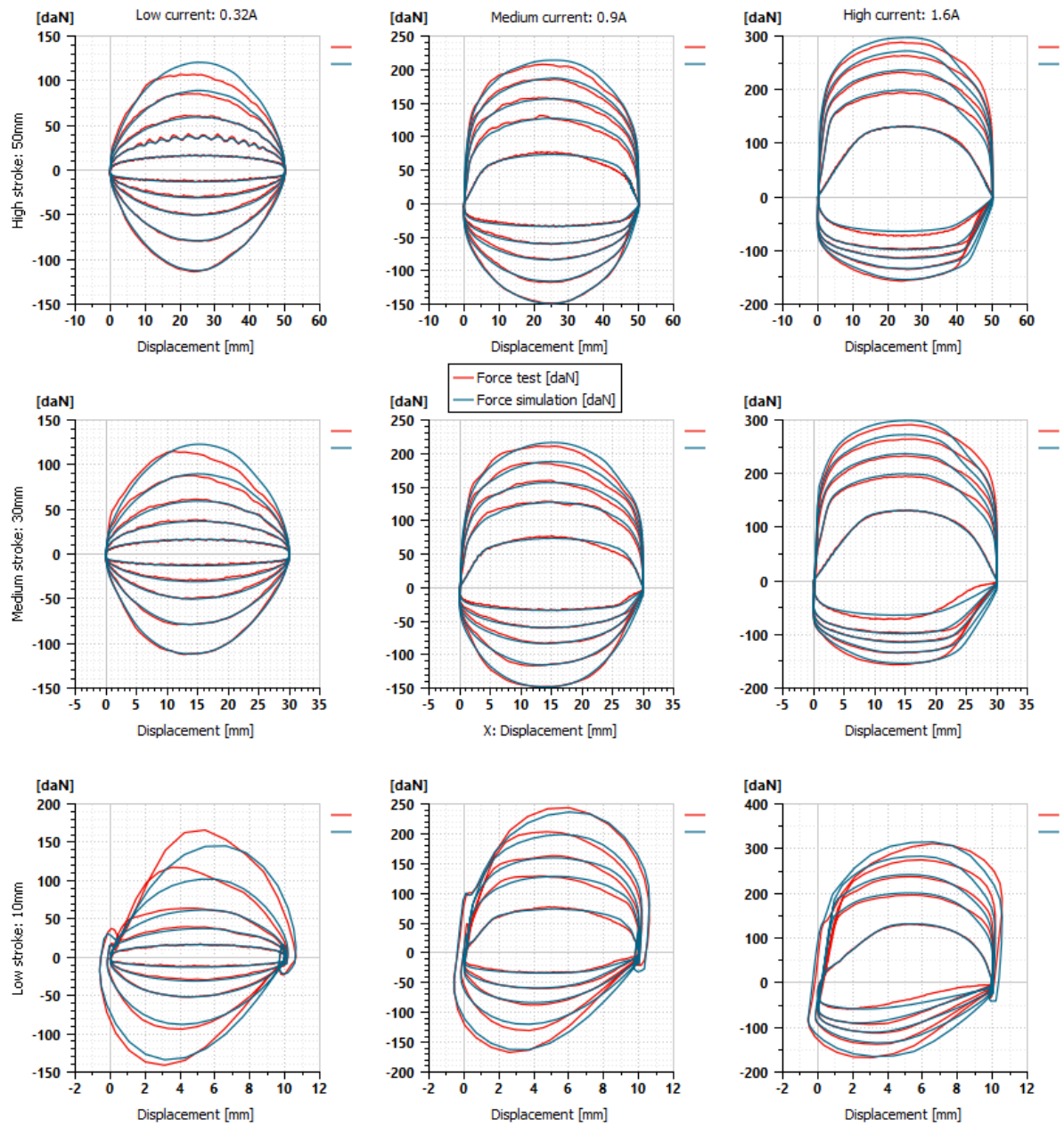


Figure 7.10: Comparison of force-displacement characteristics obtained from simulation and physical test

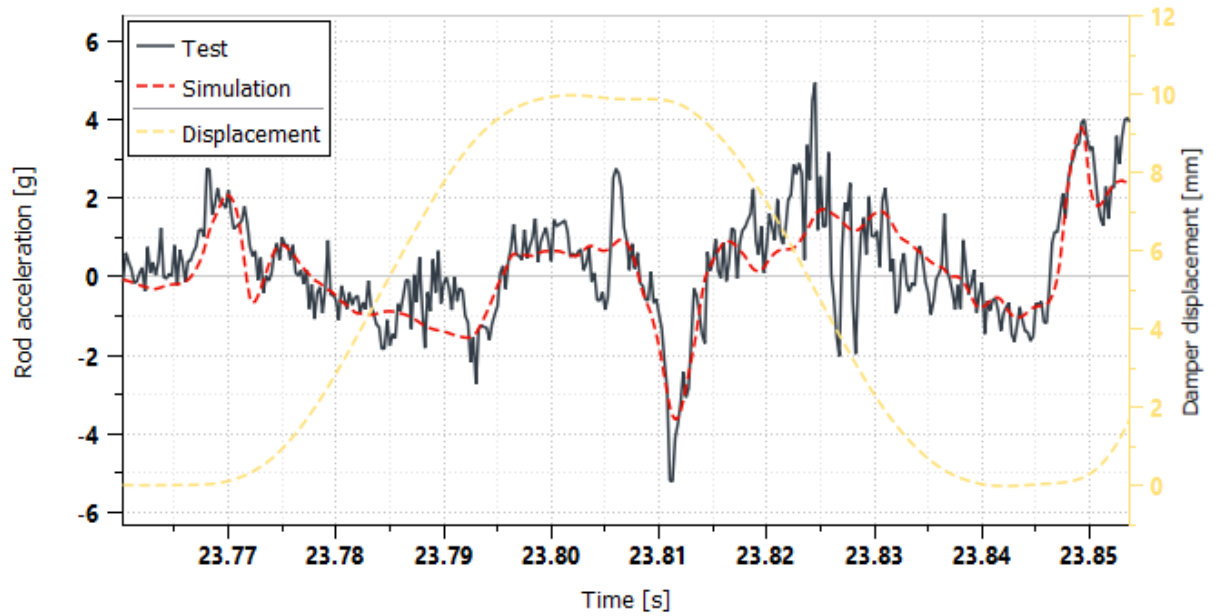


Figure 7.11: 16Hz excitation 0.5m/s at 10mm stroke with 0.32A active valve current

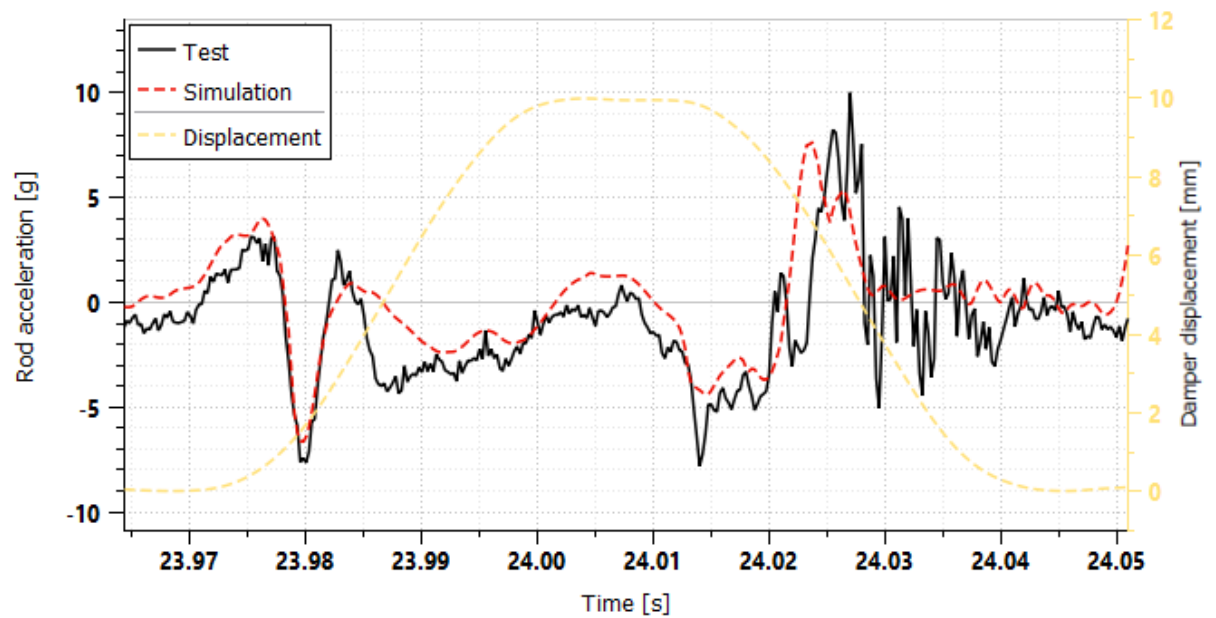


Figure 7.12: 16Hz excitation 0.5m/s at 10mm stroke with 0.9A active valve current

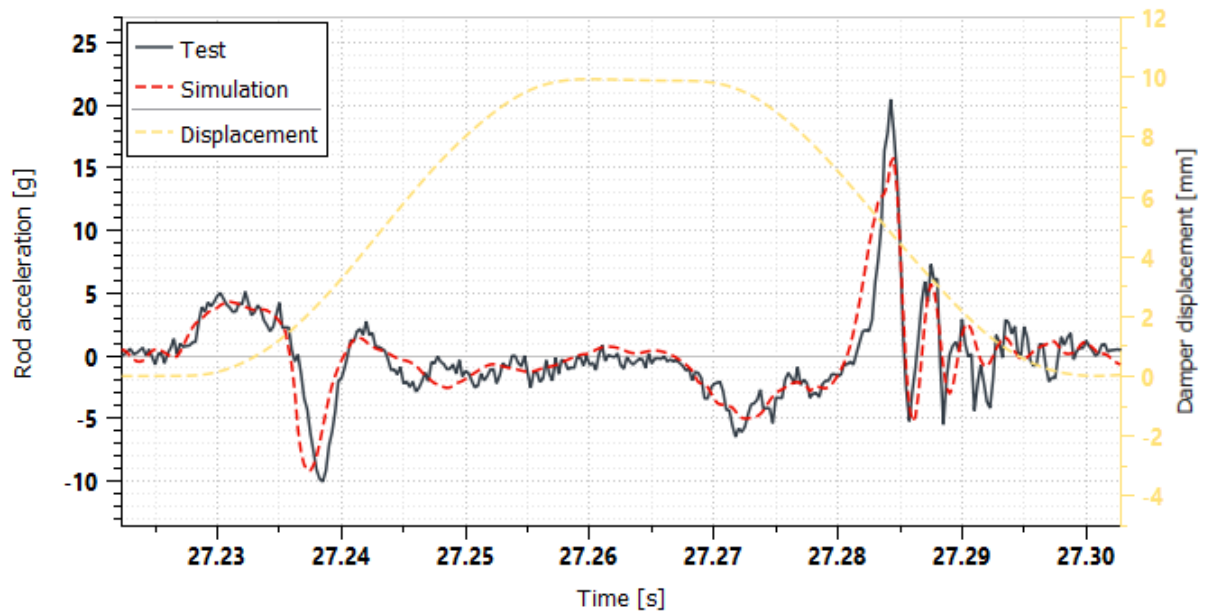


Figure 7.13: 16Hz excitation 0.5m/s at 10mm stroke with 1p6A active valve current

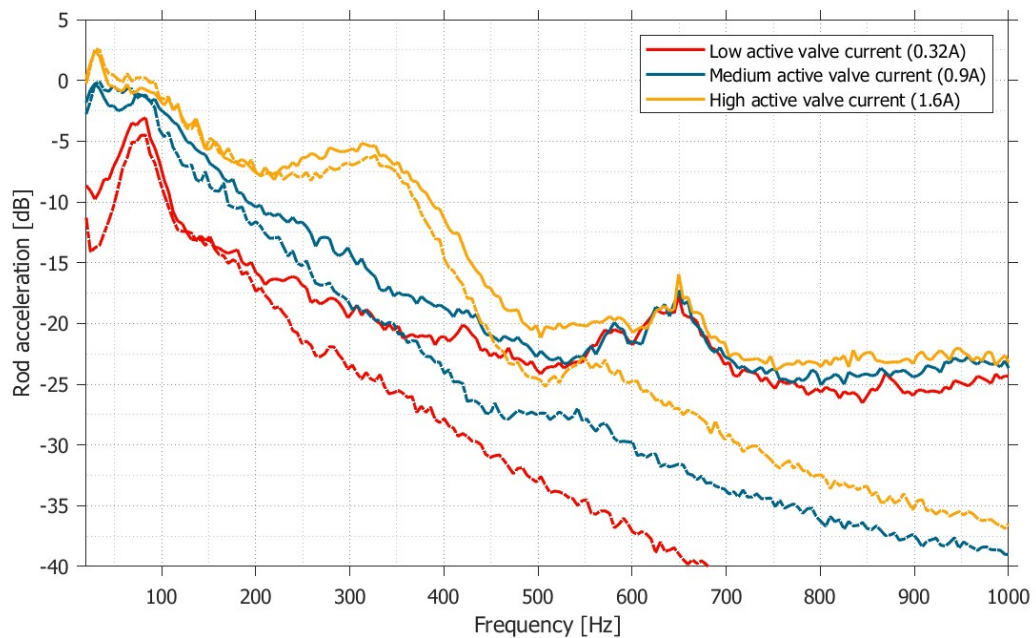


Figure 7.14: Comparison of power spectra of rod acceleration signals obtained from simulation and physical test, solid line - test, dotted line - simulation results

# Chapter 8

## Summary and discussion

It is probably not uncommon, that the initial goals formulated at the beginning of the Ph.D. project that led to this dissertation seemed quite vague and it was not entirely clear at that stage what exactly should become the focus of the investigation and further development. There was no doubt that the dynamic behavior of the existing and newly developed shock absorber design (particularly semi-active ones) was important and that computer modeling was the most efficient approach that could be employed to enable the engineers and industrial partners to predict it at the early stages of the project.

A big part of the initial confusion was related to the fact that both, in literature as well as in industrial practices, there is a strong distinction between lateral and axial dynamics of the damper. After studying both mechanisms it has become clear that although these two aspects of the damper dynamics can influence each other (albeit, the link remains obscure), each is largely governed by different physical phenomena and most importantly, the starkly different toolset is required for the analysis of each (detailed discussion regarding both can be found in section 2.6 ). One of the relevant differentiating factors for both aspects of the damper dynamics is that axial rod vibrations, unlike lateral behavior of the damper structure, are **self-induced** due to the nonlinearities created by the combination of the excitation, internal valving, damper compliance and top mount stiffness characteristics. This makes the damper supplier a directly responsible entity for any deficiencies within this domain. Conversely, the structural lateral aspects of the damper behavior are always strongly related to the dynamic response of the entire suspension and are merely one of many elements that comprise the larger problem. For this reason as well as due to the fact that the self-induced axial damper vibrations are less predictable and understood, the industrial partner company was much more incentivized to pursue progress in this domain. Therefore, self-induced axial rod vibrations were selected as a primary subject of the modeling and investigation.

After establishing the true focus and boundaries of the project, it was imperative to perform a detailed survey of the literature as well as industrial knowledge and practices

in the relevant domains. Based on the results of that survey as well as on the results of concurrently performed consultation with the engineering community of the industrial partner company, a set of requirements for the model has been formulated (for detailed description, see section 3.3). Based on these guidelines and after the process of experimentation by trial and error with various modeling concepts, the computer model was proposed (see chapter 4). Since it has been established that a wide range of physical phenomena such as shim valve friction, hydraulic stiction forces as well as distributed compliance of the damper are important and should be captured by the simulation, the proposed model is characterized by a relatively high level of complexity. The main modeling simplifications in the form of empirical representation of the passive valve stiffness as well as active valve flow characteristics originated from the structure and organization of the engineering resources present in the systems of the industrial partner. This modeling functionality was already covered by the dedicated systems and tools (separately improved and maintained) therefore it was counterproductive to incorporate them within the developed model. In terms of the modeling environment, a strong emphasis was put on the flexibility of design modification as well as on the ability to combine the proposed model with other suspension systems (e.g. rebound or compression end-stops solutions). As a result, the proposed model can capture all the important physical phenomena that contribute to the rod accelerations and at the same time it is well suited for industrial application and integration with other components and subsystems of the automotive suspension.

However, due to its complexity, some input parameters could not be directly linked to the design features. Therefore, in order to facilitate easy implementation into the industrial standard processes, a large part of the attention was dedicated to the study of the potential ways of model calibration. For this purpose, multiple rounds of calibration activities were performed for the most important subsystems which included passive valves, compliance-related parameters as well as dynamic properties of the vibroisolator (top mount). Based on the performed parameters calibration, model accuracy was analyzed by comparing the module-level simulation results with experimental measurement. The study was performed using a one-factor-at-a-time experiment to analyze the fidelity of the model under various design scenarios (see chapter 6). Despite noticeable discrepancies in terms of rod acceleration peaks, thanks to the correct representation of the trends, the model together with the proposed model calibration procedure has been judged suitable and useful for engineering design development purposes. However, during this study of the model calibration methods, the practical difficulties related to the complexity and workload required for the parameter calibration process were observed and it has become clear that the proposed method might pose significant challenges for the application in the industrial setting. For that reason, a second approach was proposed, in which all the damper parameters are calibrated at the same time using complete damper and module

measurement (instead of isolated subsystems as proposed previously). In contrast to the previous method, in this case, the main challenge was related not to the experimental part but rather to the computational effort required for the model calibration done for a large number of parameters simultaneously. As an attempt to improve this process, the sensitivity-based calibration procedure has been proposed. The main underlying principle behind it is to utilize only those parts of the training signals (in terms of the time ranges) that are influenced by the parameters being calibrated. For example, during the operation of the shock absorber, certain valves actively contribute to the damping force generation only at specific phases of the damper actuation (i.g. compression or rebound) therefore by focusing on those time ranges, the calibration procedure can be more robust. The proposed method which was described in chapter 7 has been verified at the damper as well as the modular level. The most important comparison from the perspective of the practical application was performed for the rod accelerations under module-level, high-frequency tests (see figures 7.11, 7.12, 7.13 and 7.14) and it proved that the sensitivity-based approach for the parameter calibration indeed brings a significant improvement to the quality and the rate of the parameter tuning.

Compared to the previous approach to the parameters calibration (which is performed on the isolated subsystem level), the sensitivity-based method can only be carried out when the physical sample of the shock absorber is available. This obviously is an important limitation. On the other hand, this approach can be adopted as a basis for the digital twin design development philosophy, according to which, each physical sample (during the development process) should have its digital counterpart. This enables to shift a large part of the performance-related testing into the virtual realm. Since a typical design validation plan consists of a large number of various test requirements which are performed at various development stages, the digital twin concept can replace complex test schedules with short and cheap physical characterization tests. Another benefit of utilizing the digital twin concept is that it allows for accumulation of the product performance knowledge in a organized and formalized fashion, since as a result of the model calibration, detailed information related to the damper and its characteristics is captured. In contrast, typical experiments for the design validation plan focus only on the specific aspect of the damper such as low-frequency characteristics, hysteresis, etc.

As a result of the performed work, the computer model has been proposed which is capable of capturing all the relevant physical phenomena related to the axial rod vibration occurring in the frequency range of up to 500Hz. It can be used at various stages of damper design development and easily modified and adapted for various related activities. Two distinct parameter calibration procedures can be employed, each having its own advantages and limitations.

## 8.1 Industrial implementation

It has been recognized relatively early in the project timeline that in order to satisfy the requirements of the industrial implementation and to effectively manage the complexity of various simulation tools and parameter calibration methods together with a large number of input parameters and test data, a dedicated scripting environment will be necessary which will serve as an application programming interface for the developed tools and gathered data. As a result, the model and parameters management environment has been prepared using Python Scripting Language. It consisted essentially of two separate repositories: the Amesim simulation engine and the parameters management system. The first part encapsulated functionality related to managing simulation. Due to the software requirement, it was based on the Amesim Python distribution and facilitated remote simulation launching and results postprocessing. The second part (which due to lack of software-specific requirements was based on the separate Python distribution) included functionality related to the parameter calibration procedures which relied on the independent libraries used for various subprocesses such as optimization (using [60]) and sensitivity study (using [70]). This code repository was also responsible for the database connection (SQLight) and experimental data processing. The simulation engine part of the interface has been published on the code hosting platform github.com and can be accessed at [120]. In the later stages of the project, the prepared programming environment has been featured with the web-based interface that is part of the engineering tools platform of the industrial partner. It allows users to use already programmed parameterization methods, run simulations and analyze both simulation and experimental results, remotely, via a web browser interface without the need for any additional software installation. Thanks to the prepared programming interfaces as well as detailed user specifications, the developed methods which are inherently complex can be used as ready-to-use tool by engineers without detailed knowledge and understanding of the underlying functionality. This approach ensures that the developed methods can be practically utilized in the industrial environment.

From the perspective of experimental procedures that have to be carried out in order to calibrate future designs, it has been recognized that the initially proposed method is too complex. Although it has been documented and could be used if necessary, a second approach has been prepared that allows to perform the calibration based on a much simpler testing procedure.

# List of Figures

2.1	Relationship between ride and handling objective measures for various suspension damping and stiffness settings [114, 82] . . . . .	17
2.2	Layout of the two most common passive damper designs . . . . .	19
2.3	Example of the pressure changes in the compression and rebound chambers in dampers with rod and full displacement configuration during sinusoidal excitation . . . . .	21
2.4	Schematic view of the triple tube semi-active shock absorber with one unidirectional active valve . . . . .	22
2.5	Exemplary PQ curve with the description of its distinct ranges . . . . .	23
2.6	Overview of the valve design . . . . .	24
2.7	Simulated intake valve opening shapes . . . . .	24
2.8	Cross section of CES8700 valve [94] . . . . .	26
2.9	Schematic layout of the CES valve [12] . . . . .	26
2.10	Comparison of the PSD profile of the acceleration signals measured at various parts of the automotive suspension . . . . .	29
2.11	Exemplary design of mass absorber used to alter dynamic properties of the shock absorber structure (source: Courtesy of Tenneco Automotive Eastern Europe Sp. z o.o.) . . . . .	30
2.12	Exemplary force-displacement and force-velocity characteristics . . . . .	31
2.13	a) flow test bench, b) cross-section of the metal column: 1 – sealed nut, 2 – pin, 3 –inner tube, 4 – valve location, 5 – inflow/outflow channel [25] . . . . .	32
2.14	Exemplary sinusoidal excitation test results for the high-frequency rod acceleration analysis . . . . .	33
2.15	Exemplary spectrum of rod acceleration resulting from noise excitation test . . . . .	34
3.1	Representation of the dynamic stiffness and loss angle by the Kelvin-Voigt model [106] . . . . .	40
4.1	Schematic drawings of the valve model . . . . .	48
4.2	Friction force in the function of displacement according to Dahl’s friction model [90] . . . . .	51

4.3	View of the purposefully introduced slot that influences the low flow rate part of the P/Q curve (valve bleed) . . . . .	52
4.4	Verification of the discharge coefficient values performed based on the flow-bench test results . . . . .	53
4.5	Schematic layout of the AutoBushFD [2] . . . . .	54
4.6	Exemplary friction force-displacement and force-velocity graph for the piston sliding bearing surface [72] . . . . .	55
4.7	Surfaces at which the friction force is induced at double tube design (courtesy of Tenneco Automotive Eastern Europe Sp. z o.o.) . . . . .	55
4.8	foo bar . . . . .	58
4.9	Impact of stiction force on the force-displacement and force-velocity curves from damper level testing . . . . .	59
4.10	Impact of friction on the force-displacement and force-velocity curves from damper level testing . . . . .	60
6.1	Overview of the sample of the semi-active shock absorber used for the model calibration studies . . . . .	69
6.2	P/Q characteristic of the active valve used in the sample during model calibration studies (in relation to increasing current for the CES valve) . . . . .	70
6.3	Relationship between flow-rate and the pressure drop for all the design cases considered in the model quality assessment, measured on the flow-bench test set-up . . . . .	71
6.4	Result of the baseline design valves parameters estimation: Left column - P-Q characteristic, Middle column - comparison of the pressure, Right column - identified valve stiffness . . . . .	73
6.5	Result of the alternative design valves parameters estimation: Left column - P-Q characteristic, Middle column - comparison of the pressure, Right column - identified valve stiffness . . . . .	74
6.6	Experimental test set-up used for damper level tests . . . . .	77
6.7	Impact of gas content over the shock absorber force-velocity characteristic <sup>2</sup> . . . . .	78
6.8	Results of the compliance-related parameter estimation process - all acquired cycles . . . . .	78
6.9	Results of the compliance-related parameter estimation process - one cycle . . . . .	78
6.10	Dynamic properties in function of the frequency of the baseline top mount, obtained from the calibrated simulation and test results at different excitation amplitudes . . . . .	81
6.11	Dynamic properties in function of the frequency of the alternative design (high stiffness) top mount, obtained from the calibrated simulation and test results at different excitation amplitudes . . . . .	81

6.12	Comparison of the baseline top mount force obtained from simulation and test under random verification excitation . . . . .	82
6.13	Comparison of the alternative design top mount force obtained from simulation and test under random verification excitation . . . . .	82
6.14	Comparison of static load-deflection characteristics ( $F_{LD}(X)$ in equation 4.37) for the baseline and alternative top mount designs . . . . .	83
6.15	Test bench used for the experimental measurements . . . . .	85
6.16	Random noise signal used as an excitation reproducing vibration of the wheel knuckle . . . . .	86
6.17	Curving test results at low active valve coil current (0.32A) line: test results, dotted line: simulation results . . . . .	86
6.18	Curving test results at medium active valve coil current (0.9A) line: test results, dotted line: simulation results . . . . .	87
6.19	Curving test results at high active valve coil current (1.6A) line: test results, dotted line: simulation results . . . . .	87
6.20	Comparison of the test and simulation results of the mono-sine test (13Hz excitation at 10mm of stroke) for high active valve current (1.6A) . . . .	89
6.21	Comparison of the test and simulation results of the mono-sine test (13Hz excitation at 10mm of stroke) for medium active valve current (0.9A) . .	90
6.22	Comparison of the test and simulation results of the mono-sine test (13Hz excitation at 10mm of stroke) for low active valve current (0.32A) . . . .	91
6.23	Comparison of the test and simulation results of the mono-sine test (13Hz excitation at 10mm of stroke) for baseline and alternative top-mount designs	92
6.24	Comparison of the test and simulation results of the mono-sine test (13Hz excitation at 10mm of stroke) for baseline and increased precharge pressure (5 bar) scenario . . . . .	93
6.25	Comparison of the test and simulation results of the mono-sine test (13Hz excitation at 10mm of stroke) for baseline and different active valve designs	94
6.26	Comparison of the test and simulation results of the mono-sine test (13Hz excitation at 10mm of stroke) for baseline and lower piston intake stiffness (see fig. 6.3) designs . . . . .	95
6.27	Comparison of the test and simulation results of the mono-sine test (13Hz excitation at 10mm of stroke) for baseline and lower piston rebound stack stiffness (see fig. 6.3) designs . . . . .	95
6.28	Comparison of the test and simulation results of the mono-sine test (13Hz excitation at 10mm of stroke) for baseline and lower base-valve intake stiffness (see fig. 6.3) designs . . . . .	96

6.29	Comparison of the test and simulation results of the mono-sine test (13Hz excitation at 10mm of stroke) for baseline and lower base-valve compression stack stiffness (see fig. 6.3) designs . . . . .	96
6.30	Comparison of the test and simulation of the random excitation signal test (see signal in fig. 6.16a and 6.16b) of different active valve currents . . .	97
6.31	Comparison of the test and simulation of the random excitation signal test (see signal in fig. 6.16a and 6.16b) for baseline and alternative top-mount designs . . . . .	97
6.32	Comparison of the test and simulation of the random excitation signal test (see signal in fig. 6.16a and 6.16b) for baseline and increased precharge pressure (5 bar) scenario . . . . .	98
6.33	Comparison of the test and simulation of the random excitation signal test (see signal in fig. 6.16a and 6.16b) for baseline and different active valve designs . . . . .	98
6.34	Comparison of the test and simulation of the random excitation signal test (see signal in fig. 6.16a and 6.16b) for baseline and lower piston intake stiffness (see fig. 6.3) designs . . . . .	99
6.35	Comparison of the test and simulation of the random excitation signal test (see signal in fig. 6.16a and 6.16b) for baseline and lower piston rebound stack stiffness (see fig. 6.3) designs . . . . .	99
6.36	Comparison of the test and simulation of the random excitation signal test (see signal in fig. 6.16a and 6.16b) for baseline and lower base-valve intake stiffness (see fig. 6.3) designs . . . . .	100
6.37	Comparison of the test and simulation of the random excitation signal test (see signal in fig. 6.16a and 6.16b) for baseline and lower base-valve compression stack stiffness (see fig. 6.3) designs . . . . .	100
7.1	Training excitation signal used for the sensitivity-based parameter calibration procedure . . . . .	106
7.2	Overview of the tooling used during the module level calibration test to register displacement of the rod in relation to the top-mount housing . .	107
7.3	Test bench used for the experimental part of the sensitivity-based parameter estimation procedure . . . . .	108
7.4	Results of the top mount model calibration . . . . .	109
7.5	Dynamic characteristics obtained from the calibration top mount model simulation at different excitation frequencies and amplitudes . . . . .	110
7.6	Sensitivity signals (first-order Sobol index) and valves opening of the different passive valves. For clarity, the opening of the intake valves has been plotted with a negative sign . . . . .	111

7.7	Improvements in reduction of the residual between simulation and training force signal across the iterations for each of the concurrent genetic algorithms	112
7.8	Comparison of the force signal obtained from the test and calibrated model of shock absorber assembly under verification signal excitation . . . . .	113
7.9	Comparison of the force signal obtained from the test and model after parameters have been calibrated with sensitivity-based parameters estimation procedure . . . . .	115
7.10	Comparison of force-displacement characteristics obtained from simulation and physical test . . . . .	116
7.11	16Hz excitation 0.5m/s at 10mm stroke with 0.32A active valve current .	117
7.12	16Hz excitation 0.5m/s at 10mm stroke with 0.9A active valve current . .	117
7.13	16Hz excitation 0.5m/s at 10mm stroke with 1p6A active valve current .	118
7.14	Comparison of power spectra of rod acceleration signals obtained from simulation and physical test, solid line - test, dotted line - simulation results	118

# List of Tables

3.1	Summary of the physical phenomena related to the automotive shock absorbers reproduced by models across publications * * abbreviation of damper types: M - monotube, D - double tube, T - semiactive triple tube with one unidirectional active valve . . . . .	37
4.1	Maximum opening velocity of the valves registered during damper level test simulation . . . . .	57
5.1	Summary of all the input parameters used in the model . . . . .	65
6.1	Parameters identified with the genetic algorithm at valve level . . . . .	72
6.2	Parameters of the genetic algorithm used for valves parameters identification	75
6.3	Parameters of the genetic algorithm used for valves parameters identification	76
6.4	Summary of the top mount model parameters and the limits used for the calibration process . . . . .	79
6.5	Summary of the mono-sine test results comparison of the test and simulation	90
6.6	Summary of the random test results comparison of the test and simulation	91
7.1	Summary of the mono-sine test results of the test and simulation . . . . .	113
7.2	Summary of the random test results of the test and simulation . . . . .	113

# List of Symbols

The next list describes symbols that were used within the body of the document

$\Gamma$	Polytropic index, see eq. 4.15
$\nu$	Poisson's ratio, see eq. 4.17
$\psi$	Wall compliance, see eq. 4.17
$\rho$	Density of the hydraulic medium, see eq. 4.8
$E$	Young modulus, see eq. 4.17
$K$	Bulk modulus, see eq. 4.9
$m$	Mass, see eq. 4.8
$p$	Pressure, see eq. 4.8
$Q$	Volumetric flow rate, see eq. 4.9
$V$	Volume, see eq. 4.8

## Damper model

$A_b$	Surface area of the piston on which the compression chamber pressure is applied, see eq. 4.1
$A_r$	Surface area of the piston on which the rebound chamber pressure is applied, see eq. 4.1
$D_{PT}$	Inner diameter of the pressure tube, see eq. 4.2
$D_R$	Outer diameter of the piston rod, see eq. 4.3
$F_\mu$	Total frictional force induced at the rod guide and piston berings and sealing, see eq. 4.1
$F_d$	Rod force exerted by the shock absorber, see eq. 4.1
$F_{tm}$	Force exerted on the rod by the top mount, see eq. 4.4
$K_b$	Effective bulk modulus of the third tube chamber, see eq. 4.12
$K_c$	Effective bulk modulus of the compression tube chamber, see eq. 4.11
$K_r$	Effective bulk modulus of the rebound tube chamber, see eq. 4.10
$l_{c0}$	Length of the compression chamber at damper initial position, see eq. 4.5
$l_{r0}$	Length of the rebound chamber at damper initial position, see eq. 4.6

$M_{rod}$	Mass of the rod assembly (including all the components rigidly attached), see eq. 4.4
$P_b$	Pressure in the third tube, see eq. 4.12
$P_c$	Pressure in the compression chamber, see eq. 4.1
$P_r$	Pressure in the rebound chamber, see eq. 4.1
$Q_a$	Volumetric flow rate through the active valve, see eq. 4.12
$Q_{bp}$	Volumetric flow rate through the base valve, see eq. 4.12
$Q_{bv}$	Volumetric flow rate through the third tube orifice, see eq. 4.11
$Q_p$	Volumetric flow rate through the piston valve, see eq. 4.11
$r_i$	Inner radius of the third tube, see eq. 4.17
$r_o$	Outer radius of the third tube, see eq. 4.17
$V_b$	Volume of the third tube chamber, see eq. 4.7
$V_b$	Volume of the third tube chamber, see eq. 4.12
$V_c$	Volume of the compression chamber, see eq. 4.6
$V_r$	Volume of the rebound chamber, see eq. 4.5
$x_{tube}$	Displacement of the damper tube in relation to rod (positive $\rightarrow$ compression of the damper), see eq. 4.5

### Hydraulic medium

$\chi$	volumetric gas content of the emulsion, see eq. 4.15
$\rho_{eml}$	Density of the oil-gas emulsion, see eq. 4.15
$\rho_{gas}$	Density of the gas, see eq. 4.15
$\rho_{oil}$	Density of the oil, see eq. 4.15
$\theta$	Volumetric fraction of undissolved gas, see eq. 4.14
$K_{eml}$	Bulk modulus related to the compressibility of the hydraulic medium (oil gas emulsion), see eq. 4.13
$K_{oil}$	Bulk modulus of the oil, see eq. 4.15
$K_{total}$	Effective bulk modulus of chamber, see eq. 4.13
$K_{wall}$	Bulk modulus related to the wall compliance, see eq. 4.13
$P_{ref}$	Reference pressure, see eq. 4.15
$P_{sat}$	Oil saturation pressure, see eq. 4.15
$P_{vap}$	Oil vaporisation pressure, see eq. 4.14
$T_{ref}$	Reference temperature, see eq. 4.15

## Parameter identification

$\Theta$  Estimated parameters, see eq. 7.1

$F_{simulation}$  Force generated by shock absorber during simulation, see eq. 6.2

$F_{test}$  Force generated by shock absorber during test, see eq. 6.2

$I$  First order Sobol index

$J$  Goal function, see eq. 7.1

## Rod friction modeling

$\alpha_s$  Stribeck effect coefficient, see eq. 4.38

$a_s$  Stribeck constant, see eq. 4.41

$c_{comp}$  Tangential compliance damping coeff., see eq. 4.39

$F_c$  Coulomb friction force, see eq. 4.41

$F_s$  Static friction, see eq. 4.41

$k_b$  LuGre bristles stiffness, see eq. 4.38

$s_1$  Bristle damping coefficient, see eq. 4.38

$s_2$  Viscous friction coefficient, see eq. 4.38

$vd$  Velocity threshold, see eq. 4.39

$z$  Bristle deflection, see eq. 4.39

## Valve stiffness approximation

$a$  First stiffness approximation coefficient, see eq. 4.19

$b$  Second stiffness approximation coefficient, see eq. 4.19

$c$  Third stiffness approximation coefficient, see eq. 4.19

$d$  Fourth stiffness approximation coefficient, see eq. 4.19

## Top mount

$C_0$  Produces the roll-off observed in the experimental data at low velocities, see eq. 4.34

$C_1$  Accounts for the relaxation of the bushing impact force, see eq. 4.34

$C_3$  Represents the viscous damping observed at large velocities, see eq. 4.34

$K_0$  Represents the bushing rubber stiffness, see eq. 4.33

$K_1$  Represents the bushing rubber stiffness, see eq. 4.33

$K_3$  Rubber stiffness at high velocities, see eq. 4.33

$P_0$  Scale factor for stiffness, see eq. 4.35

$P_1$  Scale factor for stiffness, see eq. 4.35

- $P_3$  Scale factor for stiffness, see eq. 4.35
- $Q_0$  Scale factor for damping, see eq. 4.34
- $Q_1$  Scale factor for damping, see eq. 4.34
- $Q_3$  Scale factor for damping, see eq. 4.34
- $R$  The cutoff frequency related to a first order filter that acts on the input X, see eq. 4.32
- $X_{Static}$  The static force response of the bushing, see eq. 4.37
- $x_{tm}$  Top mount input displacement, see eq. 4.32

### Valve modeling

- $\alpha$  Dahl coefficient controlling shape of the stress-strain curve, see eq. 4.26
- $\Delta p_{test}$  Pressure drop during the test, see eq. 6.1
- $\lambda$  Flow number, see eq. 4.31
- $\lambda_{crit}$  Critical flow number, see eq. 4.30
- $\mu$  Viscosity of the hydraulic medium, see eq. 4.25
- $\nu$  Kinematic viscosity, see eq. 4.31
- $\sigma_0$  Dahl's friction stiffness coefficient, see eq. 4.26
- $\zeta$  Angle of the deflected oil stream, see eq. 4.23
- $A_{bleed}$  Flow area of the valve bleed
- $A_{fi}$  Flow area due to opening of the intake disc, see eq. 4.28
- $A_{fs}$  Flow area due to opening of the shim stack disk, see eq. 4.27
- $A_f$  Flow area, see eq. 4.23
- $A_{slot}$  Flow area of the valve slot
- $C_{q,max}$  Discharge coefficient at turbulent flow regime, see eq. 4.30
- $C_q$  Discharge coefficient, see eq. 4.30
- $c_v$  Valve damping, see eq. 4.20
- $D_c$  Inner diameter of the valve slot, see eq. 4.21
- $D_d$  Outer diameter of the valve disc, see eq. 4.21
- $D_{Hyd}$  Hydraulic diameter, see eq. 4.31
- $D_h$  Inner diameter of the intake valve disc
- $D_h$  Inner diameter of the intake valve disk
- $D_i$  Outer diameter of the valve slot, see eq. 4.21
- $F_{\Delta p}$  Force exerted on the valve due to pressure differential, see eq. 4.20

$F_\mu$	Force exerted on the valve by the friction forces, see eq. 4.20
$F_c$	Coulomb (dynamic) friction coefficient, see eq. 4.26
$F_k$	Force exerted on the valve due to valve stiffness, see eq. 4.20
$F_m$	Force exerted on the valve due to change of flow momentum, see eq. 4.20
$F_{preload}$	Valve stiffness preload, see eq. 4.19
$F_{st}$	Force exerted on the valve by stiction force, see eq. 4.20
$m_v$	Mass of the valve moving part, see eq. 4.20
$p_1$	Pressure in chamber above the considered valve, see eq. 4.21
$p_2$	Pressure in the chamber below considered valve, see eq. 4.21
$p_{simulation}$	Pressure during the simulation, see eq. 6.1
$T$	Total duration of the simulation or test, see eq. 6.1
$V_f$	Flow velocity, see eq. 4.23
$x_{v0}$	Initial valve separation distance for the stiction force calculation, see eq. 4.25

# Bibliography

- [1] Automobile Ride, Handling, and Suspension. *Q. Riley Enterprises*, page 83.
- [2] MotionView Documentation, 2017.
- [3] Simcenter Technical Bulletin No. 117, HYD Advanced Fluid Properties, 2019.
- [4] Simcenter Technical Bulletin No. 118, HYD Robert Bosch Fluid Properties, 2019.
- [5] The World's Fastest Reacting Suspension Technology Gets Even Faster with MagneRide 4.0. <https://media.cadillac.com/media/us/en/cadillac/vehicles/ct4-v/2021.detail.html/content/Pages/news/us/en/2020/oct/1015-technology.html>, October 2020.
- [6] CDC Dampers for Cars. <https://aftermarket.zf.com/go/en/sachs/products/cars-and-vans/shock-absorbers-and-dampers/cdc/>, 2022.
- [7] Damping Technology by ZF, 2022.
- [8] Monroe riding high on the electronic suspension market. <https://www.just-auto.com/analysis/monroe-riding-high-on-the-electronic-suspension-market-briefing/>, 2022.
- [9] SIMULIA Simpack Documentation, 2022.
- [10] Adams Solver User's Guide, 2023.
- [11] P J Allen, A Hameed, and H Goyder. Automotive Damper Model for Use in Multi-Body Dynamic Simulations. *Proceedings of the Institution of Mechanical Engineers, Part D: Journal of Automobile Engineering*, 220(9):1221–1233, September 2006.
- [12] Samuel Andre. *Optimization of Valve Damping*. Master of Science, Linköping University, Linköping, Sweden, 2013.
- [13] Kristofer Arvidsson and Róbert Már Runólfsson. *Development of Methods for Objectively Quantifying Performance of Active Suspension Systems*. Master of Science, Chalmers University of Technology, Gothenburg, 2019.

- [14] Ibrahim Badiru and W. Bradley Cwycyshyn. Customer Focus in Ride Development. In *SAE 2013 World Congress & Exhibition*, pages 2013–01–1355, April 2013.
- [15] Vijay Barethiye, G. Pohit, and A. Mitra. A combined nonlinear and hysteresis model of shock absorber for quarter car simulation on the basis of experimental data. *Engineering Science and Technology, an International Journal*, 20(6):1610–1622, December 2017.
- [16] Nicola Bartolini, Lorenzo Scappaticci, Francesco Castellani, and Alberto Garinei. The Knocking Noise on Twin Tube Shock Absorbers: Individuation and Analysis of the Phenomenon. In *SAE 2016 World Congress and Exhibition*, pages 2016–01–1549, April 2016.
- [17] D Bell and Rg Beale. Numerical Investigation of a Mono-Tube Damper with a Shim Stack. *Proceedings of the Institution of Mechanical Engineers, Part C: Journal of Mechanical Engineering Science*, 231(9):1762–1774, May 2017.
- [18] Marouane Benaziz. *Identification et Modélisation de Phénomènes Vibratoires Non-Linéaires Dans Les Amortisseurs*. PhD thesis, 2013.
- [19] Marouane Benaziz, Samuel Nacivet, Jérémie Deak, and Fabrice Thouverez. Double Tube Shock Absorber Model for Noise and Vibration Analysis. *SAE Int. J. Passeng. Cars - Mech. Syst.*, 6(2):1177–1185, May 2013.
- [20] Marouane Benaziz, Samuel Nacivet, and Fabrice Thouverez. A Shock Absorber Model for Structure-Borne Noise Analyses. *Journal of Sound and Vibration*, 349:177–194, August 2015.
- [21] John F. Blackburn and J. Lowen Shearer. *Fluid power control*. The Mit Press, Cambridge (Massachusetts), 4 ed edition, 1972.
- [22] Michael Blundell and Damian Harty. *Multibody Systems Approach to Vehicle Dynamics*. Elsevier Butterworth-Heinemann, Oxford Burlington, MA, 2004.
- [23] David Bogema, Paul Goodes, Chahe Apelian, and Michael Csakan. Noise Path Analysis Process Evaluation of Automotive Shock Absorber Transient Noise. In *SAE 2009 Noise and Vibration Conference and Exhibition*, pages 2009–01–2091, May 2009.
- [24] Rodney Bouc. Forced Vibration of Mechanical Systems with Hysteresis. In *4th International Conference on Nonlinear Oscillations*, Prague, Czechoslovakia, 1967.
- [25] Daniel Buczkowski, Szymon Zymelka, and Grzegorz Nowak. Experimental and Numerical Studies on the Development of Hysteresis in a Shock Absorber with a

- Shim Disc Valve. *International Journal of Automotive and Mechanical Engineering*, 19(2):9747–9758, June 2022.
- [26] Francesca Campolongo, Andrea Saltelli, and Jessica Cariboni. From screening to quantitative sensitivity analysis. A unified approach. *Computer Physics Communications*, 182(4):978–988, April 2011.
- [27] C. Canudas De Wit, H. Olsson, K.J. Astrom, and P. Lischinsky. A new model for control of systems with friction. *IEEE Transactions on Automatic Control*, 40(3):419–425, March 1995.
- [28] Ford Motor Company. *Ford Manual for Owners and Operators of Ford Cars*. Ford motor Company, 1915.
- [29] Francesco I Cosco, Gianluca Gatti, Alessandro Toso, and Stijn Donders. An Optimized Identification Method for Modular Models of Rubber Bushings.
- [30] Jesse Crosse. The design, development and applications of MagneRide suspension. <https://www.autocar.co.uk/car-news/new-cars/design-development-and-applications-magneride-suspension>, October 2014.
- [31] P Czop, D Sławik, P Śliwa, and G Wszolek. Simplified and Advanced Models of a Valve System Used in Shock Absorbers. *Journal of Achievements in Materials and Manufacturing Engineering*, 33(2):9, 2009.
- [32] Piotr Czop, Damian Gasiorek, Jacek Gniłka, Damian Sławik, Grzegorz Wszolek, Damian Gasiorek@polsl, Pl, Jacek Gniłka@polsl, and Grzegorz Pl. Fluid-structure simulation of a valve system used in hydraulic dampers. *Modelowanie Inzynierskie*, 45:197–205, January 2012.
- [33] Piotr Czop and Damian Sławik. A high-frequency first-principle model of a shock absorber and servo-hydraulic tester. *Mechanical Systems and Signal Processing*, 25(6):1937–1955, August 2011.
- [34] Piotr Czop, Damian Sławik, and Pawel Sliwa. Static Validation of a Model of a Disc Valve System Used in Shock Absorbers. *International Journal of Vehicle Design*, 53(4):317–342, 2010.
- [35] L. Dahil. Effect on the Vibration of the Suspension System. *Metalurgija*, 56(3-4):375–378, 2017.
- [36] R Dalbey, S Eldred, Kathryn A Maupin, Jason A Monschke, D Thomas Seidl, Laura P Swiler, and Anh Tran. *Dakota, A Multilevel Parallel Object-Oriented*

*Framework for Design Optimization, Parameter Estimation, Uncertainty Quantification, and Sensitivity Analysis*., May 2022.

- [37] Tod Dalrymple, Juan A Hurtado, I. Lapczyk, and H.R. Ahmadi. Parallel rheological framework to model the amplitude dependence of the dynamic stiffness in carbon-black filled rubber. In *Constitutive Models for Rubber IX*, pages 205–212. CRC Press, 0 edition, October 2015.
- [38] Bill Dawson and Simonetta Esposito. Tenneco’s CVSAe Suspension Technology Launching in China. <https://www.tenneco.com/news/news-detail/2021/11/02/tenneco-s-cvsae-suspension-technology-launching-in-china-on-new-zeekr-001-premium-electric-vehicle#:~:text=CVSAe%20technology%20is%20one%20of,damping%20characteristics%20at%20all%20times.,> 2021.
- [39] Matthew de Brett, Tore Butlin, Robin Langley, and Ole M Nielsen. Modelling Vibration Transmission Through a Car’s Damper and Top Mount Strut. page 8, 2019.
- [40] John C Dixon. *The Shock Absorber Handbook*. John Wiley and Sons, 2nd edition, 2007.
- [41] S. Duym, R. Stiens, G. Baron, and K. Reybrouck. Physical Modeling of the Hysteretic Behaviour of Automotive Shock Absorbers. In *SAE International Congress and Exposition*, 1997.
- [42] Stefaan Duym. Simulation Tools, Modelling and Identification, for an Automotive Shock Absorber in the Context of Vehicle Dynamics. *Vehicle System Dynamics - VEH SYST DYN*, 33:261–285, April 2000.
- [43] Stefaan Duym and Koenraad Reybrouck. Physical Characterization of Nonlinear Shock Absorber Dynamics. *Eur. j. mech. environ. eng*, 43(4):181–188, 1998.
- [44] Stefaan Duym, Randy Steins, and Koenraad Reybrouck. Evaluation of Shock Absorber Models. *Vehicle System Dynamics*, 27(2):109–127, February 1997.
- [45] Vinzenz Gregor Eck, Wouter Paulus Donders, Jacob Sturdy, Jonathan Feinberg, Tammo Delhaas, Leif Rune Hellevik, and Wouter Huberts. A guide to uncertainty quantification and sensitivity analysis for cardiovascular applications. *Int. J. Numer. Meth. Biomed. Engng.*, 32(8):e02755, August 2016.
- [46] Rafael Eder, Christian Zehetner, and Wolfgang Kunze. Comparison of Parameter Identification Techniques. *MATEC Web Conf.*, 70:09007, 2016.

- [47] Mathias Eickhoff, Alexander Kruse, Andreas Tischer, Jörg Pagel, and Hendrik Marquar. Dynamic Characteristics of a Shock Absorber Module: Optimization of Vehicle Acoustics. *ATZ Worldwide*, 111:28–35, 2009.
- [48] Mathias Eickhoff, Reinhard Sonnenburg, and Anja Stretz. Piston Rod Vibrations in Damper Modules — Causes and Remedies. *ATZ Worldw*, 112(1):24–29, January 2010.
- [49] Gershon Elber. Interpolation using bézier curves. In *Graphics Gems III (IBM Version)*, pages 133–136. Elsevier, 1992.
- [50] R. D. Eyres, A. R. Champneys, and N. A. J. Lieven. Modelling and Dynamic Response of a Damper with Relief Valve. *Nonlinear Dyn*, 40(2):119–147, April 2005.
- [51] Jianguang Fang, Yunkai Gao, Guangyong Sun, and Qing Li. Development of a novel identification platform for automotive dampers. *International Journal of Vehicle Design*, 66(3):272, 2014.
- [52] Alireza Farjoud, Mehdi Ahmadian, Michael Craft, and William Burke. Nonlinear Modeling and Experimental Characterization of Hydraulic Dampers: Effects of Shim Stack and Orifice Parameters on Damper Performance. *Nonlinear Dynamics*, 67, June 2012.
- [53] J. W. Fash. Modeling of Shock Absorber Behavior using Artificial Neural Networks. In *International Congress & Exposition*, page 940248, March 1994.
- [54] Urszula Ferdek. The Modelling and Analysis of Shock Absorbers with Stroke-Dependent Damping. *CT*, (1), 2018.
- [55] Urszula Ferdek and Jan Łuczko. Modeling and Analysis of a Twin-Tube Hydraulic Shock Absorber. *JOURNAL OF THEORETICAL AND APPLIED MECHANICS*, 50(2):627–638, 2012.
- [56] Marek Fidali. Application of evolutionary algorithm to limitation of a set of statistical features of thermovision images. *Computer Assisted Mechanics and Engineering Sciences*, 14(4):601–609, 2007.
- [57] Marek Fidali and Wojciech Jamrozik. Concept of Database Architecture Dedicated to Data Fusion Based Condition Monitoring Systems. In Stanislaw Kozielski, Dariusz Mrozek, Pawel Kasprowski, Bożena Małysiak-Mrozek, and Daniel Kostrzewa, editors, *Beyond Databases, Architectures, and Structures*, volume 424, pages 515–526. Springer International Publishing, Cham, 2014.

- [58] Bartłomiej Franczyk, Michał Maniowski, and Janusz Gołdasz. Frequency-dependent automotive suspension damping systems: State of the art review. *Proceedings of the Institution of Mechanical Engineers, Part D: Journal of Automobile Engineering*, page 095440702311742, May 2023.
- [59] Andrew Frankel. Smooth sailing: How to build the most comfortable car. *Autocar*, April 2019.
- [60] Ahmed Fawzy Gad. PyGAD: An Intuitive Genetic Algorithm Python Library. *arXiv*, page 7, 2021.
- [61] Anders Gällsjö and Mattias Johansson. *Physical Modelling and Automatic Configuration of CES Valve*. Master of Science, Linköping University, Linköping, Sweden, 2012.
- [62] C T T Geluk. *Vehicle Vibration Comfort: The Influence of Dry Friction in the Suspension*. Master of Science, Technische Universiteit Eindhoven, Eindhoven, 2005.
- [63] Janusz Gołdasz. High-Frequency Model of Monotube Shock Absorbers. *Modelowanie Inżynierskie*, (39):81–88, 2010.
- [64] Janusz Gołdasz and Bogdan Sapiński. *Insight into Magnetorheological Shock Absorbers*. Springer International Publishing : Imprint: Springer, Cham, 1st ed. 2015 edition, 2015.
- [65] Joseph H.A. Guillaume, John D. Jakeman, Stefano Marsili-Libelli, Michael Asher, Philip Brunner, Barry Croke, Mary C. Hill, Anthony J. Jakeman, Karel J. Keesman, Saman Razavi, and Johannes D. Stigter. Introductory overview of identifiability analysis: A guide to evaluating whether you have the right type of data for your modeling purpose. *Environmental Modelling & Software*, 119:418–432, September 2019.
- [66] P. Hagedorn and J. Wallaschek. On Equivalent Harmonic and Stochastic Linearization for Nonlinear Shock-Absorbers. In F. Ziegler and G. I. Schuëller, editors, *Nonlinear Stochastic Dynamic Engineering Systems*, pages 23–32. Springer Berlin Heidelberg, Berlin, Heidelberg, 1988.
- [67] B B Hall and K F Gill. Performance of a Telescopic Dual-Tube Automotive Damper and the Implications for Vehicle Ride Prediction. *Proceedings of the Institution of Mechanical Engineers, Part D: Transport Engineering*, 200(2):115–123, April 1986.
- [68] Matthew Harrison. Vehicle Refinement - Controlling Noise and Vibration in Road Vehicles. <https://www.elsevier.com/books/vehicle-refinement/harrison/978-0-7506-6129-4>, August 2004.

- [69] Bernd Heissing and Metin Ersoy, editors. *Chassis Handbook: Fundamentals, Driving Dynamics, Components, Mechatronics, Perspectives*. ATZ. Vieweg + Teubner, Wiesbaden, 1st edition edition, 2011.
- [70] Jon Herman and Will Usher. SALib: An open-source Python library for Sensitivity Analysis. *The Journal of Open Source Software*, 2(9):97, January 2017.
- [71] F. Herr, T. Mallin, J. Lane, and S. Roth. A Shock Absorber Model Using CFD Analysis and Easy5. In *International Congress & Exposition*, pages 1999–01–1322, March 1999.
- [72] Ludwig Herzog. *Theoretical and Experimental Investigations of the Friction Behavior of Automotive Shock Absorbers*. PhD thesis, TU Ilmenau, December 2021.
- [73] Takuya Iwanaga, Will Usher, and Jon Herman. Toward SALib 2.0: Advancing the accessibility and interpretability of global sensitivity analyses. page 16, 2022.
- [74] Hanen Jrad, Jean Luc Dion, Franck Renaud, Imad Tawfiq, and Mohamed Haddar. Non-Linear Generalized Maxwell Model for Dynamic Characterization of Viscoelastic Components and Parametric Identification Techniques. In *Volume 1: 24th Conference on Mechanical Vibration and Noise, Parts A and B*, pages 291–300, Chicago, Illinois, USA, August 2012. American Society of Mechanical Engineers.
- [75] Sourabh Katoch, Sumit Singh Chauhan, and Vijay Kumar. A review on genetic algorithm: Past, present, and future. *Multimedia Tools and Applications*, 80(5):8091–8126, February 2021.
- [76] Marc C. Kennedy and Anthony O’Hagan. Bayesian Calibration of Computer Models. *Journal of the Royal Statistical Society: Series B (Statistical Methodology)*, 63(3):425–464, 2001.
- [77] H E Khalifa and X Liu. Analysis of Stiction Effect on the Dynamics of Compressor Suction Valve. In *International Compressor Engineering Conference*, page 13, 1998.
- [78] David E Kline. *Geometric Design of Independent Suspension Linkages*. Doctor of Philosophy, University of Michigan, Michigan, USA, 2018.
- [79] Don Knowles. *Automotive Suspension & Steering Systems*. Today’s Technician. Thomson/Delmar Learning, Clifton Park, NY, 4th ed edition, 2007.
- [80] Peter Koch, Christian Angrick, Denise Beitelschmidt, Günther Prokop, and Peter Knauer. Influence of Rubber Temperature on Transfer Functions of Bushings. *SAE International Journal of Passenger Cars - Mechanical Systems*, 8(4):1209–1217, December 2015.

- [81] Alexander Kruse. Characterizing and Reducing Structural Noises of Vehicle Shock Absorber Systems. In *SAE 2002 World Congress & Exhibition*, pages 2002–01–1234, March 2002.
- [82] Ferit Küçükay. *Fahrzeugschwingungen*. Institut für Fahrzeugsystemtechnik, Braunschweig, Germany, 2011.
- [83] Harold Harvey Lang. *A Study of the Characteristics of Automotive Hydraulic Dampers at High Stroking Frequencies*. PhD thesis, 1977.
- [84] Ill-Yeong Lee and Dan Dan Sun. Evaluation of Effective Bulk Modulus of Oil in Automotive Hydraulic Dampers. In *SICE Annual Conference*, Sapporo, 2004.
- [85] Kwangjin Lee. Numerical Modelling for the Hydraulic Performance Prediction of Automotive Monotube Dampers. *Vehicle System Dynamics*, 28(1):25–39, July 1997.
- [86] Jason L Loeppky, Derek Bingham, and William J Welch. Computer Model Calibration or Tuning in Practice. page 21.
- [87] Michael W. Neal, Walter Cwycyshyn, and Ibrahim Badiru. Tuning Dampers for Ride and Handling of Production Vehicles. *SAE International Journal of Commercial Vehicles*, 8(1):152–159, April 2015.
- [88] Tommy Nilsson and Matteo Pelosi. *2-Way FSI Simulations on a Shock Absorber Check Valve*. Master of Science, KTH Royal Institute of Technology, Stockholm, Sweden, 2015.
- [89] Jin-Kyu Ok, Jeong-Hyun Sohn, and Wan-Suk Yoo. Development of Nonlinear Coupled Mode Bushing Model Based on the Bouc-Wen Hysteretic Model. In *Volume 5: 6th International Conference on Multibody Systems, Nonlinear Dynamics, and Control, Parts A, B, and C*, pages 1987–1994, Las Vegas, Nevada, USA, January 2007. ASMEDC.
- [90] H. Olsson, K. J. Åström, C. Canudas de Wit, M. Gäfvert, and P. Lischinsky. Friction Models and Friction Compensation. *European Journal of Control*, 4(3):176–195, January 1998.
- [91] Kyushik Park, Jeongrae Kim, and Dongshin Kim. A Study on the Dynamic Characteristics of the Continuously Variable Shock Absorber for Semi-Active Damping Control System. In *SAE 2005 World Congress & Exhibition*, pages 2005–01–1711, April 2005.

- [92] Margie Pazikas and Simonetta Esposito. Tenneco Introduces New Adaptive Damping Technology On The Ford Focus RS High Performance Road Car. <https://www.tenneco.com/news/news-detail/2015/09/16/tenneco-introduces-new-adaptive-damping-technology-on-the-ford-focus-rs-high-performance-road-car>, 2015.
- [93] Enrico Pellegrini, Guido Koch, and Boris Lohmann. Physical Modeling of a Nonlinear Semi-Active Vehicle Damper. *IFAC Proceedings Volumes*, 43(7):324–329, July 2010.
- [94] Matteo Pelosi, Kashyap Subramanya, and Jonas Lantz. Investigation on the Dynamic Behavior of a Solenoid Hydraulic Valve for Automotive Semi-Active Suspensions Coupling 3D and 1D Modeling,. In *13th Scandinavian International Conference on Fluid Power, June 3-5, 2013, Linköping, Sweden*, pages 241–250, September 2013.
- [95] Francesca Pianosi, Keith Beven, Jim Freer, Jim W. Hall, Jonathan Rougier, David B. Stephenson, and Thorsten Wagener. Sensitivity analysis of environmental models: A systematic review with practical workflow. *Environmental Modelling & Software*, 79:214–232, May 2016.
- [96] O. Polach. Modelling of Rubber Components Using Estimated Parameters. In *The Dynamics of Vehicles on Roads and Tracks*, pages 977–986. CRC Press, 0 edition, March 2016.
- [97] D. J. Purdy. Theoretical and Experimental Investigation into an Adjustable Automotive Damper. *Proceedings of the Institution of Mechanical Engineers, Part D: Journal of Automobile Engineering*, 214(3):265–283, March 2000.
- [98] Na Qiu, Chanyoung Park, Yunkai Gao, Jianguang Fang, Guangyong Sun, and Nam H. Kim. Sensitivity-Based Parameter Calibration and Model Validation Under Model Error. *Journal of Mechanical Design*, 140(1):011403, January 2018.
- [99] M. D. Rao and S. Gruenberg. Measurement of Equivalent Stiffness and Damping of Shock Absorbers. *Exp Tech*, 26(2):39–42, March 2002.
- [100] Mohan D. Rao, Scott Gruenberg, and Homa Torab. Measurement of Dynamic Properties of Automotive Shock Absorbers for NVH. In *Noise & Vibration Conference & Exposition*, pages 1999–01–1840, May 1999.
- [101] Koenraad Reybrouck. A Non Linear Parametric Model of an Automotive Shock Absorber. In *International Congress & Exposition*, page 940869, March 1994.

- [102] German Sacramento and Jorge Biera. Simulation tool for shock absorber noise prediction in time and frequency domains. *International Journal of Vehicle Noise and Vibration*, 3(3):217, 2007.
- [103] Andrea Saltelli. Making best use of model evaluations to compute sensitivity indices. *Computer Physics Communications*, 145(2):280–297, May 2002.
- [104] Andrea Saltelli, Paola Annoni, Ivano Azzini, Francesca Campolongo, Marco Ratto, and Stefano Tarantola. Variance based sensitivity analysis of model output. Design and estimator for the total sensitivity index. *Computer Physics Communications*, 181(2):259–270, February 2010.
- [105] Sergio Matteo Savaresi, Charles Poussot-Vassal, Cristiano Spelta, Luc Dugard, and Olivier Sename. *Semi-Active Suspension Control Design for Vehicles*. Butterworth-Heinemann, Oxford Burlington, Mass, 1e éd edition, 2010.
- [106] Christian Scheiblegger, Jinhuai Lin, and Hannes Karrer. New Nonlinear Bushing Model for Ride Comfort and Handling Simulation: Focussing on Linearization and the Implementation into MBS Environment. In SAE-China and FISITA, editors, *Proceedings of the FISITA 2012 World Automotive Congress*, volume 198 of *Lecture Notes in Electrical Engineering*, pages 461–473. Springer Berlin Heidelberg, Berlin, Heidelberg, 2013.
- [107] Kai Sedlaczek, Sven Dronka, and Jochen Rauh. Advanced modular modelling of rubber bushings for vehicle simulations. *Vehicle System Dynamics*, 49(5):741–759, May 2011.
- [108] L. Segel and H. H. Lang. The Mechanics of Automotive Hydraulic Dampers at High Stroking Frequencies. *Vehicle System Dynamics*, 10(2-3):82–85, September 1981.
- [109] Marian Sikora. Pomiary Drgań i Ciśnienia w Amortyzatorze Hydraulicznym w Zawieszeniu Samochodowym. *CT*, 8(4), 2017.
- [110] Marian Sikora. Modeling and Operational Analysis of an Automotive Shock Absorber with a Tuned Mass Damper. *Acta Mechanica et Automatica*, 12(3):243–251, September 2018.
- [111] Marian Sikora. *Selected Aspects of Dynamic Behaviour of Automotive Hydraulic Shock Absorbers*. PhD thesis, 2021.
- [112] Paweł Skalski and Klaudia Kalita. Role of Magnetorheological Fluids and Elastomers in Today’s World. *Acta Mechanica et Automatica*, 11(4):267–274, December 2017.

- [113] I.M Sobol'. Global sensitivity indices for nonlinear mathematical models and their Monte Carlo estimates. *Mathematics and Computers in Simulation*, 55(1-3):271–280, February 2001.
- [114] Ama Soliman and Mms Kaldas. Semi-active suspension systems from research to mass-market – A review. *Journal of Low Frequency Noise, Vibration and Active Control*, 40(2):1005–1023, June 2021.
- [115] R. Sonnenburg and A. Stretz. Damper Modules with Adapted Stiffness Ratio. *Arch Appl Mech*, 81(7):853–862, July 2011.
- [116] B.F. Spencer Jr, S.J. Dyke, M.K. Sain, and J.D. Carlson. Phenomenological Model of a Magnetorheological Damper. *ASCE Journal of Engineering Mechanics*, 1996.
- [117] D. Storer, G. Guerci, C. Morari, V. Tanfoglio, X. Lauwerys, and K. Reybrouck. Case Studies Involving the Identification of Problematic Impulsive Effects on Vibration Signals. In *SAE Noise and Vibration Conference and Exposition*, page 971894, May 1997.
- [118] C. Surace, K. Worden, and G. R. Tomlinson. An improved nonlinear model for an automotive shock absorber. *Nonlinear Dynamics*, 3(6):413–429, December 1992.
- [119] C Surace, K Worden, and G R Tomlinson. On the Non-Linear Characteristics of Automotive Shock Absorbers. *Proceedings of the Institution of Mechanical Engineers, Part D: Journal of Automobile Engineering*, 206(1):3–16, January 1992.
- [120] Żymelka Szymon. Amesim interface.
- [121] Michael S. Talbott and John Starkey. An Experimentally Validated Physical Model of a High-Performance Mono-Tube Damper. In *Motorsports Engineering Conference & Exhibition*, pages 2002–01–3337, December 2002.
- [122] M.J. Garcia Tarrago, N. Gil Negrete, and J. Vinolas. Viscoelastic models for rubber mounts: Influence on the dynamic behaviour of an elastomeric isolated system. *International Journal of Vehicle Design*, 49(4):303, 2009.
- [123] Joris Van Haver. Structure-Borne Shock Absorber Noise: Non-Linear Noise Source Characterization in a Laboratory Environment. In *SAE Noise and Vibration Conference and Exposition*, page 951255, May 1995.
- [124] Jörg Wallaschek. Dynamics of Non-Linear Automobile Shock-Absorbers. *International Journal of Non-Linear Mechanics*, 25(2-3):299–308, January 1990.

- [125] M. Weigel, W. Mack, and A. Riepl. Nonparametric Shock Absorber Modelling Based on Standard Test Data. *Vehicle System Dynamics*, 38(6):415–432, October 2002.
- [126] Klaus Wolff, Jannis Hoppermans, and Rob Kraaijeveld. Objective Evaluation of Subjective Driving Impressions. In *FISITA 2008 World Automotive Congress*, Munich, Germany, September 2008. VDI.
- [127] Jingli Xu, Jinli Chu, and Hongwei Ma. Hybrid Modeling and Verification of Disk-Stacked Shock Absorber Valve. *Advances in Mechanical Engineering*, 10(2):168781401875639, February 2018.
- [128] Hiroshi Yamauchi, Toshihiko Sugahara, Masaru Mishima, and Eishin Noguchi. Theoretical Analysis and Proposition to Reduce Self-Excited Vibration of Automotive Shock Absorber. May 2003.
- [129] Victor Y. B. Yung and David J. Cole. Modelling High Frequency Force Behaviour of Hydraulic Automotive Dampers. *Vehicle System Dynamics*, 44(1):1–31, January 2006.
- [130] V.Y.B. Yung and D. J. Cole. Analysis of High Frequency Forces Generated by Hydraulic Automotive Dampers. *Vehicle System Dynamics*, 37(sup1):441–452, January 2002.
- [131] Christoph Zach, Werner Mack, Gabriele Fruhmann, and Werner Tieber. On the performance of rheological shock absorber models in full vehicle simulation. *Vehicle System Dynamics*, 45(11):981–999, November 2007.
- [132] Szymon Żymełka. Modes pairing strategies for model updating procedure performed on spatially incomplete modal data. *International Journal of Vehicle Noise and Vibration*, 17(1/2):82, 2021.
- [133] Szymon Żymełka. The Diagnostic Procedure of Internal Characteristics Identification of the Semi-active Automotive Shock Absorber Using a Numerical Model. In Andrzej Puchalski, Bogusław Edward Łazarz, Fakher Chaari, Iwona Komorska, and Radosław Zimroz, editors, *Advances in Technical Diagnostics II*, volume 21, pages 154–165. Springer Nature Switzerland, Cham, 2023.